CR 137529
AVAILABLE TO
THE PUBLIC

FINAL REPORT

ANALYSIS OF THE WIND TUNNEL TEST OF A TILT ROTOR POWER FORCE MODEL

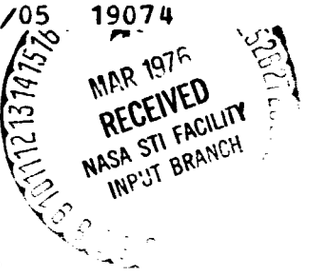

REPORT 301-099-004

NASA CONTRACT NAS 2-8084

BELL HELICOPTER COMPANY
POST OFFICE BOX 482 FORT WORTH TEXAS 76101 A Textron COMPANY

CR 137529
AVAILABLE TO
THE PUBLIC

ANALYSIS OF THE WIND TUNNEL TEST OF A TILT ROTOR POWERED FORCE MODEL

by

R. L. Marr
D. G. Ford
S. W. Ferguson

Bell Helicopter Company Report No. 301-099-004
June 1, 1974

Prepared Under Contract No. NAS2-8084 by
Bell Helicopter Company, A Textron Company
Fort Worth, Texas

for

National Aeronautics and Space Administration
Ames Research Center

This data is furnished in accordance with the
provisions of Contract NAS2-8084

Foreword

This report is prepared by the Bell Helicopter Company, Fort Worth, Texas, for the National Aeronautics and Space Administration, Ames Research Center, Moffett Field, California, under Contract NAS2-8084.

The Administrative Contacting Officer was Mr. Dennis Brown. The Technical Monitor was Mr. Kip Edenborough, Tilt Rotor Research Aircraft Project Office.

TABLE OF CONTENTS

LIST OF ILLUSTRATIONS

LIST OF ILLUSTRATIONS (Continued)

LIST OF ILLUSTRATIONS (Continued)

LIST OF ILLUSTRATIONS (Continued)

LIST OF ILLUSTRATIONS (Continued)

LIST OF ILLUSTRATIONS (Continued)

LIST OF ILLUSTRATIONS (Continued)

LIST OF TABLES

LIST OF SYMBOLS

Symbol	Description	Units
A	Rotor disc area	m^2 (ft^2)
AF	Axial force	N (lbf)
a_H	Horizontal stabilizer lift curve slope	1/deg
a_1	Fore and aft flapping angle	deg
B_1	Fore and aft cyclic angle, reference to the shaft	deg
B.L.	Buttline location	
b_w	Wing span	m (ft)
b_1	Lateral flapping angle	deg
C_{AF}	Aircraft axial force coefficient, AF/qS_w	
C_D	Aircraft drag coefficient, $Drag/qS_w$	
C_{D_o}	Profile drag coefficient of the wing	
C_L	Aircraft lift coefficient, L/qS_w	
C_{L_s}	Slipstream lift coefficient, L/q_sS_w	
$C_{L_{V_T}}$	$L/\rho AV_T^2$	
C_ℓ	Aircraft stability axis rolling moment coefficient about the aircraft center of gravity, RM/qS_wb_w	
C_m	Aircraft stability axis pitching moment coefficient about the aircraft center of gravity, $PM/qS_w\bar{c}_w$	
$C_{m_{H_T}}$	Aircraft pitching moment coefficient, due to horizontal stabilizer in rotor wake	

LIST OF SYMBOLS (Continued)

Symbol	Description	Units
$C_{m_{i_{H_T}}}$	Aircraft pitching moment coefficient, due to horizontal stabilizer incidence in rotor wake	
$C_{m_{s_{C/4}}}$	Slipstream pitching moment coefficient about the wing quarter chord	
$C_{m_{\delta_{e_T}}}$	Aircraft pitching moment coefficient, due to elevator in rotor wake	
C_{NF}	Aircraft normal force coefficient, NF/qS_w	
C_n	Aircraft stability axis yawing moment coefficient about the aircraft center of gravity, $YM/qS_w b_w$	
C_p	Rotor power coefficient, $Q/\rho AV_T^2 R$	
C_{PM}	Aircraft body axis pitching moment coefficient, $PM/qS_w c_w$	
C_{PM_R}	Rotor pitching moment coefficient	
C_{RM}	Aircraft body axis rolling moment coefficient, $RM/qS_w b_w$	
C_{RM_R}	Rotor rolling moment coefficient	
C_{RM_s}	Slipstream rolling moment coefficient	
C_T	Rotor thrust coefficient - helicopter notation, $T/\rho AV_T^2$	
C_{SF}	Aircraft body axis side force coefficient, SF/qS_w	
C_{SF_s}	Slipstream side force coefficient	

LIST OF SYMBOLS (Continued)

Symbol	Description	Units
C_{X_s}	$C_D\ q/q_s$	
C_y	Aircraft stability axis side force coefficient, SF/qS_w	
C_{YM}	Aircraft body axis yawing moment coefficient, $YM/qS_w b_w$	
C_{YM_s}	Slipstream yawing moment coefficient	
c_f	Flap chord	m (ft)
c_w	Wing chord	m (ft)
D	Rotor diameter	m (ft)
F.S.	Fuselage station	
g	gravity	m/sec^2 (ft/sec^2)
h	Height of rotor disc above the ground	m (ft)
h/D	Height to diameter ratio	
IGE	In-ground-effect	
i_H	Horizontal stabilizer incidence, positive leading edge up	deg
i_N	Nacelle incidence (i_N = 0 airplane mode)	deg
K_β	Rotor sidewash factor	
L	Lift	N (lbf)
ℓ_H	Horizontal tail arm	m (ft)
ℓ_m	Length of mast	m (ft)
MAC	Mean aerodynamic chord	m (ft)
MSF	Model scale factor	
NF	Normal force	N (lbf)

LIST OF SYMBOLS (Continued)

Symbol	Description	Units
OGE	Out-of-ground effect	
PM	Aircraft pitching moment	N-m (ft-lbf)
PM_R	Rotor pitching moment	N-m (ft-lbf)
Q	Rotor torque (per rotor)	
q	Free stream dynamic pressure	N/m^2 (lbf/ft^2)
q_s	Slipstream dynamic pressure, q + T/A	N/m^2 (lbf/ft^2)
R	Radius of rotor	m (ft)
RM	Aircraft rolling moment	N-m (in-lbf)
RM_R	Rotor rolling moment measured on rotor balance	N-m (ft-lbf)
R_N	Reynolds number	
RPM	Rotor speed	rev/min
SF	Side force	N (lbf)
S_H	Area of horizontal stabilizer	m^2 (ft^2)
S_w	Area of wing	m^2 (ft^2)
S'_w	Area of wing under rotor (blocked area for zero flaps)	m^2 (ft^2)
T	Rotor thrust (per rotor)	N (lbf)
T_c	Aircraft thrust coefficient, T/qS_w	
T_{c_s}	Aircraft slipstream thrust coefficient, T/q_sS_w	
$V_{F.S.}$	Full scale aircraft airspeed	kt
$\bar{V}_H$	Horizontal tail volume coefficient	
$V_{M.S.}$	Model scale airspeed	m/sec (ft/sec)

LIST OF SYMBOLS (Continued)

Symbol	Description	Units
V_{H_R}	Velocity of the rotor wake at the horizontal stabilizer	m/sec (ft/sec)
V_T	Tip speed	m/sec (ft/sec)
W.L.	Waterline location	
W_{i_R}	Induced velocity at rotor disc	m/sec (ft/sec)
$W_{i_{R/H}}$	Induced velocity from the rotor in the plane of the horizontal stabilizer	m/sec (ft/sec)
X_{LT}	Lateral stick position	m (in)
YM	Yawing moment	N-m (ft-lbf)
α_F	Fuselage angle of attack	deg
α_H	Angle of attack at horizontal stabilizer	deg
α_w	Wing angle of attack	deg
δ_a	Flaperon delfection angle, positive down	deg
δ_e	Elevator deflection, positive down	deg
δ_f	Flap deflection angle, positive down	deg
δ_3	Pitch flap coupling	deg
$\epsilon_{R/H}$	Rotor wake deflection at horizontal stabilizer, positive down	deg
ϵ_T	Wing plus rotor wake deflection at horizontal stabilizer, positive down	deg
$\epsilon_{W/H}$	Wing wake deflection at horizontal stabilizer, positive down	deg
η_{H_R}	Dynamic pressure ratio of the horizontal stabilizer, due to rotor interference	
η_{H_T}	Dynamic pressure ratio at the horizontal stabilizer, due to wing-body-rotor interference	

LIST OF SYMBOLS (Continued)

Symbol	Description	Units
$\eta_{H_{WB}}$	Dynamic pressure ratio at the horizontal stabilizer, due to wing-body interference	
η_{V_T}	Dynamic pressure ratio at the vertical stabilizer, due to wing-body-rotor interference	
$\eta_{V_{T_{WB}}}$	Dynamic pressure ratio at the vertical stabilizer, due to wing-body interference	
θ_{TIP}	Rotor blade collective pitch setting at tip	deg
μ	Advance ratio	
ν	Kinematic viscosity	m^2/sec (ft^2/sec)
ρ	Density	Kg/m^3 ($slugs/ft^2$)
τ_e	Elevator effectiveness parameter	
ϕ	Roll angle, positive right wing down	deg
ψ	Fuselage yaw angle, positive nose right	deg
Ω	Rotor speed	rev/sec
$\partial\sigma/\partial\beta$	Sidewash factor	

I. SUMMARY

Two series of tests were made to determine performance, stability and control, and rotor wake interaction on the airframe, using a one-tenth scale powered force model of a tilt rotor aircraft (Figure 1). Testing covered hover (IGE/OGE), helicopter, conversion, and airplane flight configurations. These tests took place in the NASA-Langley V/STOL wind tunnel. The first test was in September 1972 and was terminated because of insufficient collective pitch actuator capability of the model to complete the high power and high speed airplane flight conditions. Modifications were made to the collective pitch actuator and testing was completed during the second tunnel entry in October 1973. Wind tunnel testing was performed under NASA Contract NAS1-11582.

Forces and moments were recorded for the model from predetermined trim attitudes. Control positions were adjusted to trim flight (one-g lift, pitching moment and drag zero) within the uncorrected test data balance accuracy. Pitch and yaw sweeps were made about the trim attitudes with the controls held at the trimmed settings to determine the static stability characteristics. Tail on, tail off, rotors on, and rotors off configurations were tested to determine the rotor wake effects on the empennage.

Data obtained during this testing will be presented in a NASA TM.[1] Information presented in this report will cover the analysis of the test data. This analysis covers only information useful for tilt rotor aircraft (rotor wake effects) and does not include any analysis of the aerodynamic characteristics for the tilt rotor model tested. Results from this test will be used to supplement information obtained from other model tests.[2] Documentation of this analysis is covered under NASA Contract NAS2-8084.

The principal results from this analysis are as follows:

(1) Rotor Interference on the Wing

Hover tests in-ground-effect showed wing download to be in agreement with previous model tests. Correlation was established when wing download is presented in terms of blade twist, thrust, blockage, and flap deflection. Reynolds number corrections are required to determine the full-scale aircraft wing download. Wing download does not appear to decrease significantly for full span flap deflections greater than 50 degrees. Flaperon deflection is more effective than flap deflection in reducing download.

Rotor interference on the wing was found to be negligible above 40 knots for all conversion angles tested.

(2) Rotor Wake on the Empennage

The interaction of the rotor wake with the horizontal stabilizer is to produce an upload during low speed helicopter flight and changes to downwash during airplane flight. The downwash measured for rotors on in airplane flight is that due to the wing wake and is the same as measured for rotors off.

Rotor-induced velocity at the empennage was found to correlate with previous model test data. The rotor wake effect was also shown to become insignificant as the nacelles are tilted forward and as speed increases above 120 knots.

(3) Rotor Flapping

Lateral flapping in helicopter mode was higher than estimated using low disc loading and low twist rotor induced velocity correction factor. Flapping angles were in agreement with previous model test results and estimates using the modified induced velocity correction factor for high disc loading and high twist rotor.

(4) Roll Stability (IGE)

The roll instability during hover IGE measured during this testing was found to be in agreement with previous test results for tilt rotor aircraft. The roll instability can be controlled with a small lateral stick input with the control power available for the models tested.

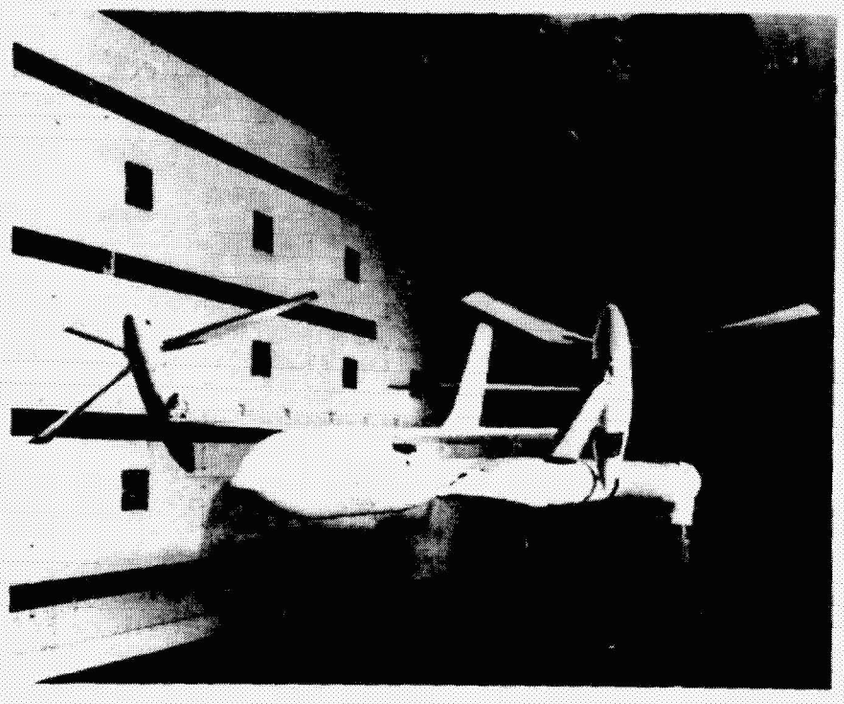

Figure I-1. Powered Model on Rotary Sting Mount, Langley V/STOL Tunnel

II. INTRODUCTION

This report presents the analysis of a wind tunnel test of a one-tenth scale powered force model of a tilt rotor aircraft. Testing was accomplished to determine the performance, stability and control, and rotor wake interaction on the airframe during hover, helicopter, conversion, and airplane flight. The Bell Model C100-F1B is a powered aerodynamic scale model of the Bell Model D270 tilt rotor aircraft.[3] A three-component rotor balance was installed in each nacelle to allow separation of rotor forces and moments from those measured from the tunnel balance for the overall model. This capability allowed analysis for rotor airframe interaction to be made in addition to that obtained from previous model tests. Rotor wake effects obtained from this analysis are applicable to tilt rotor aircraft configurations.

The principal objectives of this report are to analyze the test data and compare it with other model test data and analytical methods. Results are summarized for application to the design of existing and future tilt rotor aircraft. The documentation was accomplished under NASA Contract NAS2-8084.

A. Previous Testing

Most of the tilt rotor model testing by Bell Helicopter Company has been with a one-fifth scale model of the Bell Model 300 as reported in Reference 2. These tests were directed at determining the performance, stability and control, and aeroelastic characteristics for the XV-15 Tilt Rotor Research Aircraft. Rotor wake interaction obtained with that model was limited in scope due to tunnel capability (inadequate for high speed airplane flight) and model capability (no rotor balance). Therefore, results obtained from the test presented in this report will be used to supplement the information obtained from the fifth-scale model tests.

B. Technical Background

Tilt rotor model testing was initiated to address problem areas encountered during the XV-3 flight test program. These problem areas were primarily noted during hover and low speed helicopter flight and were related to the rotor wake interaction on the airframe. A detailed discussion as to the approach to correct these problems is presented in Reference 2. This test investigated these problem areas.

C. Tunnel Description

The wind tunnel test was accomplished in the NASA-Langley V/STOL wind tunnel. The V/STOL tunnel has a 4.88-meter (16-foot) test section and can operate through a speed range of 6.1 to 76.2 meters per second (20 to 250 feet per second), with the walls down. With the tunnel walls raised, the test section is opened to eliminate wall effects and can be operated through a speed range of 0 to 18.3 meters (60 feet per second). The model was mounted on a rotary sting support with a six-component internal balance. Adjustments could be made for pitch, roll, and yaw at the desired h/D (height above ground to rotor diameter) to obtain ground effect information. This capability allowed the model to be tested at all configurations from helicopter to airplane flight.

D. Objectives of This Analysis

This analysis has the following specific objectives:

1. Determine the rotor wake effect on the wing. This includes evaluating the effects of various design parameters on wing download during hover and changes in wing download during forward flight.

2. Determine the rotor wake effects on the empennage in sufficient detail to supplement existing data for use in the mathematical model for flight simulation of tilt rotor aircraft.[4] Rotor wake characteristics for two types of empennage configurations will be shown.

3. Compare measured rotor performance with estimated.

4. Evaluate roll static stability during hover in-ground-effect.

5. Evaluate rotor flapping characteristics.

These objectives were accomplished and the results are discussed in the following sections.

III. DESCRIPTION OF THE MODEL

The model tested, designated the Bell Model C100-F1B, is a one-tenth length scaled aerodynamically similar model of the Bell Model D-270 tilt rotor aircraft. The model was developed under Phase I of Air Force Contract F33615-69-C-1578. The model has two five-foot diameter rotors that are mechanically interconnected. They are driven by two fuselage-mounted TASK variable frequency motors having a continuous operating rating of 25,353 watts (34 horsepower) each. The span of the model between rotor centers is 1.95 meters (6.4 feet); with the rotors turning, the span is 3.47 meters (11.4 feet). Overall model length is 2.47 meters (8.1 feet). The model was supported during the test on a fuselage-mounted six component balance rotary sting support. A list of scale factors, full-scale and model-scale parameters for the rotor, wing, fuselage, and empennage are given in Table III-1. These are the parameters used during data reduction and analysis.

A. Construction and Design Parameters

A description of the model components are as follows:

1. Fuselage

The basic fuselage backbone, from the wing aft to the empennage, was a square steel tube with aluminum plate bulkheads to support removable fiberglass fairing shells. Forward of the wing bulkhead, four aluminum longerons extend forward to support the motors, center gearbox mounting bulkheads, and the nose section. The cylindrical fuselage section ahead of the wing is formed by two removable shells of curved aluminum plate.

2. Empennage

The vertical stabilizer has a steel spar and was attached to the aft portion of the fuselage backbone. The drive motor and potentiometer for remote control and position indicator of the elevator was housed at the base of the vertical stabilizer in the spar. A rudder was not required for this test. The horizontal stabilizer was mounted midway up the vertical stabilizer. The elevator could be remotely varied ±20 degrees. Horizontal stabilizer incidence could be manually varied ±5 degrees by changing fillet blocks which attached the horizontal stabilizer to the vertical stabilizer. The aerodynamic shape for the horizontal and vertical stabilizers was formed from wood panels.

3. Wing

The basic wing structure was a hogged-out aluminum channel section which was closed to form a torque box by means of a bolted on, lower surface aluminum cover plate. At the root end of each wing box, a fork-shaped steel root fitting was attached to the upper part of the center gearbox. The rotor interconnect power shaft was through the wing box and attached the center gearbox to the wing tip mounted rotors. Brackets were available to adjust the flaps (δ_f) to 50 degrees down, and flaperons (δ_a) to 20 degrees down. Taping of the flaperons was required to permit full span flap testing to 62.5 degrees to evaluate the effect of flap position on wing download during hover. The aerodynamic contours for the wing, flaps, and flaperons were shaped from wood panels attached to the metal spars.

4. Nacelles

The nacelles were mounted on the wing tips and housed the rotor controls, balance, and transmission. Non-structural fiberglass fairings were attached to aluminum plate bulkheads which supported the transmission. Conversion struts were available for manual adjustment of the nacelle from 90 degrees (helicopter) to 0 degrees (airplane) in fifteen-degree increments.

5. Rotors and Controls

The five-foot diameter rotors were provided with remotely controlled collective pitch and longitudinal monocyclic pitch control for each rotor. The rotors have three blades per rotor. Each blade was mounted to a gimbal hub to permit rotor flapping. Flapping was restrained by hub springs located in the rotating system and was recorded using a strain gaged flexure referenced to the rotor shaft. The rotor blades were dynamically scaled in stiffness and mass distribution based on a model tip speed of 0.6 times full scale tip speed. The model rotors were operated up to 1884 rpm which was representative of a full-scale hover tip speed of 251 meters per second (822 feet per second). The blades were provided with strain gages for monitoring beam, chord, and torsion loads.

Cyclic pitch range was $\pm$12 degrees. The collective pitch range was from -11 to +33 degrees (measured at tip of blade). Cyclic and collective control positions were

5. (Continued)

instrumented for both rotors. The collective pitch could be changed simultaneously for both rotors, or to the right rotor independently for trim capability. Loads generated by the model collective and cyclic control system did not cross the rotor balances, but were monitored from an instrumented pitch link for each rotor.

6. Rotor Drive System

The rotor drive system consisted of two TASK motors mounted in the fuselage driving aft through flexible couplings into a coupling gearbox which reduced the motor speed by a factor of three. The outputs of the gearbox are coupled to the interconnect shafts with universal joints. Wing tip gearboxes are provided for a further reduction of shaft speed by a ratio of two to one. The wing tip gearboxes are modified Bell Model 47 helicopter, 90 degree, tail rotor gearboxes. Each rotor shaft was strain gaged to sense rotor torque. The rotor shafts were extended to carry an instrumented slip ring to measure rotor blade loads, flapping, etc., and a tachometer/azimuth wheel for driving a magnetic pulse pickup.

7. Rotor Balance

A three-component rotor balance was installed in each nacelle. The primary measurement was rotor axial force for use in evaluating the rotor/airframe lift distribution data. Longitudinal and lateral moments were measured and included in the balance equations to improve the accuracy of the axial force measurement in addition to providing supplemental rotor data. Dual thrust and torque bridges were incorporated in each balance to permit the tunnel test to continue if the signal from one bridge was lost.

8. Instrumentation

The model was instrumented to measure the parameters as listed in Table III-2. This data was presented on oscillograph recorders and on the V/STOL tunnel data recorder system for monitoring during the test. Model motor temperatures were monitored using a Brown temperature recorder.

TABLE III-1. FULL SCALE/MODEL SCALE PARAMETERS

Scale Factors	Model/Full Scale
Length	0.10
Velocity	0.60
Force	0.0036
Power	0.00216

Design Parameters	Full Scale	Model Scale
Aircraft:		
C.G. Location (Mid)		
F.S. @ i_N = 90°	529	52.9
W.L.	199	19.9
F.S. @ i_N = 0°	510	51.0
W.L.	171	17.1
Design Gross Weight, N (lbf)	293,568 (66,000)	1059 (238)
Rotors:		
Blades Per Rotor	3	3
Diameter, m (ft)	15.24 (50)	1.524 (5.0)
Blade Chord, cm (in)	101.6 (40)	10.16 (4.0)
Blade Twist, deg	25	25
RPM		
Helicopter	314	1884
Conversion	268	1604
Airplane	228	1372
Mast Length, m (ft)	3.106 (10.19)	.3106 (1.019)
Hub Spring, m-N/deg (ft-lbf/deg)	1242 (916)	.447 (.33)
δ_3, deg	-25	-25
Conversion Axis		
F.S.	526	52.6
W.L.	195.4	19.54
B.L.	385.5	38.55
Wing:		
Span (Rotor Centerline), m (ft)	19.58 (64.25)	1.958 (6.425)
Area, m^2 (ft^2)	65.59 (706)	.6559 (7.06)
Aspect Ratio	5.85	5.85
MAC, m (ft)	3.38 (11.1)	.338 (1.11)
Location of 1/4 MAC		
F.S.	514	51.4
W.L.	195.4	19.54
B.L.	180.6	18.06
Leading Edge Sweep, deg	-6	-6
Dihedral, deg	2	2

TABLE III-1. FULL SCALE/MODEL SCALE PARAMETERS (Continued)

	Full Scale	Model Scale
Flaperons:		
Span Per Side, cm (in)	335 (132)	33.5 (13.2)
Chord/Wing Chord	.275	.275
Flaps:		
Span Per Side, cm (in)	381 (150)	38.1 (15.0)
Chord/Wing Chord	.275	.275
Fuselage:		
Length, cm (in)	2261 (890)	226.1 (89.0)
Diameter, cm (in)	304.8 (120)	30.48 (12.0)
Horizontal Stabilizer:		
Span, cm (in)	1016 (400)	101.6 (40.0)
Area, m^2 (ft^2)	23.23 (250)	.2323 (2.50)
Aspect Ratio	4.45	4.45
Sweep of 1/4 Chord, deg	15	15
MAC, m (ft)	2.30 (7.56)	.230 (.756)
Location of 1/4 MAC		
F.S.	1004.5	100.45
W.L.	291.1	29.11
Elevator:		
Area, m^2 (ft^2)	4.74 (51)	.0474 (.51)
Chord/Stabilizer Chord	.265	.265
Vertical Stabilizer:		
Span, cm (in)	548.6 (216)	54.86 (21.6)
Area, m^2 (ft^2)	19.04 (205)	.1904 (2.05)
Aspect Ratio	1.6	1.6
Sweep of 1/4 Chord, deg	32	32
MAC, m (ft)	3.53 (11.58)	.353 (1.158)
Location of 1/4 MAC		
F.S.	955	95.5
W.L.	291.1	29.11
Rudder:		
Area, m^2 (ft^2)	4.08 (43.9)	None

TABLE III-2. MODEL INSTRUMENTATION*

Blade beamwise loads (27.3% R) Blade chordwise loads (27.3% R) Blade torsion loads (27.3% R) Blade flapping Pitch link loads Rotor torque Rotor speed and azimuth Rotor axial force Rotor pitching moment Rotor yawing moment Collective pitch position Cyclic pitch position Elevator position Wing tip gearbox temperatures Interconnect drive shaft bearing temperatures Center gearbox temperatures Motor temperatures Motor frequency control and amperage
*Rotor, blade, and motor parameters were recorded for both left and right rotors.

IV. DESCRIPTION OF TESTS

Testing was accomplished in the NASA-Langley V/STOL wind tunnel during two tunnel entries. The first entry, V/STOL test number 31, was from August 22, 1972, through September 13, 1972. The second entry, V/STOL test number 69, was from October 11, 1973, through November 9, 1973. Both tests were accomplished to fulfill the same test plan; therefore, run numbers were made continuous for both tests. Total occupancy time was 440 hours. Rotors-on testing, rotors turning, accounted for 70 hours of this time resulting in a 18.5% utilization. Rotors-off testing accounted for only 42 hours. A total of 359 runs were made for a run average of 0.82 run per hour.

The model was mounted on the V/STOL tunnel rotary sting support system with an internal, six component strain gage balance to record aircraft force and moment data. Fuselage pitch attitude was generally varied from -16 to +20 degrees and yaw angles were varied from -2 to +16 degrees. Both hover and forward flight was investigated. Yaw sweeps during the V/STOL test 31 were made with and without the horizontal stabilizer. Dynamic characteristics of the model were such that removal of the empennage mass would cause the model to vibrate. Only pitch characteristics with yaw were obtained. During the second tunnel entry, a simulated empennage mass was inserted in the tail cone fairing to allow complete empennage off testing.

Initial control positions and trim aircraft attitudes were determined prior to testing using the Bell Helicopter Company computer program C81. Static stability data were obtained during pitch and yaw sweeps from the trim conditions. Control settings were held constant during the sweep. In order to obtain wake effects on the horizontal stabilizer, both elevator sweeps and horizontal stabilizer incidence sweeps were made. Tests were also accomplished with the empennage and/or the rotors removed. The model is shown mounted on the sting in Figures IV-1 through IV-4 for the various configurations tested.

The wing download was measured during hover at h/D ratios from 0.525 through 1.825. Various combinations of flap and flaperon settings were tested at h/D of 1.825 to determine the effect of flap settings on wing download. Settings tested were 0, 20, 50, and 62.5 degree, all full span flap settings.

The rotary sting permitted the model to be set at various roll angles and h/D ratios. Rolling moment was measured to determine the influence of the wing/rotor interaction on roll stability.

Several tunnel wall configurations were tested to determine the wall interference effects on the model performance. These configurations were with the 1) walls up (open test section), 2) walls down (closed test section), and 3) walls down/slots open (slots in walls, floor, and ceiling opened).

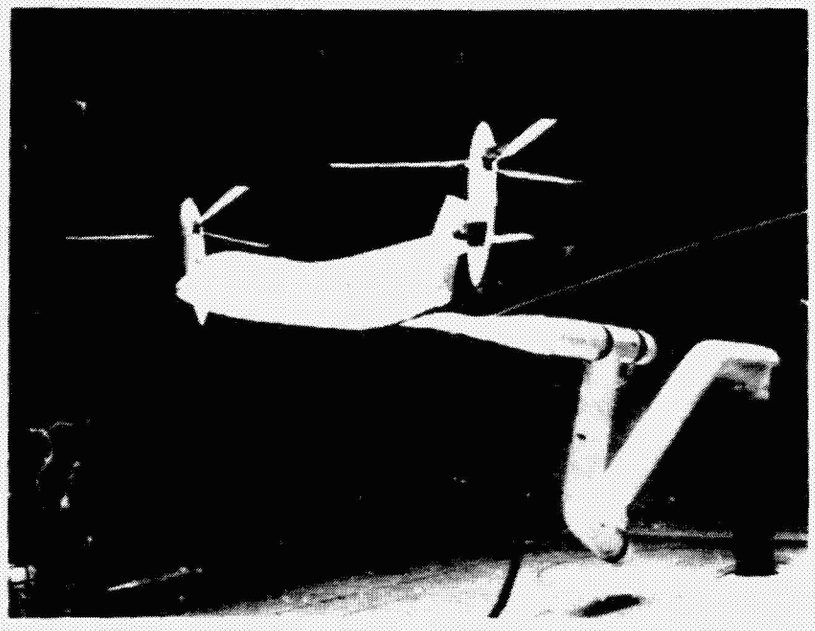

Figure IV-1. Helicopter Configuration, Nacelle Incidence 90°, OGE, Walls Up

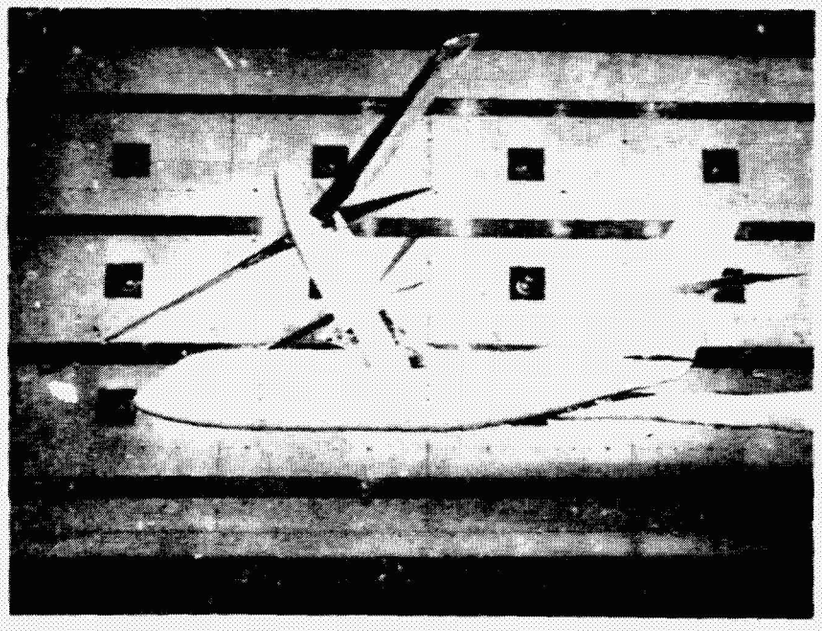

Figure IV-2. Conversion Configuration, Nacelle Incidence 60°, OGE, Walls Down

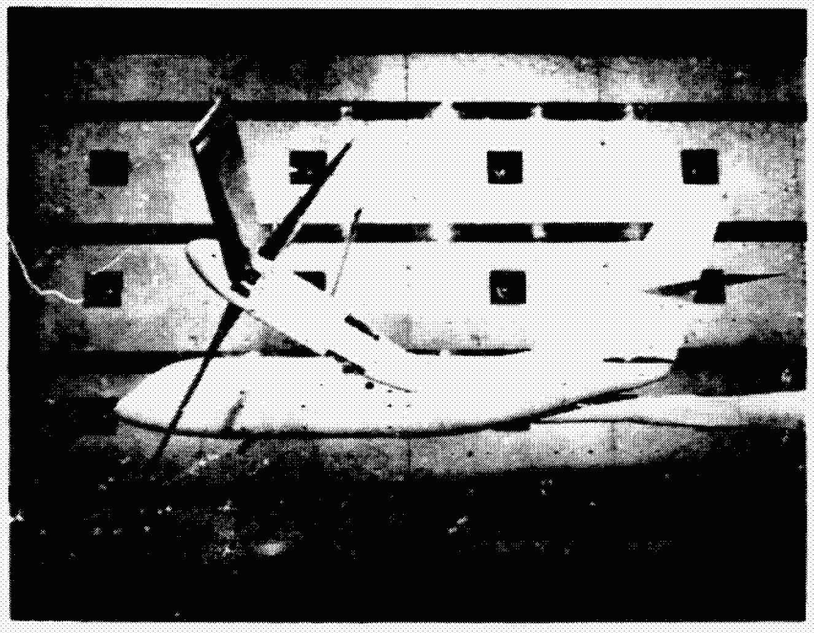

Figure IV-3. Conversion Configuration, Nacelle Incidence 30°, OGE, Walls Down

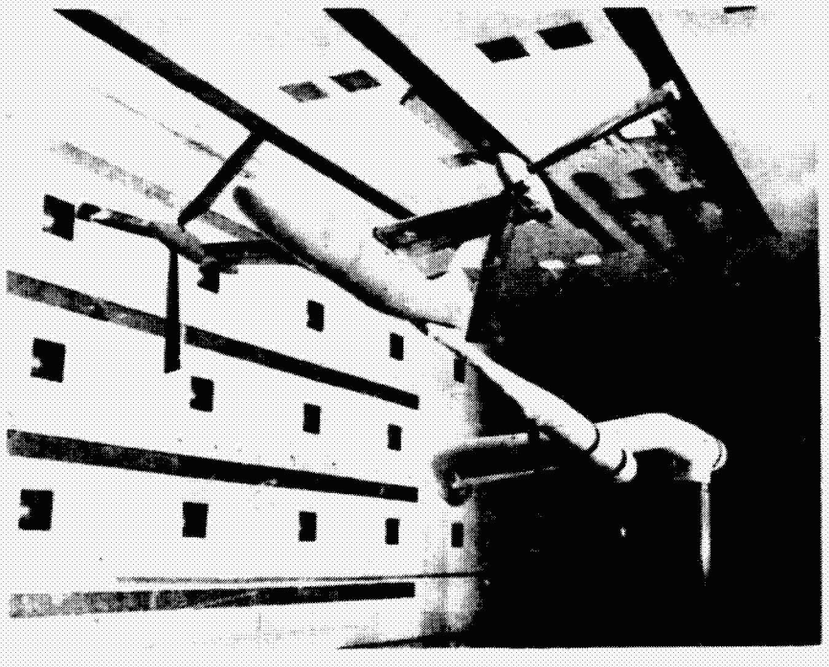

Figure IV-4. Airplane Configuration, Nacelle Incidence 0°, OGE, Walls Down

V. DATA REDUCTION

Force and moment data measured on the wind tunnel six-component internal balance and rotor balances were reduced using a NASA-Langley data reduction program. Corrections were included for tunnel wall effects and interference effects of the sting support. The tunnel test data was tabulated in a format as listed in Table V-1. Also included in Table V-1 is a comparison of the symbols used in the tabulated test data presented in Reference 1 and those used in this report. This is intended to give the user a means of correlating the data presented in the two reports. Control positions and test conditions (airspeed, angle of attack, sideslip, etc.) are also listed. The force and moment sign convention used for the rotor and airframe is shown in Figure V-1. The configuration code used is listed in Table V-2. A run schedule summary is given in Appendix A.

The data reference center for the internal sting balance was station line 52.6, water line 11.0, and butt line 0.0. Data was corrected to a center-of-gravity location equivalent to a mid-cg as listed in Table V-3. Maximum Reynolds number tested was 1.28×10^6 referenced to the wing chord of .338 meters (1.11 feet).

Airspeed presented throuout the text of this report, in the figures and the Appendix, is given as equivalent full-scale airspeed ($V_{F.S.}$). For the scale of the model tested, the equivalent full-scale value in knots is nearly equal to the model scale test airspeed ($V_{M.S.}$) in feet per second as shown below:

$$V_{F.S.}(\text{KTS}) = \frac{V_{M.S.}(\text{FPS})}{.6\left(\frac{\text{M.S.}}{\text{F.S.}}\right) * 1.681\left(\frac{\text{FPS}}{\text{KTS}}\right)} = .99\ V_{M.S.}(\text{FPS})$$

TABLE V-1. DATA REDUCTION

Information	Tabulated Data	
	Computer Notation As In Ref. 1	Symbol As Defined In Report
I. Configuration		
A. Tunnel Setting	V, FS	$V_{F.S.}$
	VTUN	$V_{M.S.}$
	MU	μ
	Q	q
	QS	q_s
B. Model Attitude	ALC	α_F
	BETA	$-\psi$
	PHI	ϕ
C. Rotor Controls, left and right rotor	THL, THR	θ_{TIP}
	B1L, B1R	B_1
	ELEV	δ_e
	RPM	RPM
II. Airframe Aerodynamics		
A. Lift	NF	NF
	CNF	C_{NF}
	CL	C_L
	CLS	C_{LS}
	CLVT	$C_{L_{V_T}}$
B. Drag	AF	AF
	CAF	C_{AF}
	CD	C_D
	CXS	C_{X_S}
C. Pitching Moment	PM	PM
	CPM	C_{PM}
	CM	C_M

TABLE V-1. DATA REDUCTION
(Continued)

Information	Tabulated Data	
	Computer Notation As In Ref. 1	Symbol As Defined In Report
II. Airframe Aerodynamics		
C. Pitching Moment (Continued)	CMS4C	$C_{m_{s_{C/4}}}$
D. Rolling Moment	RM	RM
	CRM	C_{RM}
	CR	C_{ℓ}
	CRS	C_{RM_s}
E. Yawing Moment	YM	YM
	CYW	C_{YM}
	CYM	C_n
	CYMS	C_{YM_s}
F. Side Force	SF	SF
	CSF	C_{SF}
	CY	C_y
	CSFS	C_{SF_s}
III. Rotor Aerodynamics		
A. Thrust average, left and right rotor	TAV, TL, TR	T
	CTAV, CTL, CTR	C_T
	TCT, TCL, TCR	T_{c_s}
	CTAAV, CTAL, CTAR	T_c
B. Torque average, left and right rotor	QAV, QL, QR	Q
	CQAV, CQL, CQR	C_p

TABLE V-1. DATA REDUCTION
(Continued)

Information	Tabulated Data	
	Computer Notation As In Ref. 1	Symbol As Defined In Report
III. Rotor Aerodynamics		
C. Moments left and right rotor	PML, PMR	PM_R
	CPML, CPMR	C_{PM_R}
	RML, RMR	RM_R
	CRML, CRMR	C_{RM_R}

TABLE V-2. CONFIGURATION CODE

Airframe/Rotor:

Code	Flaps	Stabilizer Horizontal	Stabilizer Vertical	Rotors
1	50/20	ON	ON	ON
2	50/20	OFF	ON	ON
3	50/20	ON	ON	OFF
4	50/20	OFF	ON	OFF
5	0/0	ON	ON	ON
6	0/0	OFF	ON	ON
7	0/0	ON	ON	OFF

Horizontal Stabilizer:

Code	Incidence
0	Tail off (Horizontal Only)
1	-5°
2	0
3	5°
4	Empennage Off

Nacelle Setting:

Code	Nacelle Incidence
0	0
2	30
4	60
5	75
6	90 (Helicopter)

Code as shown in the run schedule listed in Appendix is written:

airframe-empennage-nacelle

TABLE V-3. CENTER-OF-GRAVITY POSITIONS

Nacelle Incidence (deg)	F.S.	W.L.
90 (Helicopter)	52.9	19.9
75	52.6	19.5
60	52.3	19.0
30	51.7	18.0
0	51.0	17.1

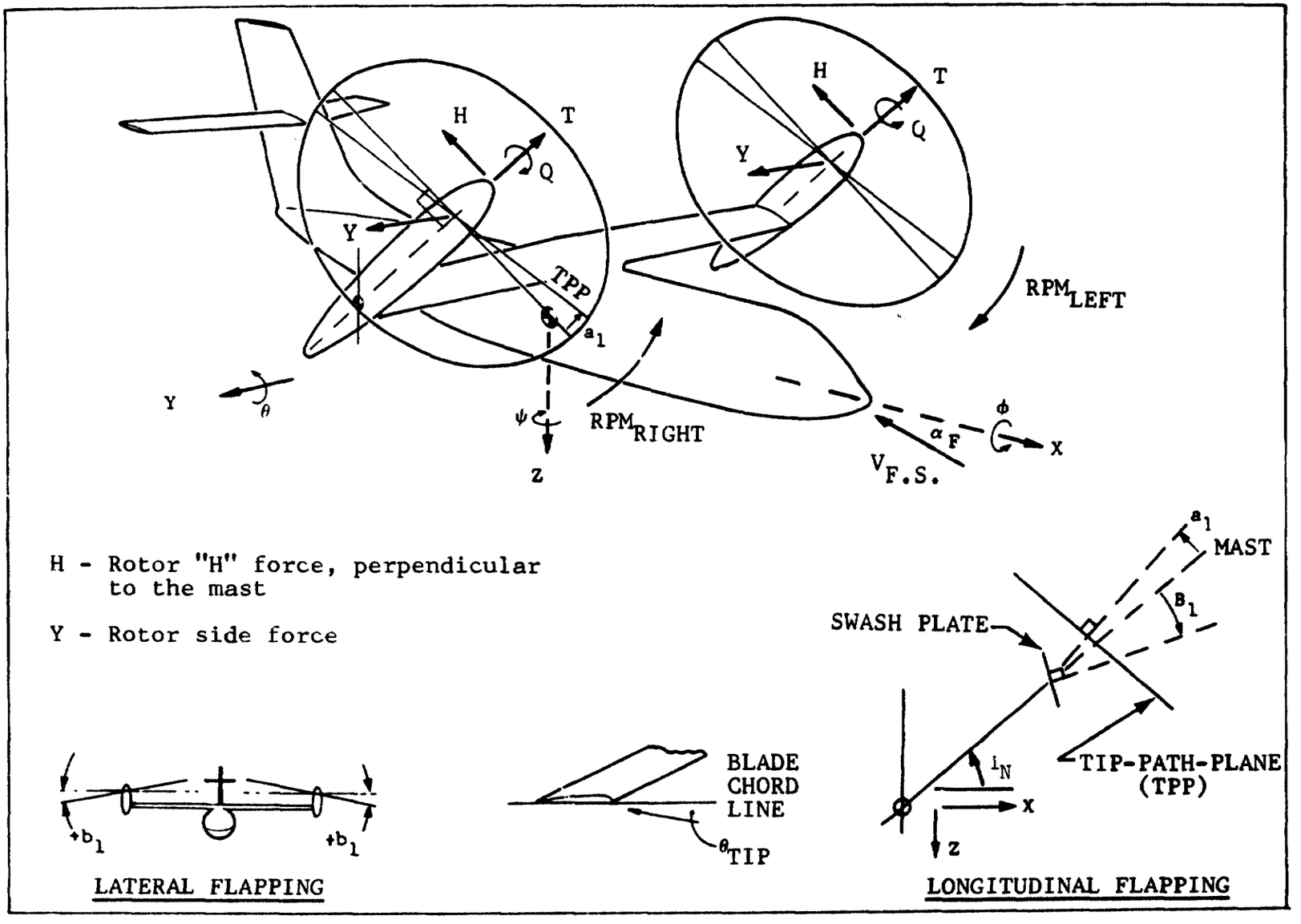

Figure V-1. Force and Moment Sign Convention.

VI. RESULTS OF TEST

A. Roll Stability - In Ground Effect

Roll stability was measured in and out of ground effect by rolling the model at h/D ratios of .53, .67, .83, 1.00, and 1.84. Aircraft rolling moment measured is given in Figure VI-1.

Roll stability versus height above the ground is summarized by Figure VI-2 in terms of the amount of lateral stick required to maintain trim and rolling moment per degree roll angle between ±2 degrees of roll. The amount of lateral stick required to maintain trim was determined by dividing the model data roll control power into the rolling moment per degree roll measured during the test. As indicated, the model was found to have positive roll stability near touchdown, h/D <.60. Between h/D = .60 and 1.67, the model showed negative roll stability. The maximum instability occurred at approximately h/D = .85. Above h/D = 1.67, or OGE, the model was again stable. Also illustrated is the small amount of lateral control required to trim at the maximum instability height. As an example, for a ten-degree wing drop in-ground-effect, the lateral stick for trim would be 1.12 cm (.44 inch).

Roll characteristics obtained during this test were found to be in agreement with those determined during similar tests on other tilt rotor models for small roll angles. The nonlinear roll effect shown above 5 degrees roll were not apparent during the other model test (Reference 2). A comparison of the results of these tests are given in Figure VI-3. With the control power available on current tilt rotor aircraft and with SCAS, the roll instability is not expected to present the problem as it did for the XV-3. These levels of instability have been incorporated into the tilt rotor simulation and have received no unfavorable pilot comment concerning hover handling qualities.

B. Wing Download

Wing download was obtained during hover in and out of ground effect by making collective sweeps and comparing rotor thrust required to hover at an equivalent full-scale gross weight. The collective pitch required to hover OGE was increased by approximately two degrees from that required to hover IGE. The wing download in percent rotor thrust at the height to diameter ratios tested is summarized in Figure VI-4. For a full-span flap configuration, the download varied from 9.5 percent OGE to -6.5 percent (upload) IGE. Raising the flaperons to a conversion flap/flaperon setting increased the download, OGE, by 3 percent for a total of 12.5 percent.

B. (Continued)

The effect of flap deflection on wing download for full-span flap OGE is shown in Figure VI-5. (The faired curve shown is based on comparison of results of other model tests as discussed in Section VII.) Test results indicate very little improvement in relieving wing download for flap deflections above 50 degrees. For comparison purposes the test point for flaperon setting of 20 degrees was plotted as 20-degree flap deflection. It is nearly in agreement with the full span flap results indicating that most of the reduction in download occurs from flaperon deflection or, in general, from deflecting a surface which is in the projected plane of the rotor.

Rotor/wing interference was determined for forward flight at various nacelle incidence angles. The rotor/wing lift sharing with nacelle incidence is shown in Figure VI-6. Comparison is shown between rotors on and rotors off to illustrate the rotor wake effect on the wing lift. Airframe lift was obtained by taking the difference between the lift recorded on the main balance (airframe plus rotor) and subtracting the rotor thrust measured on the rotor balances. Comparison with the rotors-off tests indicate that the wing lift is not influenced by the rotor wake above 40 knots, and the wing download in hover changes to an upload with forward flight. As shown, the wing begins to contribute lift at an airspeed of 35 knots, whereas linearized rotor wake theory would predict the wing to be immersed in the rotor wake at that low airspeed.

Flow visualization tests on another model[2] were in agreement with these test results. As observed during that test, the rotor induced a strong upwash at the wing leading edge and on the inboard wing section at speeds as low as 20 knots. At 30 knots, the rotor wake was nearly completely off the wing. The nonuniform induced velocity distribution of the tilt rotor is considered to be the reason for the rotor wake moving off the wing at these low airspeeds. Because of this effect, the aircraft lift was higher than originally estimated prior to the first tunnel entry. Further discussion on differences between estimated and test can be found in Section VI.C.

C. Static Stability Characteristics

Stability data are shown in terms of lift, pitching moment, and yawing moment coefficients. Force and moment data were obtained for rotors and/or empennage on and off to evaluate rotor wake effects. Pitch and yaw sweeps were made about predetermined trim attitudes for level flight. Test conditions are shown in Figures VI-7 through VI-45 for speed range of 40 to 130 knots and nacelle incidence range of 90

C. (Continued)

(helicopter) to 0 degrees. Information shown is for combinations of test data that were used in the analysis of the rotor wake on the empennage.

Two types of procedures were followed in determining trim settings and obtaining wake data for the empennage. During the first tunnel entry, trim attitudes and control positions were set from predetermined estimates for rotor wake effects on the wing and empennage. As noted in Section VI.B., it was found that the rotor wake on the wing was different than estimated. This was also found to be the case for the empennage (to be shown later). The rotor performance versus collective pitch setting was also found to be different than estimated. As the result of all these differences, the aircraft was not tested in a completely trimmed configuration during the first tunnel entry. Because of the improved lift of the wing over that estimated, the model was trimmed for level flight at one g, although not necessarily at trimmed angle of attack or cyclic control position. These corrections to the rotor wake characteristics were made in the theoretical estimates prior to the second tunnel entry. The procedure followed during the second tunnel entry was to set the model at a specified trim attitude and trim both lift and drag by adjusting the controls to obtain trim thrust and power. The elevator was coordinated with cyclic position to trim aircraft pitching moment. Rolling and yawing moments were monitored to insure lateral-directional trim also. Rotor torque was found to be a good indicator for control setting repeatability when repeating a test condition going from tail on to off, and making incidence sweeps and yaw sweeps. During the sweeps from trim, the controls were not changed.

Both elevator sweeps and horizontal stabilizer incidence sweeps were used to evaluate rotor wake characteristics on the horizontal stabilizer. During the first tunnel entry, only elevator sweeps were made. Incidence sweeps were made during the second tunnel entry.

1. Lift Coefficient

A comparison between rotors on and rotors off lift coefficients for the range of airspeed and nacelle incidence angles tested is shown in Figures VI-7 through VI-21. Lift coefficient is presented versus fuselage angle of attack and is referenced to wing area and free stream dynamic pressure. Comparison was also made between the two tunnel entries for several airspeeds. The second

1. (Continued)

entry, V/STOL test 69, sometimes had higher lift coefficient rotors on than the first entry because of the different trim procedure as discussed above.

These figures illustrate the amount of lift sharing between the rotor and airframe as speed increases and the nacelles are tilted forward. Figure VI-6 summarizes the lift sharing in terms of percent wing lift to total lift for the conditions tested. As shown, at speeds above 120 knots and nacelle incidence angles 60 degrees, the rotors do not provide much additional lift to the aircraft.

2. Pitching Moment Coefficient

Pitching moment characteristics for the same range of airspeeds and nacelle incidence angles are shown in Figures VI-22 through VI-36. Again, comparisons are shown between rotors on, rotors off, and for the two tunnel entries. Rotor-off tests were not made for all speeds tested for rotors on. Comparative plots were made for rotors off with airspeed to determine the effects on pitching moment for the range of Reynolds number tested. The faired lines shown are for rotors off and are the result of the comparison. It was found that for the speed range tested, Reynolds number did not have a large effect on rotors-off pitching moment. When rotors-off runs are made at the same conditions as tested for rotors on, the data analyses is easier and eliminates any Reynolds number effects that may exist. Although some small differences existed, it is felt that the analysis of the rotor wake is still valid. As shown, the rotor wake produces a nose-down pitching moment during low speed helicopter flight and is effectively reduced to that of the wing wake above 120 knots. This change is caused from the wake changing from an upwash during low speeds to a downwash at high speeds. Trends are similar to those obtained from the powered aeroelastic model test[2] (see Section VII for a more detailed discussion of rotor wake effects). The aircraft was stable with empennage on for the speeds tested for both rotors on and off.

The pitch up at around 8 degrees angle of attack for 75 degrees nacelle incidence at 40 and 80 knots (Figure VI-28) is similar to that observed on the aeroelastic model. The pitch angle range tested for nacelle incidence at 90 degrees was not large enough to determine if the pitch up occurred at that nacelle incidence. Comparisons made between the two model tests indicated the same trends would occur at 90 degrees. To properly analyze this effect would require the velocity distribution of the rotor as the model changes angle of attack.

3. Yawing Moment Coefficient

Directional stability for the airspeeds and nacelle incidence angles tested is shown in Figures VI-37 through VI-45. Yaw sweeps made during this testing were limited due to a model dynamic problem (Section IV) and the time required to make the sweep. Therefore, a complete set of rotors-on and rotors-off data combinations were not obtained for each airspeed as tested for longitudinal stability. Where rotors-off runs are not available, runs from other airspeeds are shown for comparison.

During low speed helicopter flight, directional stability was shown to be improved with rotors on over that for rotors off. This was apparently due to the stabilizing effect of the rotors since with the empennage off, the aircraft was directionally stable. As airspeed increased, the rotor wake effects became less effective. This empennage configuration has lower directional stability for sideslip angles less than 8 degrees than that above 8 degrees. These are the characteristics of the fuselage/empennage configuration tested and have been shown also during other model tests. At small sideslip angles the wake from the wing/fuselage intersection reduces the dynamic pressure at the base of the fin. At higher sideslip angles, the fin is in the free stream which provides increased stability.

4. Rotor Performance

Rotor performance was measured during hover in and out of ground effect, helicopter, conversion, and airplane flight. Data presented in Figures VI-46 through VI-56 show the average power coefficient and thrust coefficient of both rotors for the airspeeds tested during a collective pitch sweep.

Figures VI-46 and VI-47 are a comparison of the effect of tunnel wall interference on rotor performance. With the tunnel walls up (open test section) there was a slight increase in power for the same collective pitch setting. Thrust increased for 20 knots and decreased at 40 knots for the same collective pitch setting. Figure VI-49 shows rotor power coefficient in ground effect compared with the faired curve out of ground effect from Figure VI-46. Ground effect was shown not to have an influence on rotor power. Some ground effect on thrust was evident in Figure VI-50. Very little change occurred until the model was at a h/D = .53 or near touchdown.

Rotor performance is summarized at trim attitude for the airspeed and nacelle incidence angles tested in Figures VI-57 and VI-58. The test data are compared with estimated performance using the digital flight simulation program. Pretest estimates were made using linearized rotor wake

4. (Continued)

theory. Post-test estimates are made using rotor wake effects based on tunnel test results. The primary differences between these two methods are the trim angle of attack and wing downloading. Pretest estimates were used to set the model trim attitude; therefore, comparisons made with post-test estimates are not necessarily at the same angle of attack.

Preliminary analysis made between tunnel entries indicated differences between estimated and test. As a result, improvements were made to the rotor data tables in one of the digital simulation programs (C81). The tilt rotor simulation program used in post-test estimates has been shown to be in agreement with the full-scale wind tunnel rotor test. In order to use the tilt rotor digital simulation program, a change was required to make fuselage drag and blade twist at the three quarter radius input parameters. As shown in Figures VI-57 and VI-58, the post-test estimates for power coefficients are in closer agreement with test than pretest estimates. Both estimates for thrust coefficients were in close agreement with test.

Reynolds number effects on the airframe and rotor were not accounted for in the estimates. These effects were accounted for in the analysis of data from Reference 2 and indicated that closer agreement could be obtained between estimated and test. Because of time, this was not included in this analysis since these effects were previously established.

5. Rotor Flapping

Rotor flapping angles measured at trim attitude are shown in Figure VI-59 for the airspeed and nacelle incidence angles tested. Total flapping angle measured was similar in magnitude to that measured during the aeroelastic model test. A comparison is shown with post-test estimated fore/aft and lateral flapping angles.

Rotor lateral flapping for low speed helicopter, obtained during both powered model tests, was higher than originally estimated. This was found to be the result of the induced velocity representation being used.[2] Pretest prediction methods used a triangular distribution of induced velocity which includes a factor to modify the triangular distribution for forward flight. The factor was derived for low disc loading, low twist rotors, and has provided reasonable correlation with such rotors. This factor was revised to reflect the higher disc loading and twist for the tilt rotor resulting in better correlation between estimated and test. These factors are summarized in Reference 5.

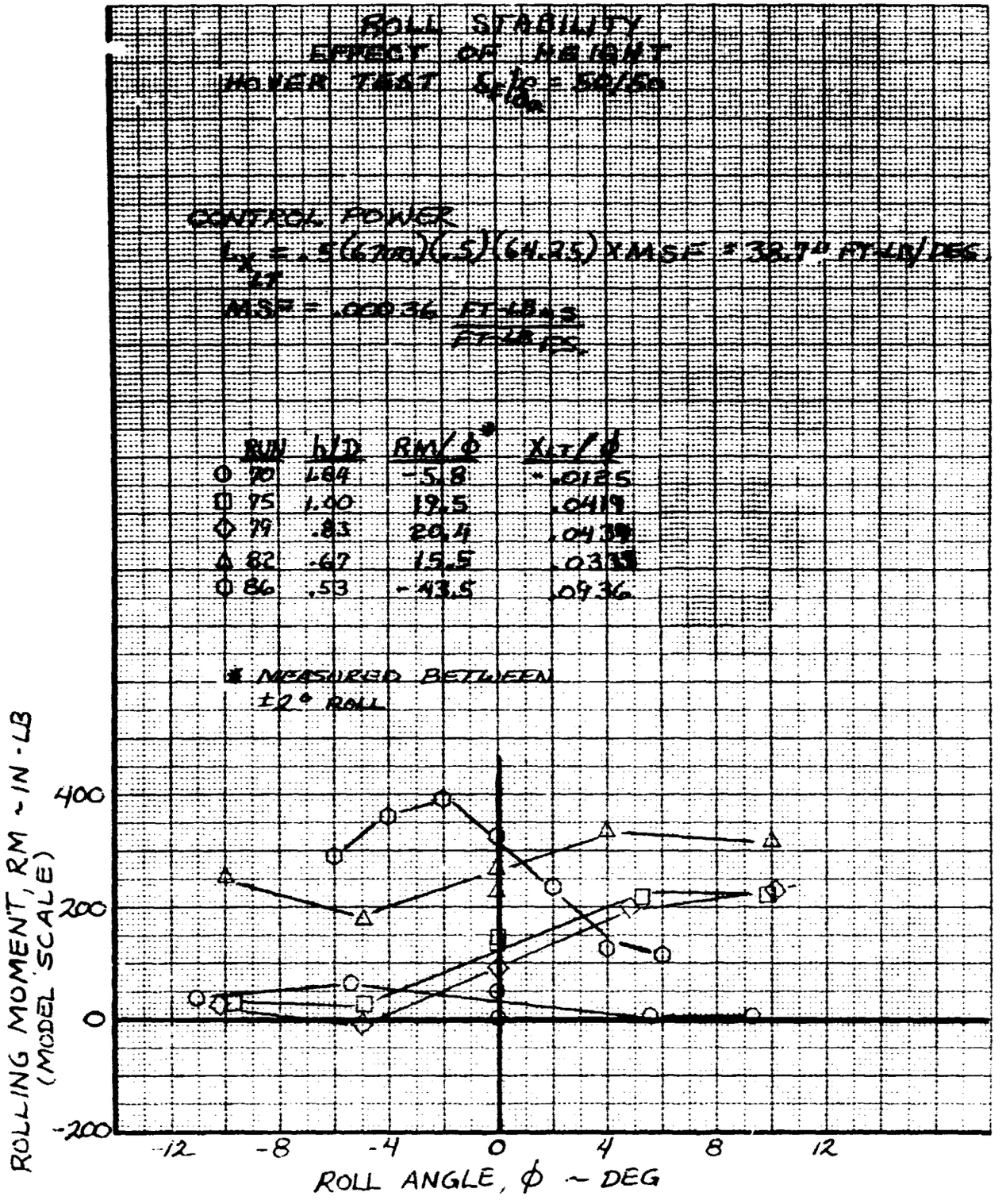

Figure VI-1. Rolling Moment in Hover.

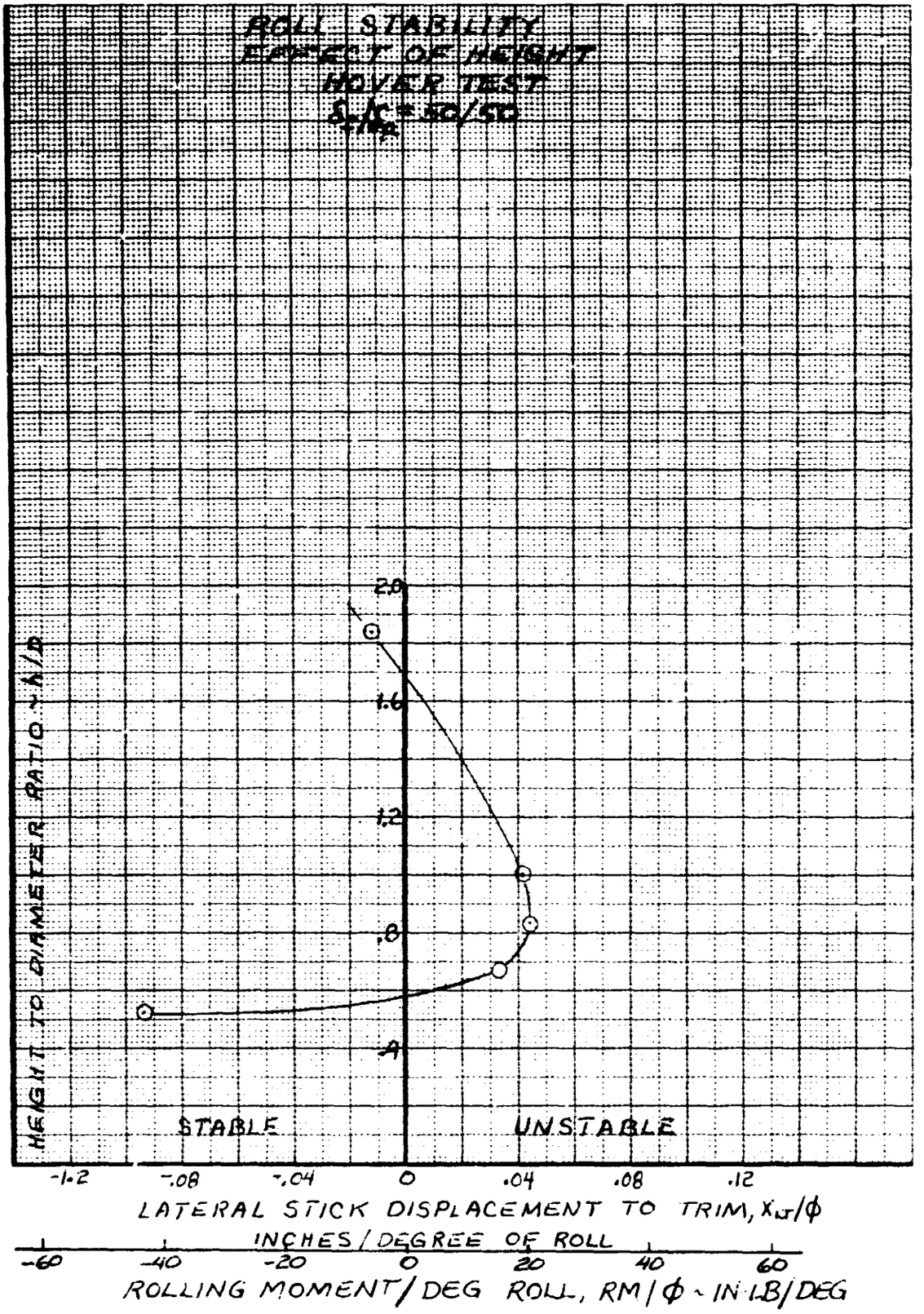

Figure VI-2. Roll Stability Characteristics in Hover.

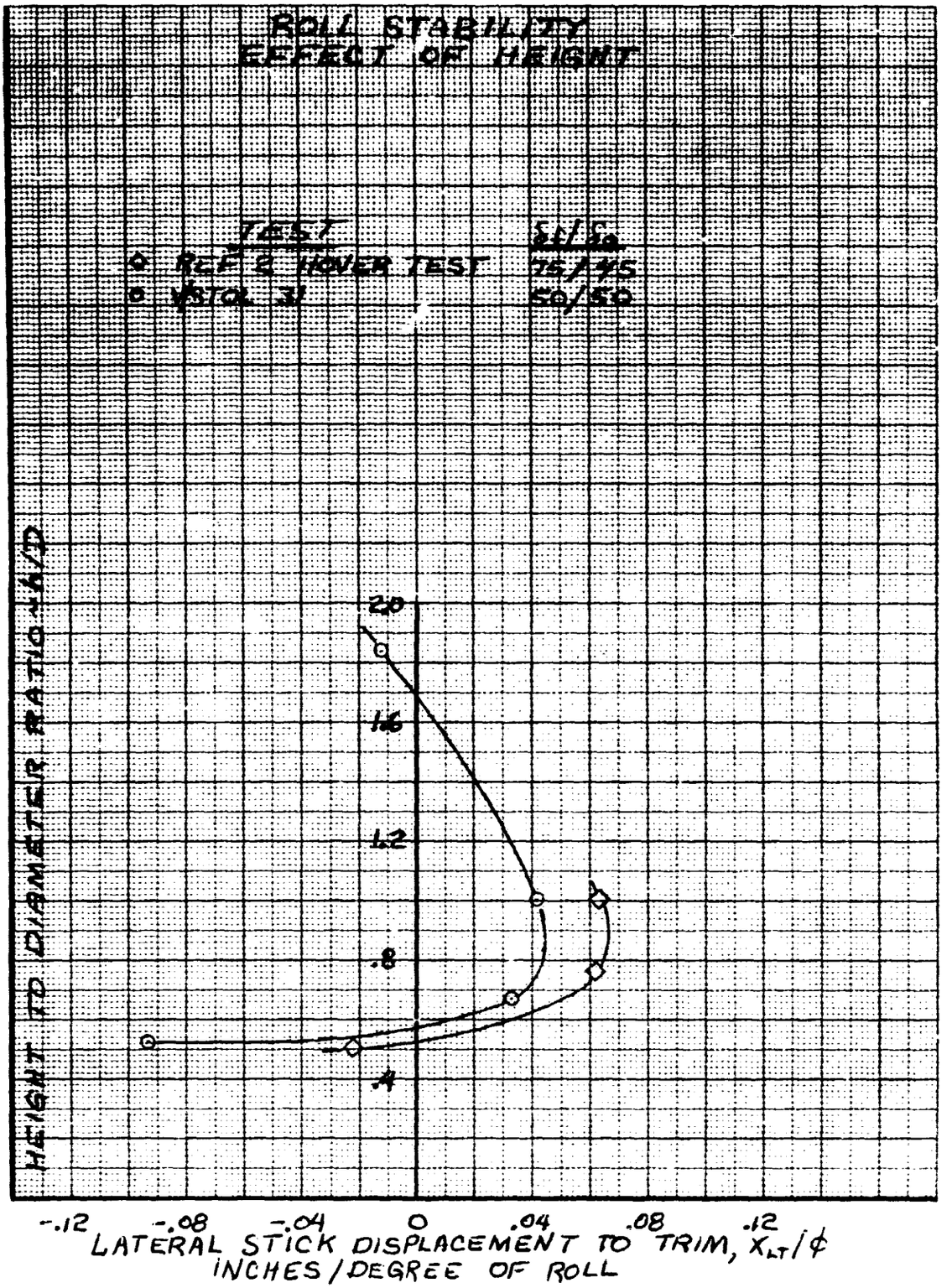

Figure VI-3. Roll Stability Summary in Hover

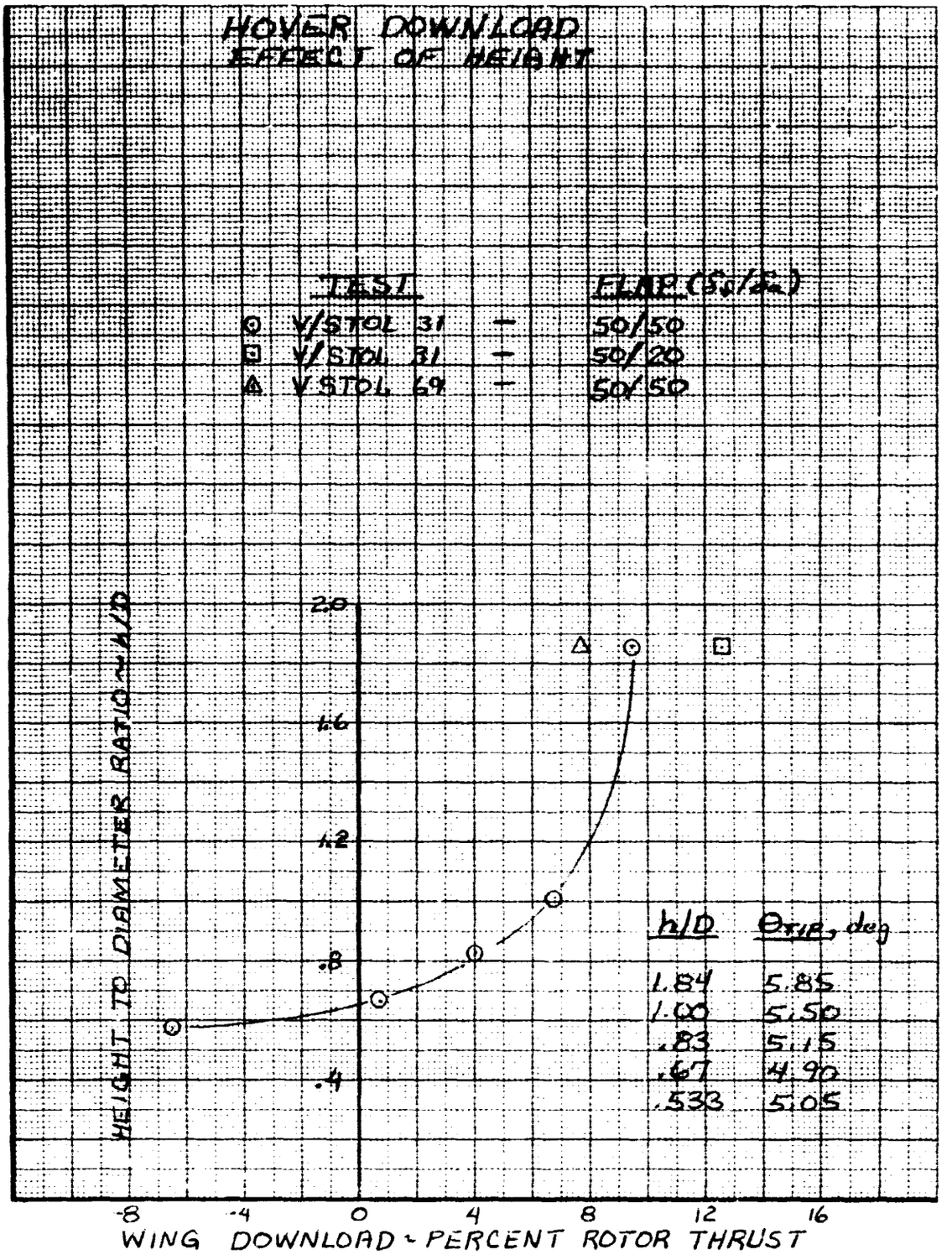

Figure VI-4. Wing Download in Hover

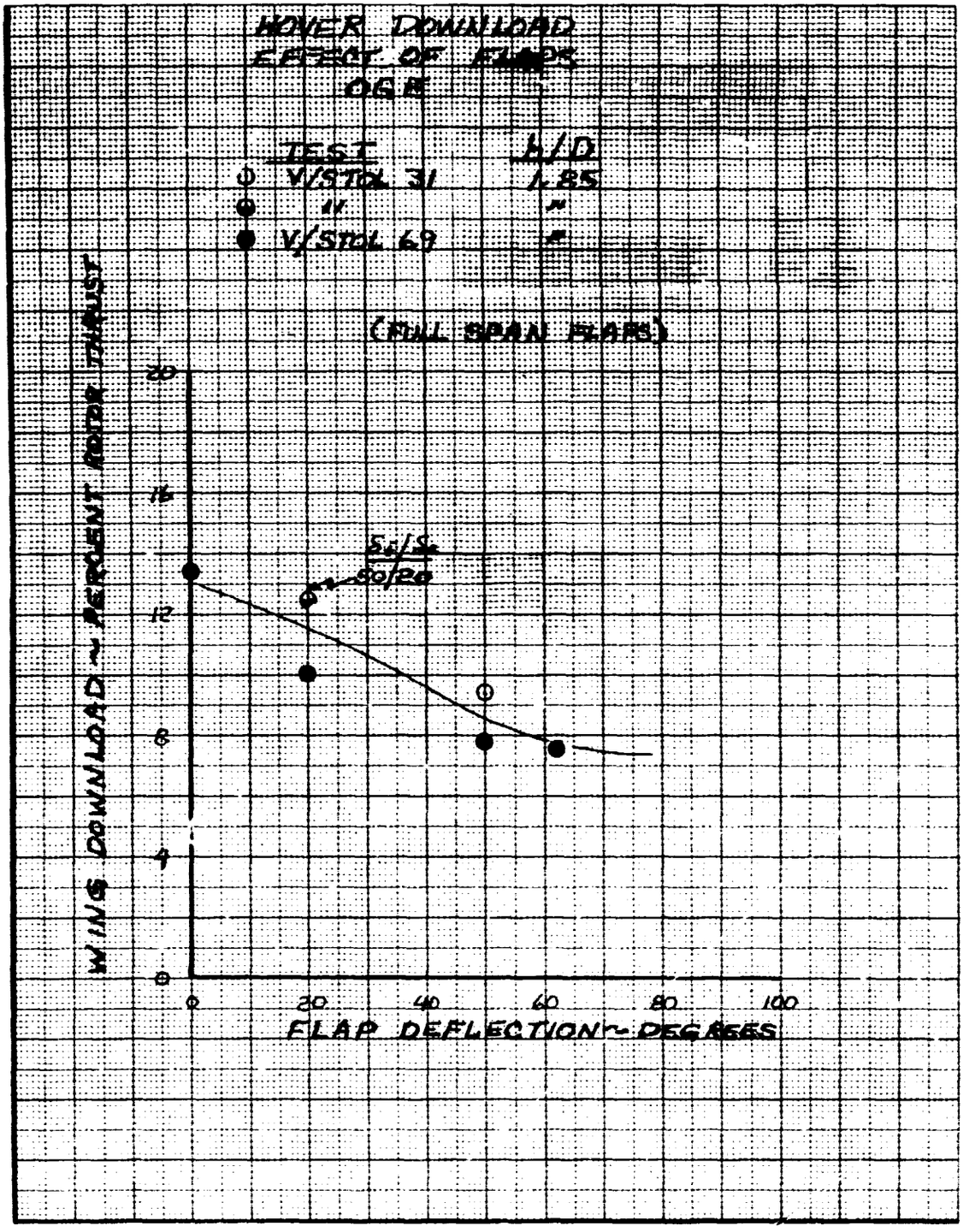

Figure VI-5. Wing Download Variation With Flap Deflection in Hover, OGE.

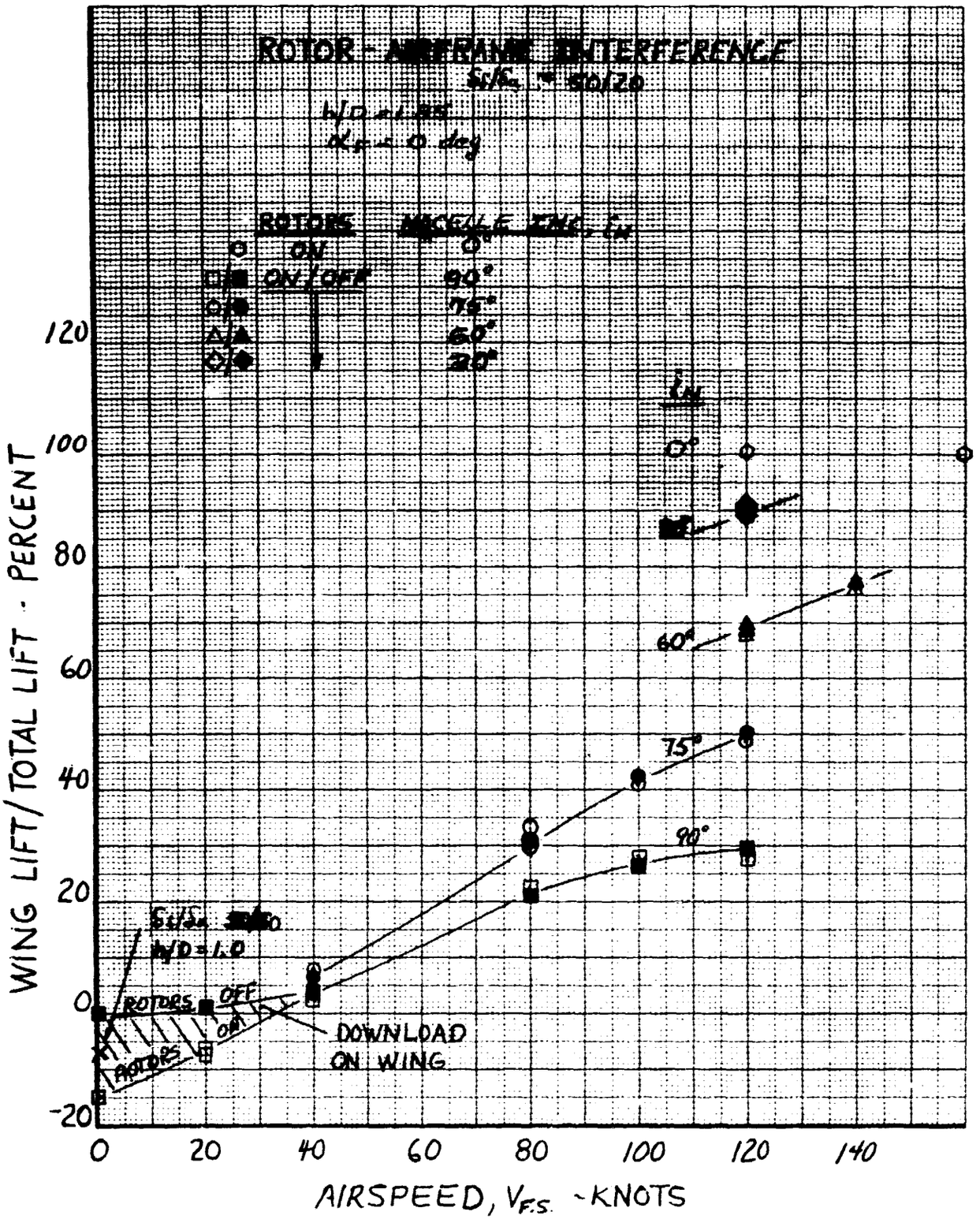

Figure VI-6. Wing Download in Forward Flight, OGE.

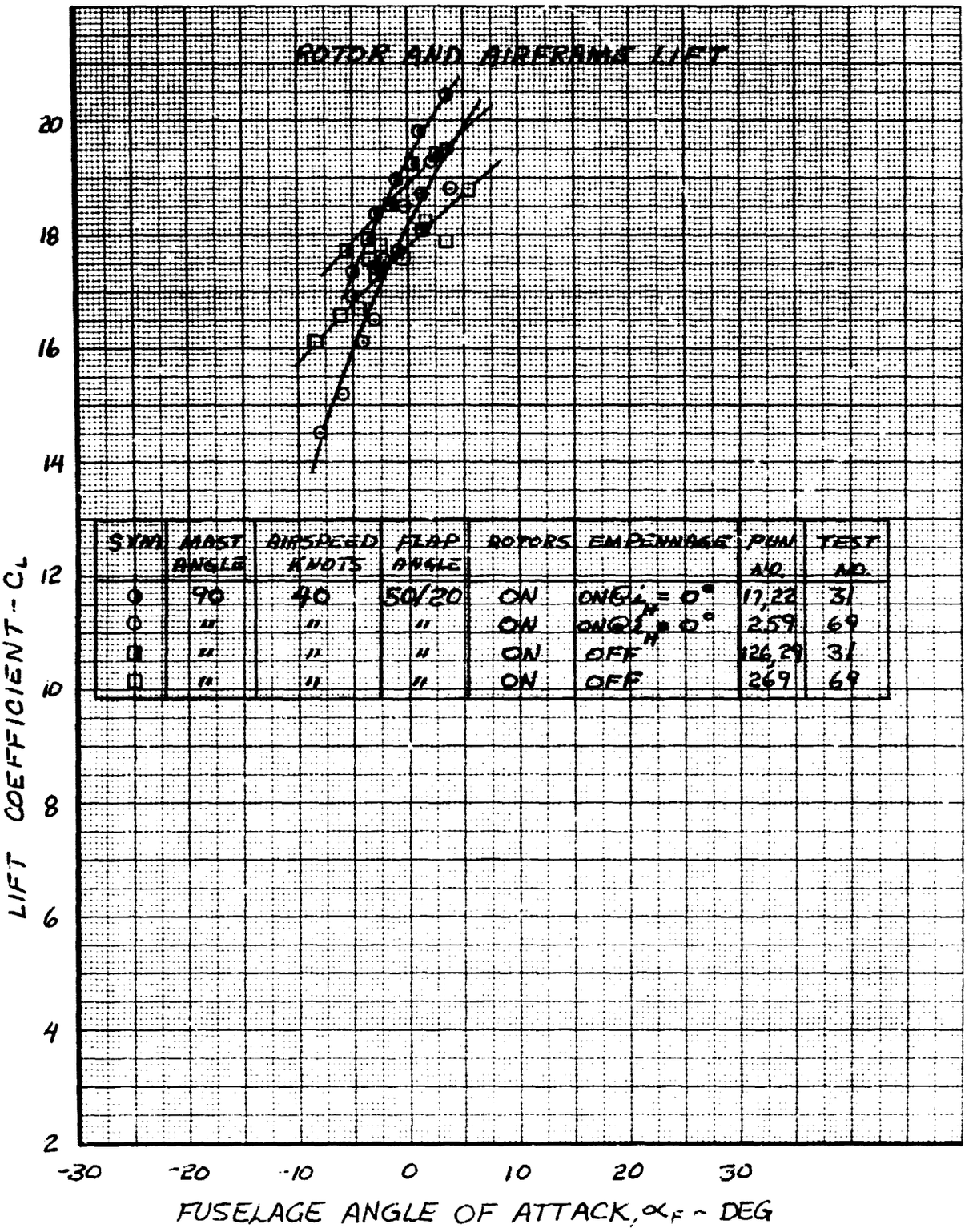

Figure VI-7. Lift Coefficient Versus Fuselage Angle of Attack, Nacelle Incidence 90°, Airspeed 40 Knots.

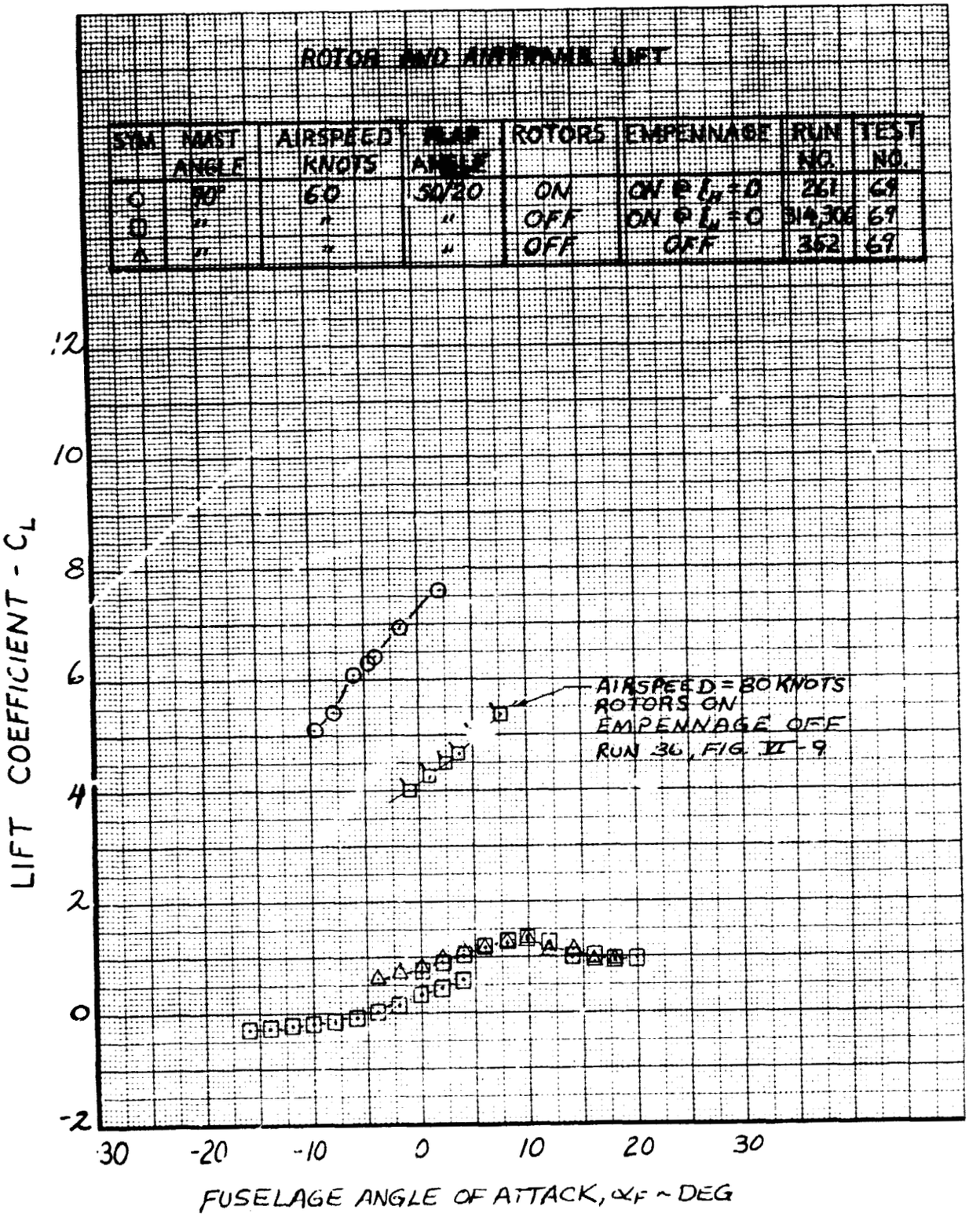

Figure VI-8. Lift Coefficient Versus Fuselage Angle of Attack, Nacelle Incidence 90°, Airspeed 60 Knots.

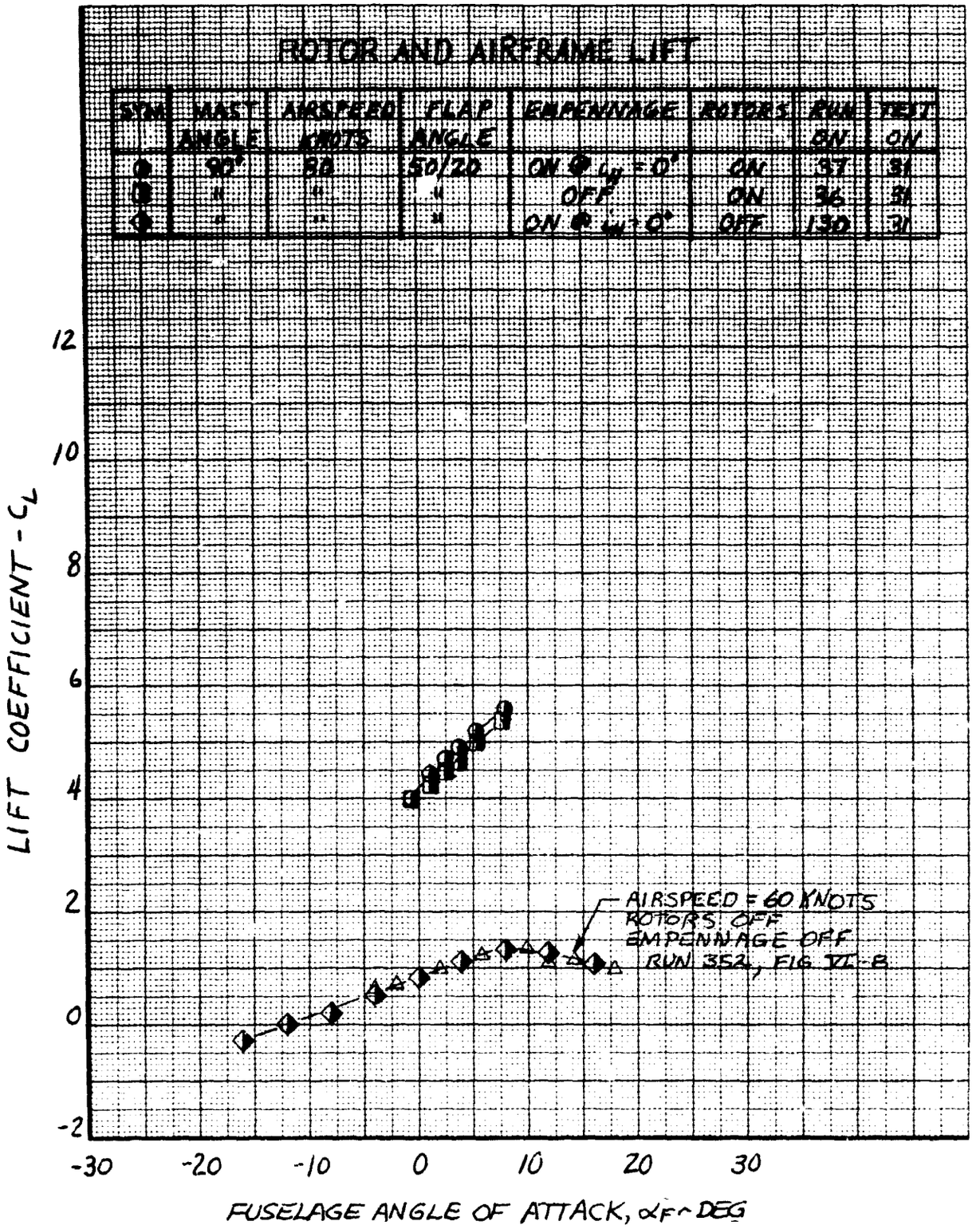

Figure VI-9. Lift Coefficient Versus Fuselage Angle of Attack, Nacelle Incidence 90°, Airspeed 80 Knots.

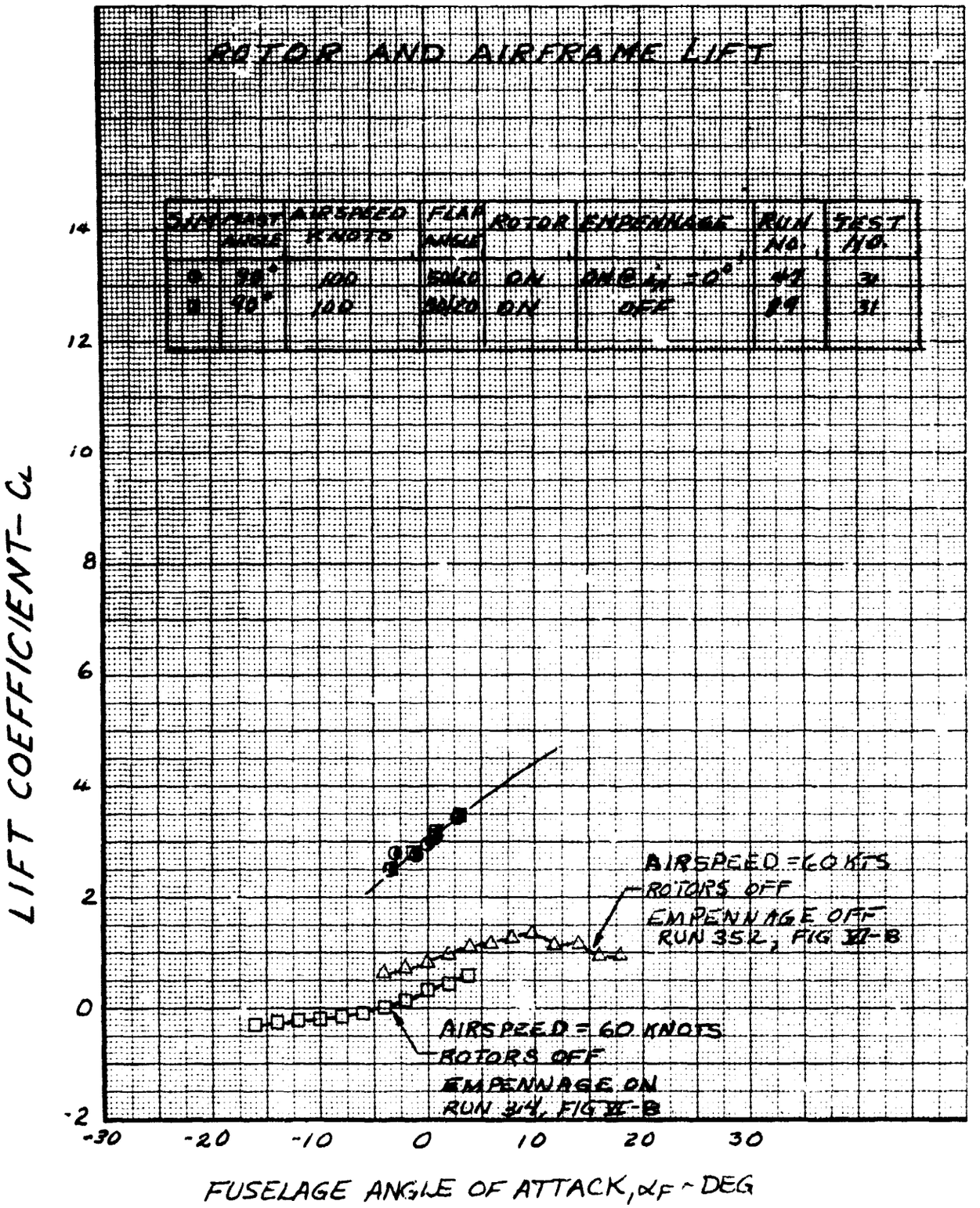

Figure VI-10. Lift Coefficient Versus Fuselage Angle of Attack, Nacelle Incidence 90°, Airspeed 100 Knots.

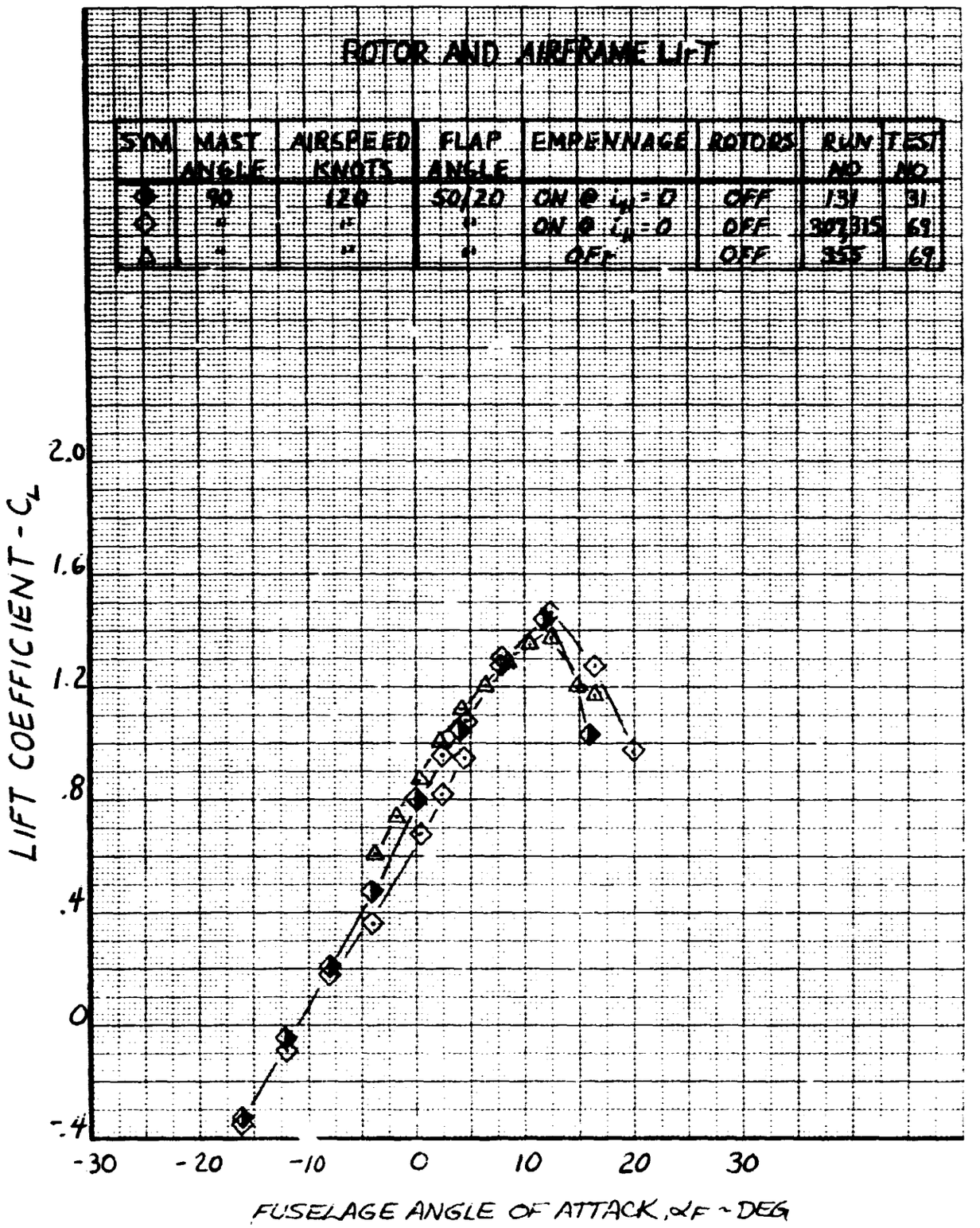

Figure VI-11. Lift Coefficient Versus Fuselage Angle of Attack, Nacelle Incidence 90°, Airspeed 120 Knots.

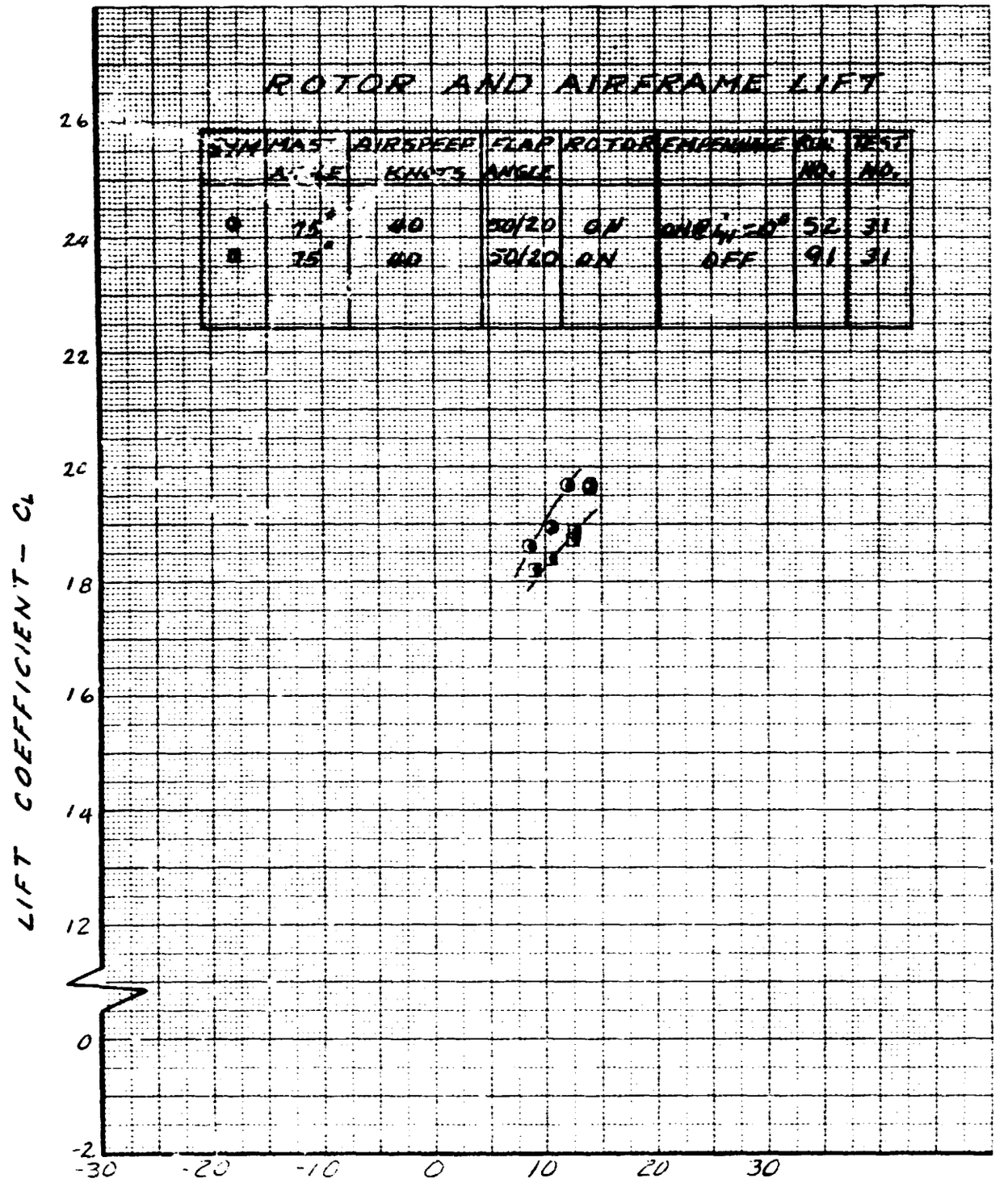

Figure VI-12. Lift Coefficient Versus Fuselage Angle of Attack, Nacelle Incidence 75°. Airspeed 40 Knots.

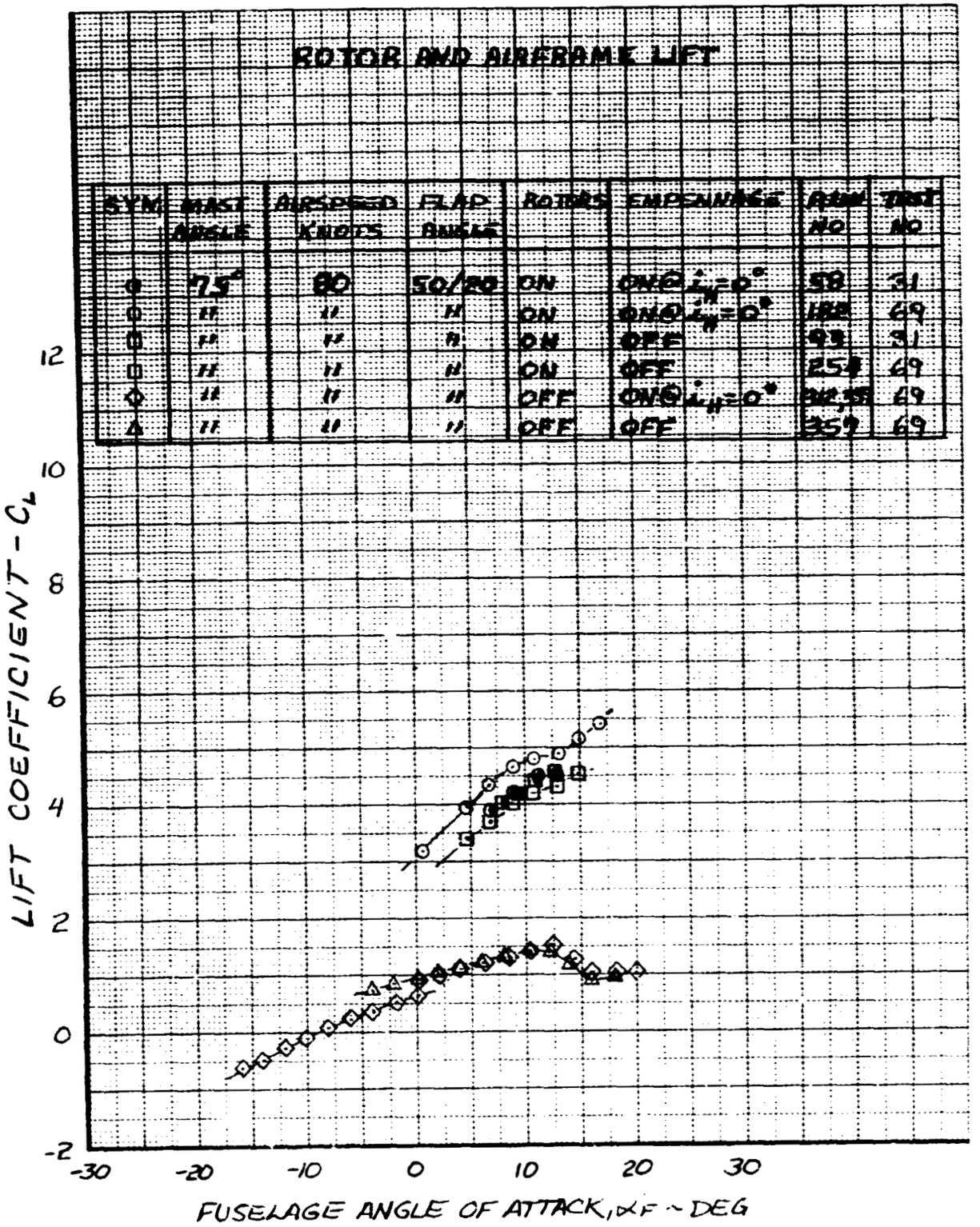

Figure VI-13. Lift Coefficient Versus Fuselage Angle of Attack, Nacelle Incidence 75°, Airspeed 80 Knots.

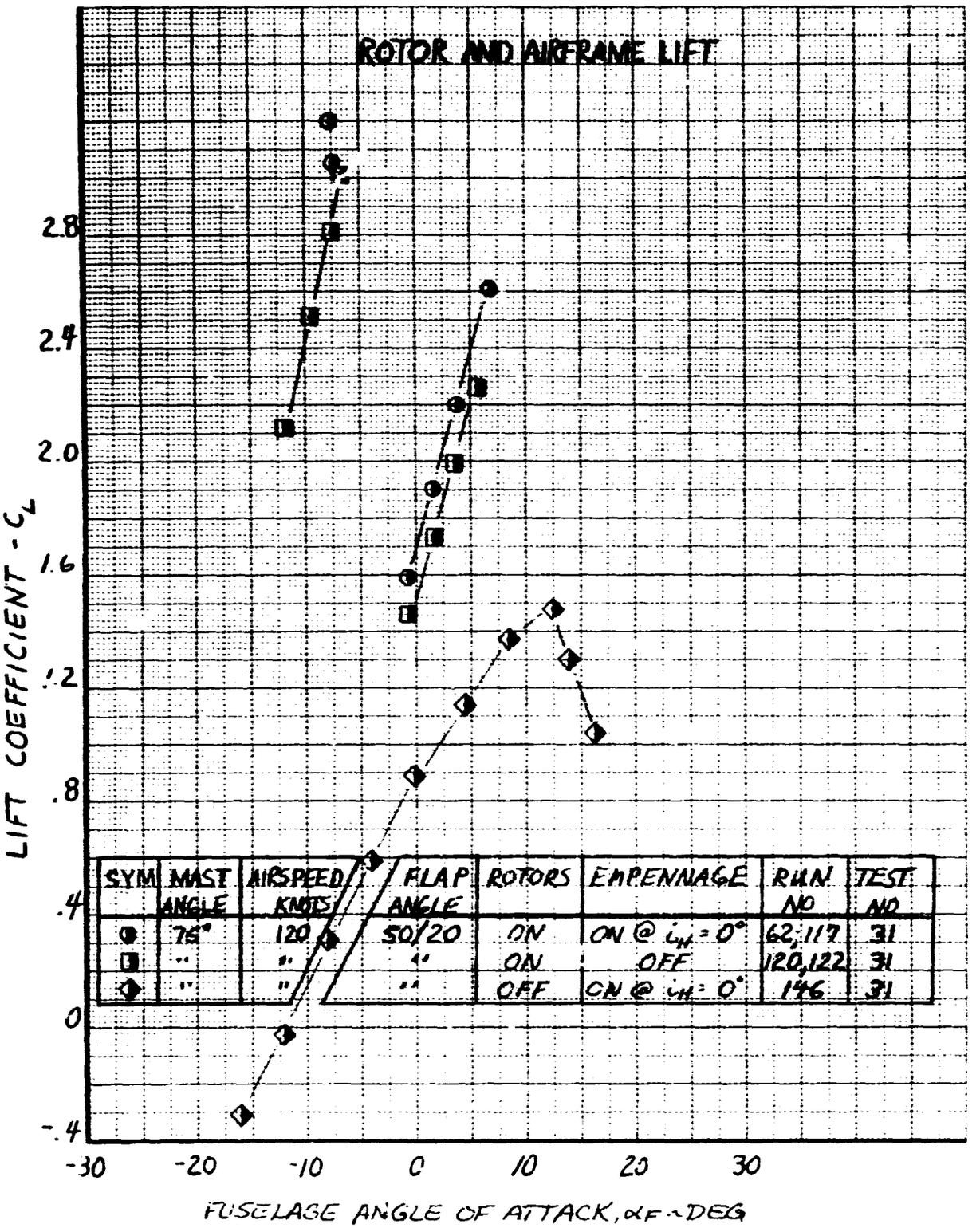

Figure VI-14. Lift Coefficient Versus Fuselage Angle of Attack, Nacelle Incidence 75°, Airspeed 120 Knots.

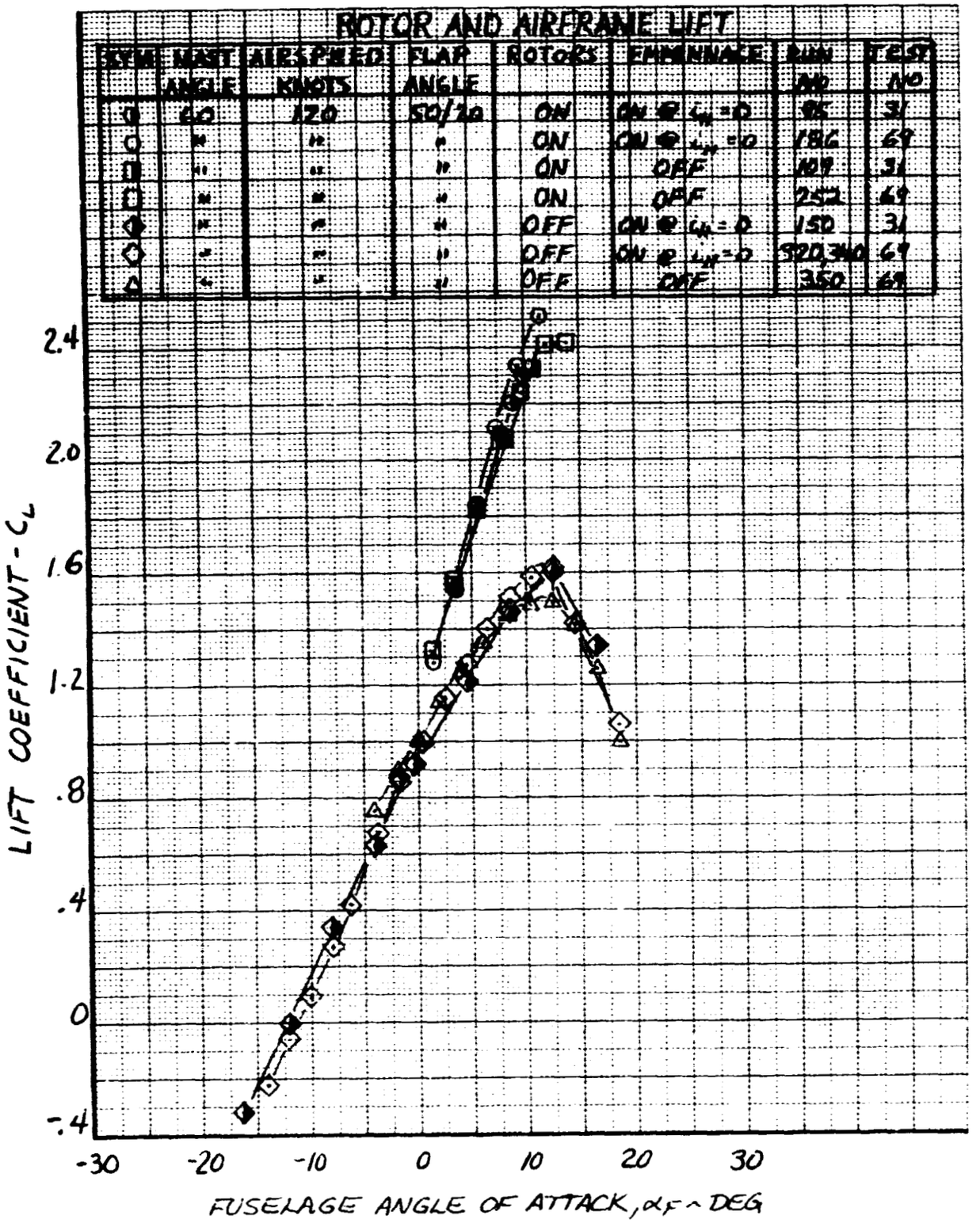

Figure VI-15. Lift Coefficient Versus Fuselage Angle of Attack, Nacelle Incidence 60°, Airspeed 120 Knots.

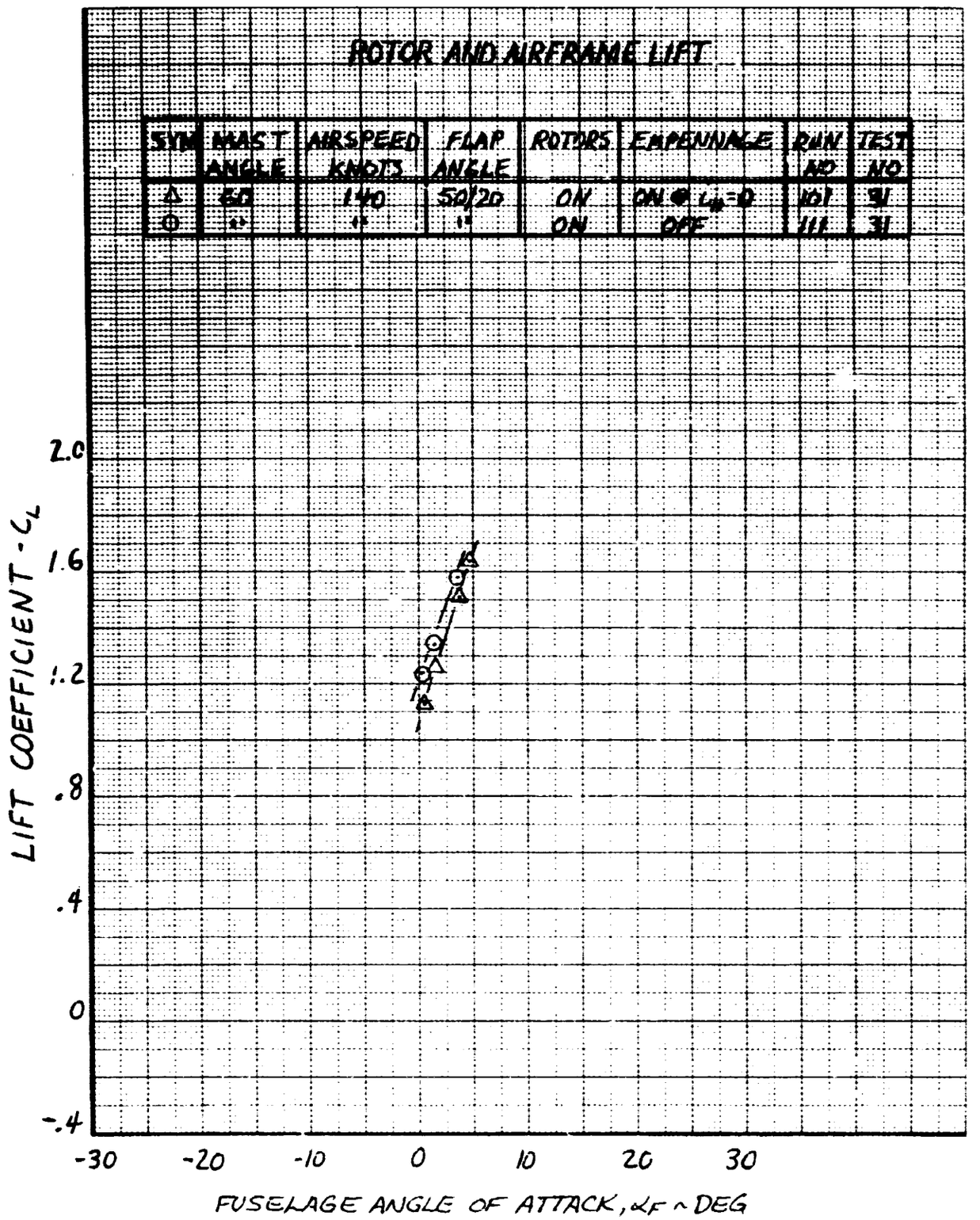

Figure VI-16. Lift Coefficient Versus Fuselage Angle of Attack, Nacelle Incidence 60°, Airspeed 140 Knots.

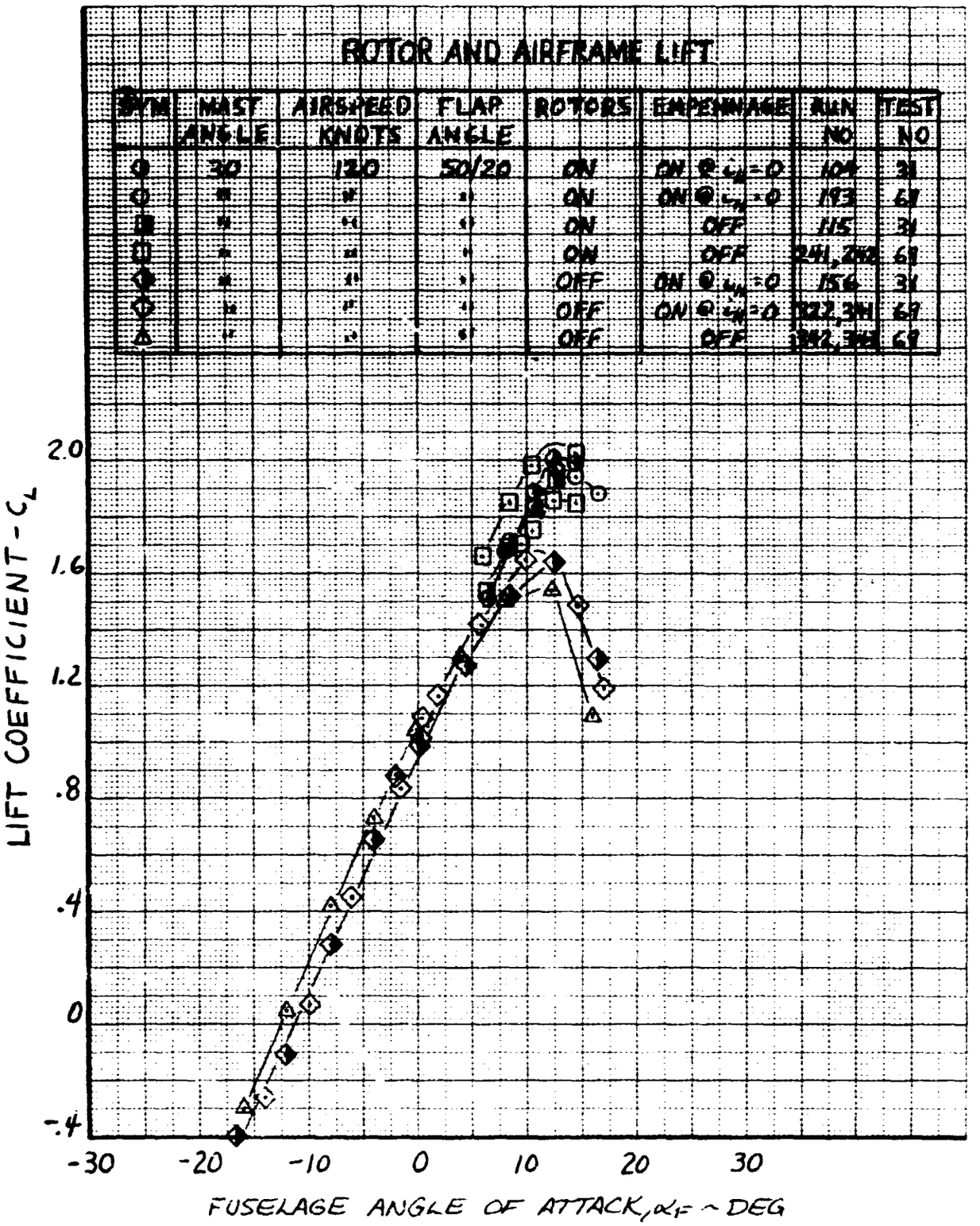

Figure VI-17. Lift Coefficient Versus Fuselage Angle of Attack, Nacelle Incidence 30°, Airspeed 120 Knots.

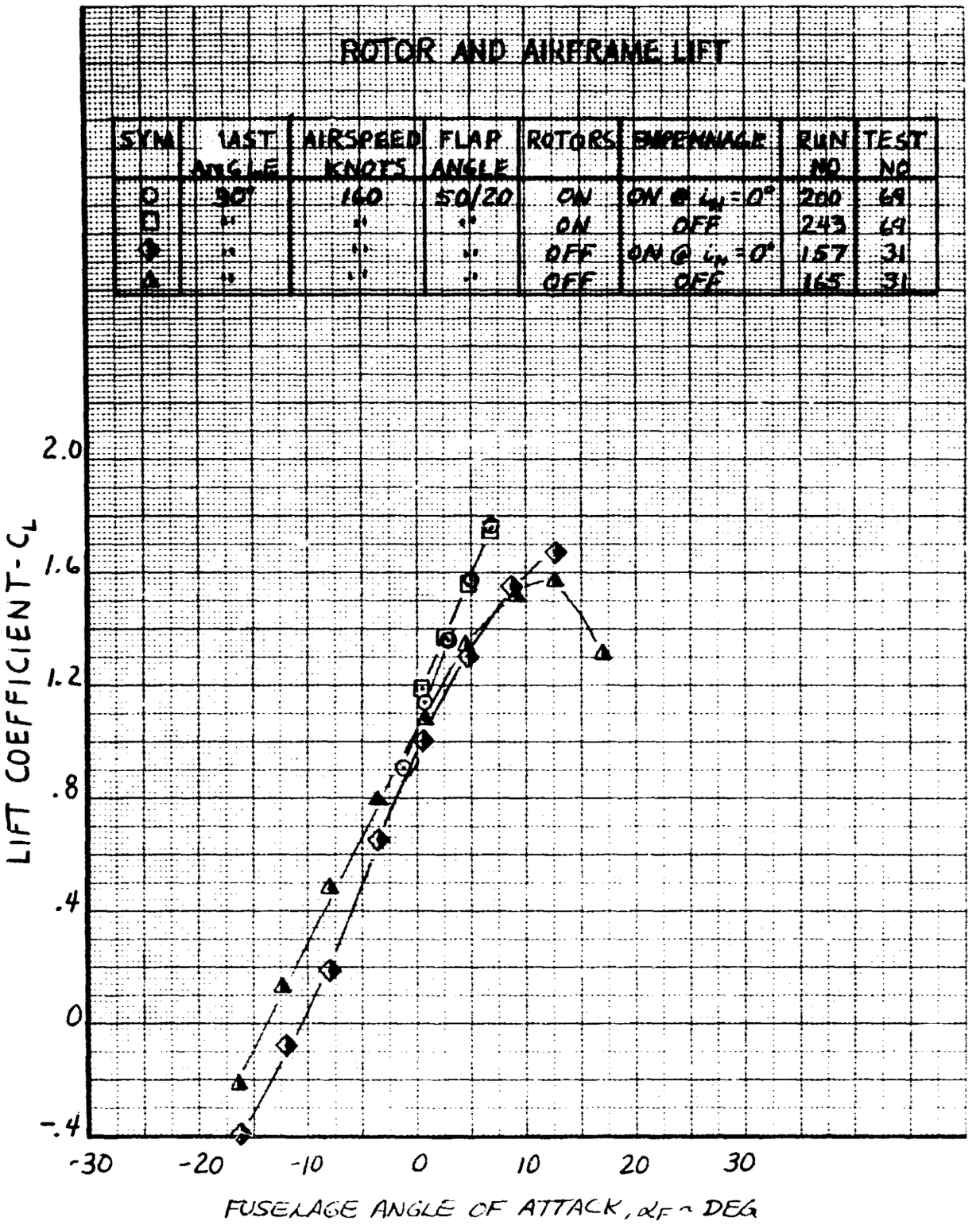

Figure VI-18. Lift Coefficient Versus Fuselage Angle of Attack, Nacelle Incidence 30°, Airspeed 160 Knots.

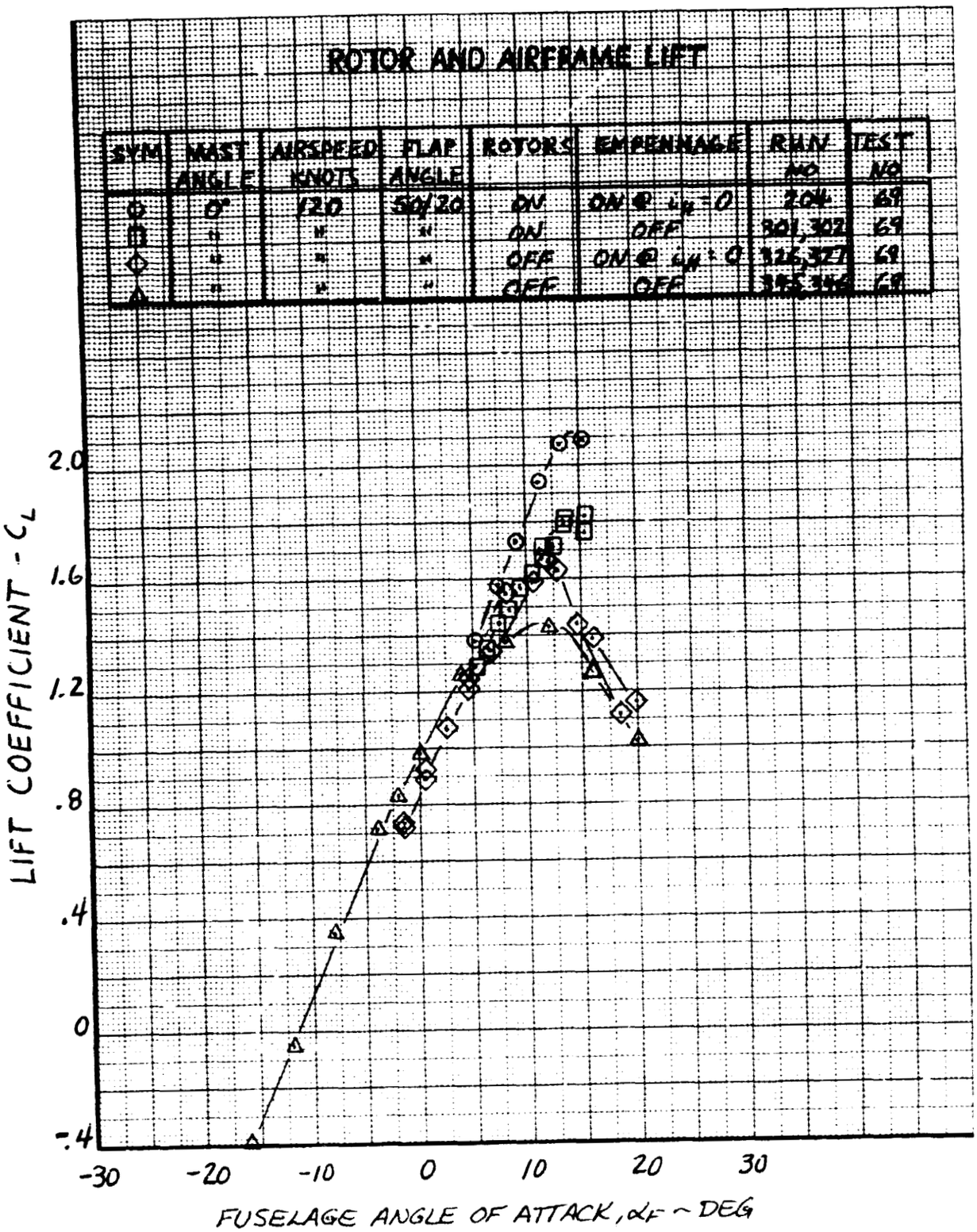

Figure VI-19. Lift Coefficient Versus Fuselage Angle of Attack, Nacelle Incidence 0°, Airspeed 120 Knots.

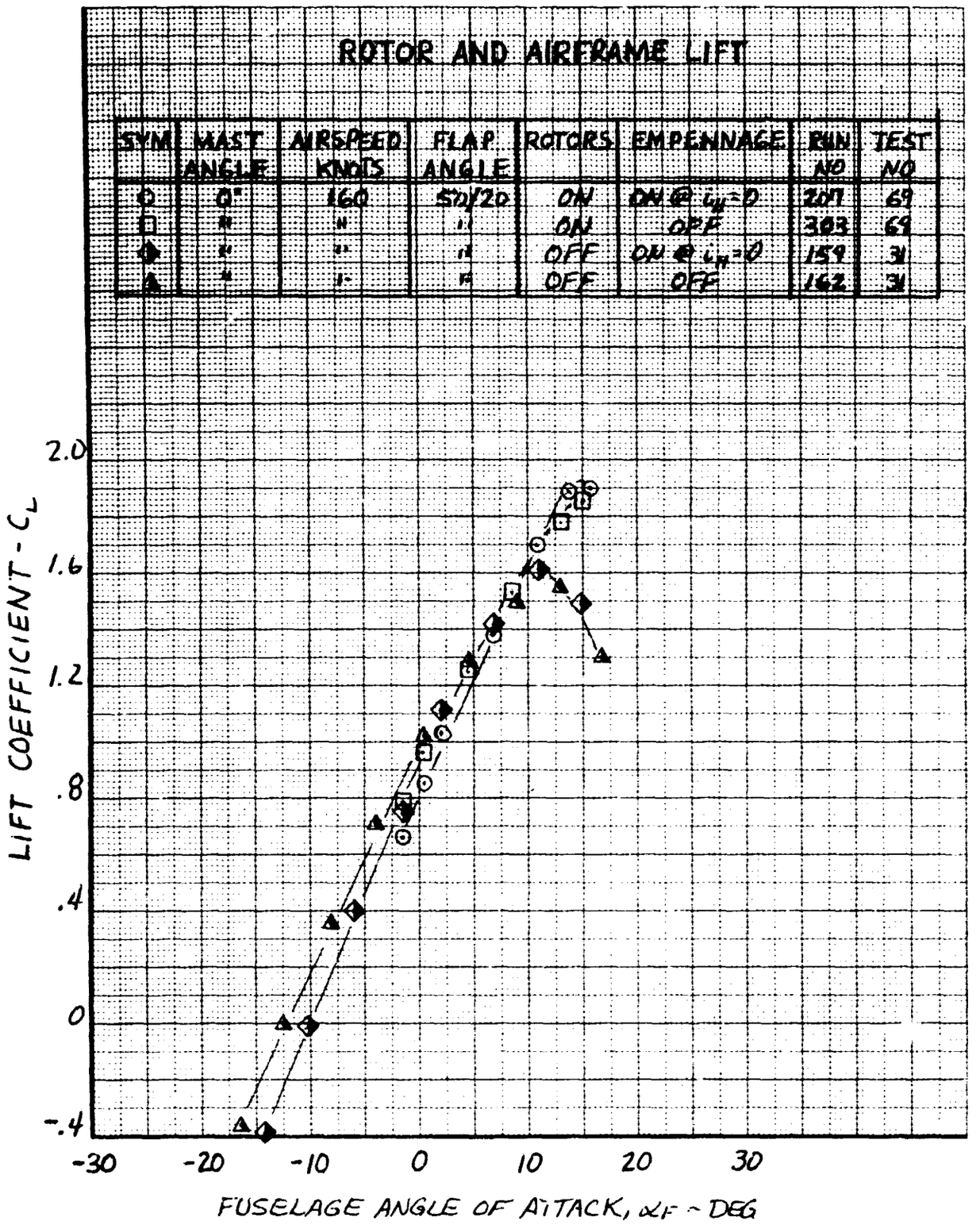

Figure VI-20. Lift Coefficient Versus Fuselage Angle of Attack, Nacelle Incidence 0°, Airspeed 160 Knots.

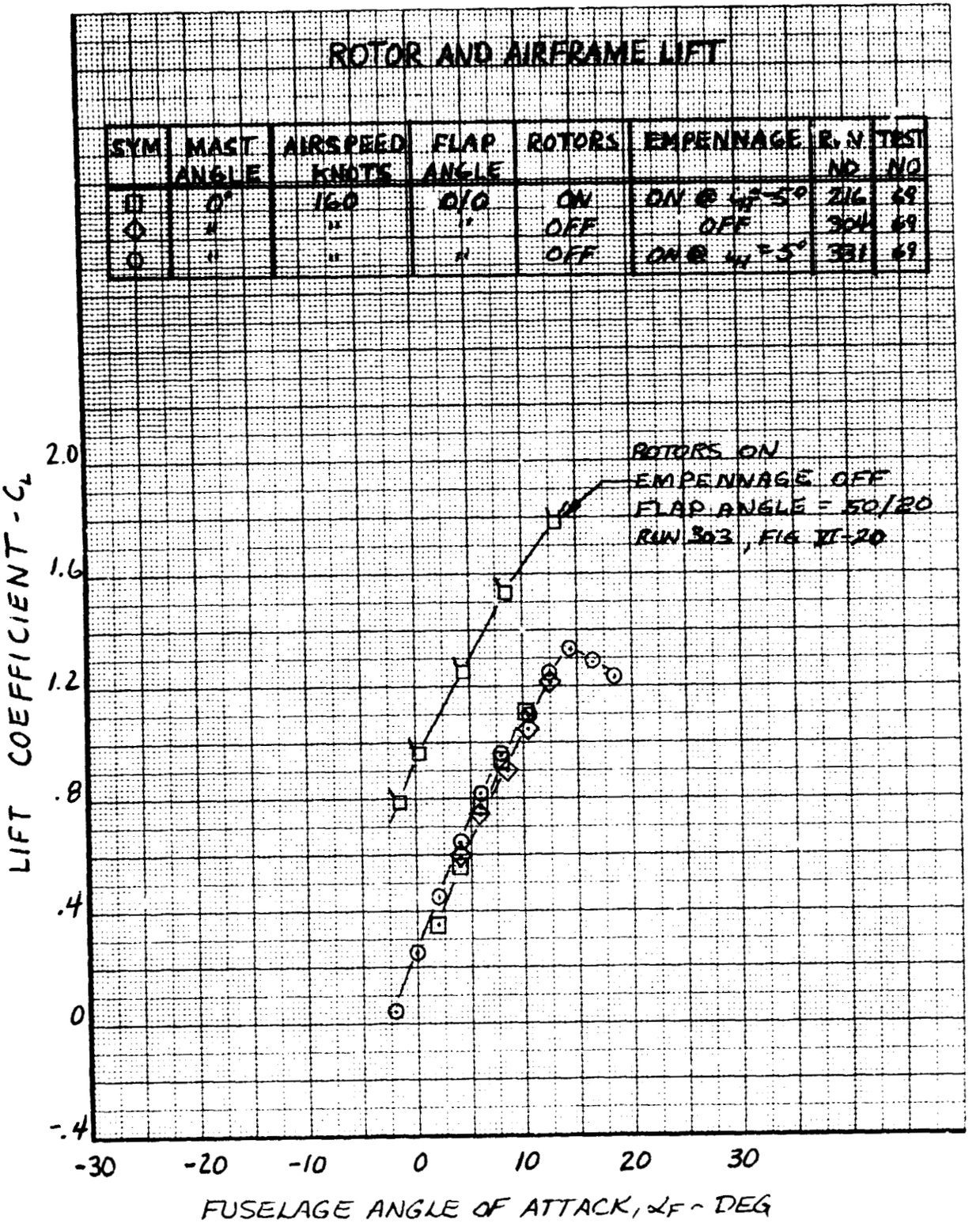

Figure VI-21. Lift Coefficient Versus Fuselage Angle of Attack, Nacelle Incidence 0^o, Airspeed 160 Knots.

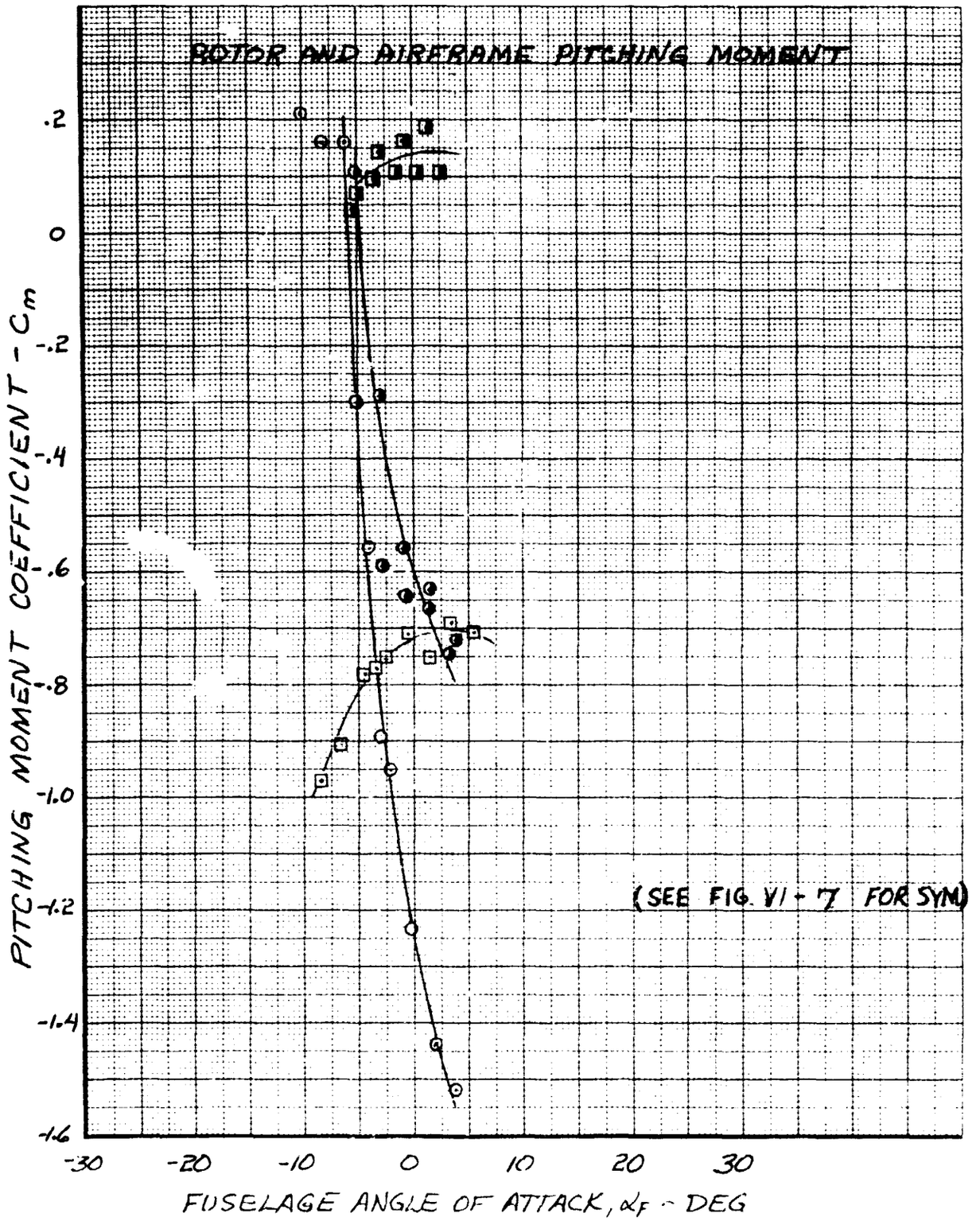

Figure VI-22. Pitching Moment Versus Fuselage Angle of Attack, Nacelle Incidence 90°, Airspeed 40 Knots.

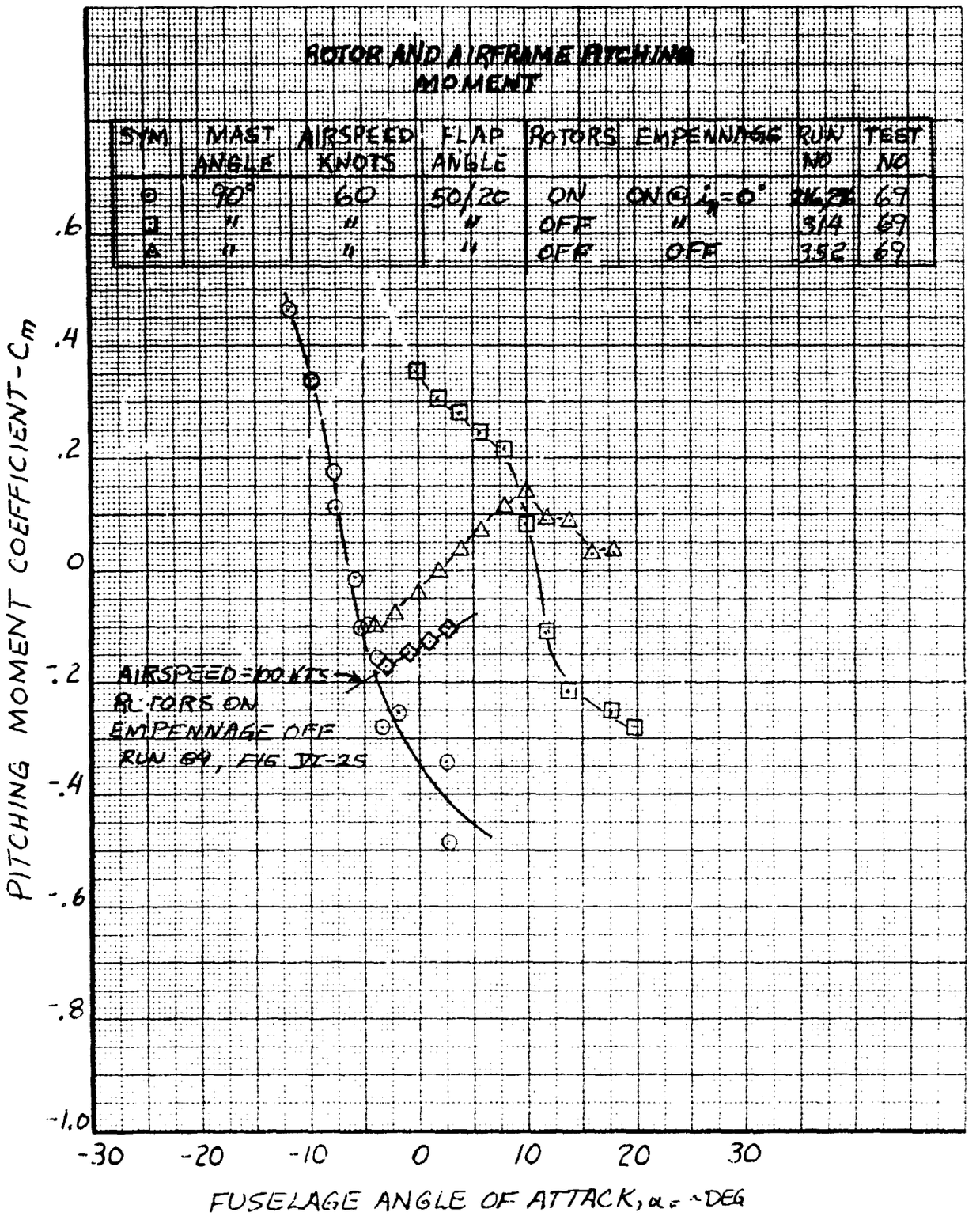

Figure VI-23. Pitching Moment Versus Fuselage Angle of Attack, Nacelle Incidence 90°, Airspeed 60 Knots.

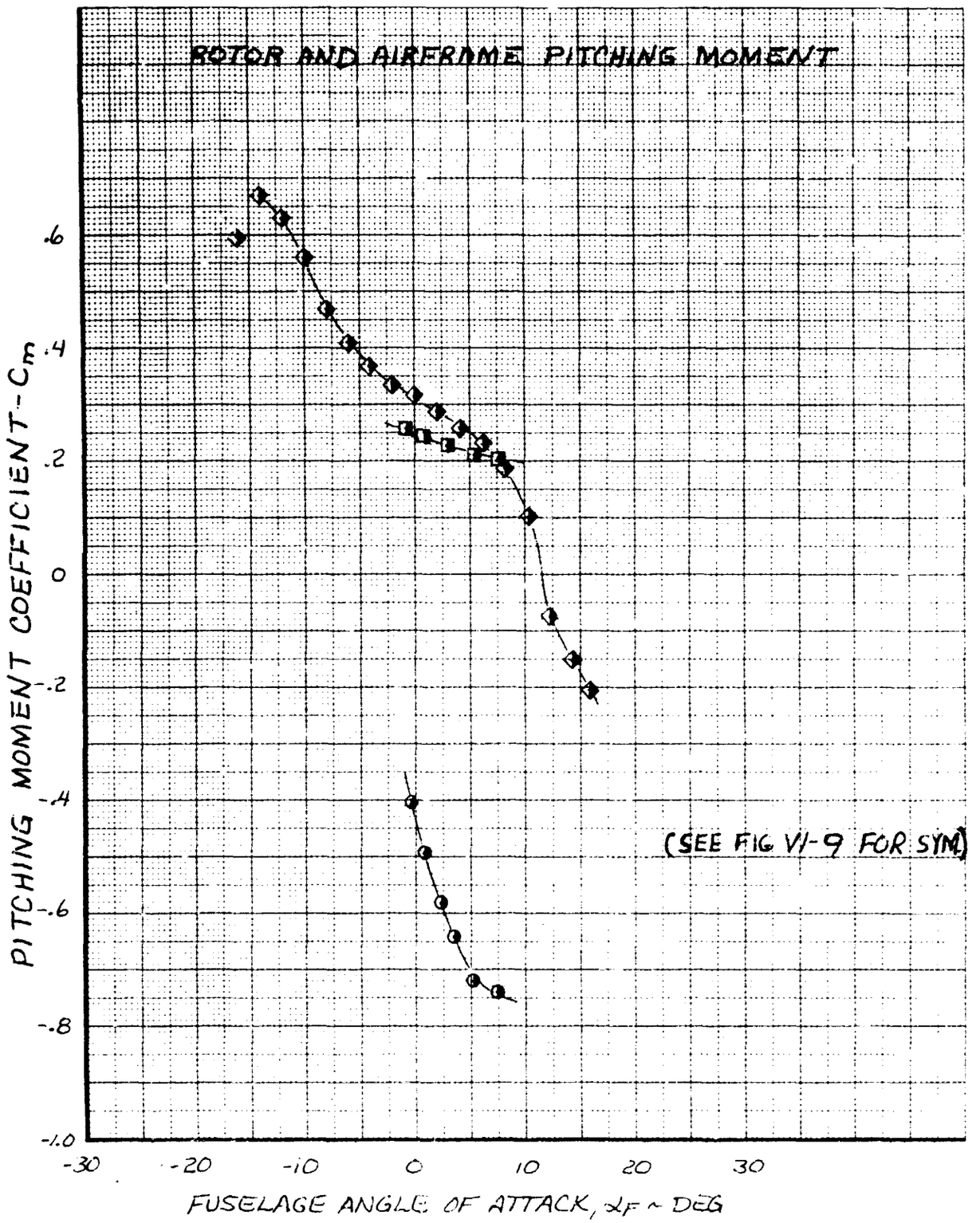

Figure VI-24. Pitching Moment Versus Fuselage Angle of Attack, Nacelle Incidence 90°, Airspeed 80 Knots.

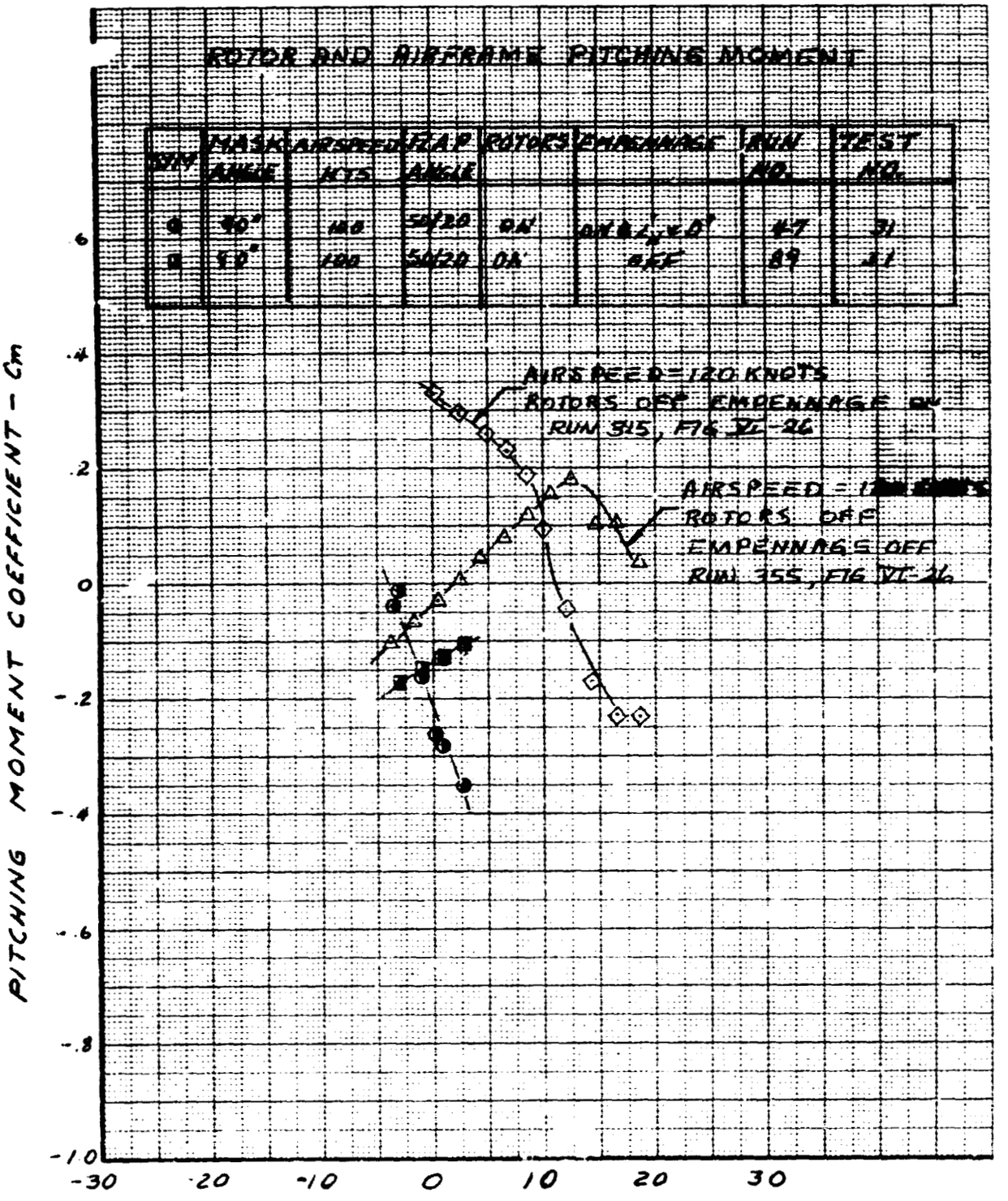

Figure VI-25. Pitching Moment Versus Fuselage Angle of Attack, Nacelle Incidence 90°, Airspeed 100 Knots.

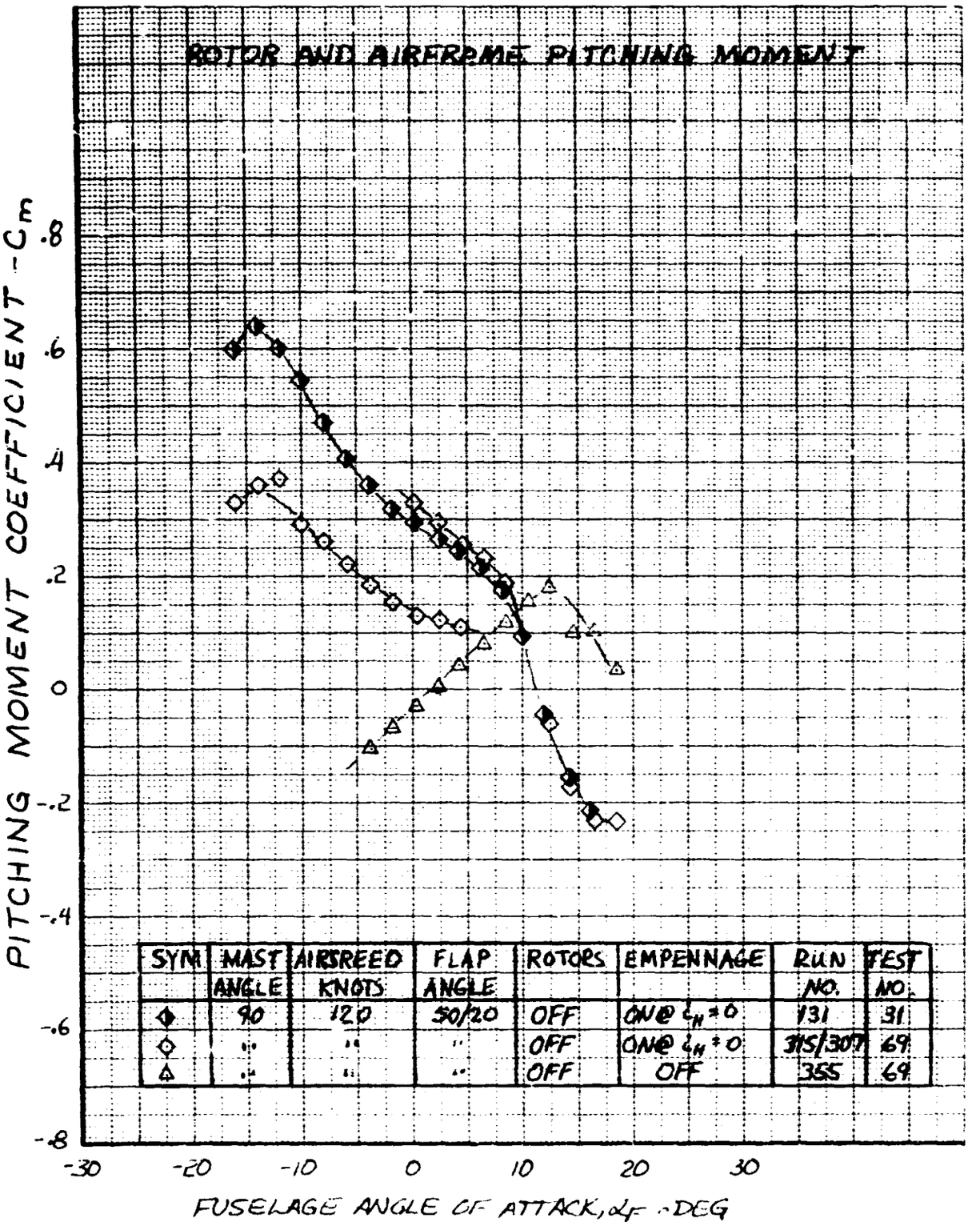

Figure VI-26. Pitching Moment Versus Fuselage Angle of Attack, Nacelle Incidence 90°, Airspeed 120 Knots.

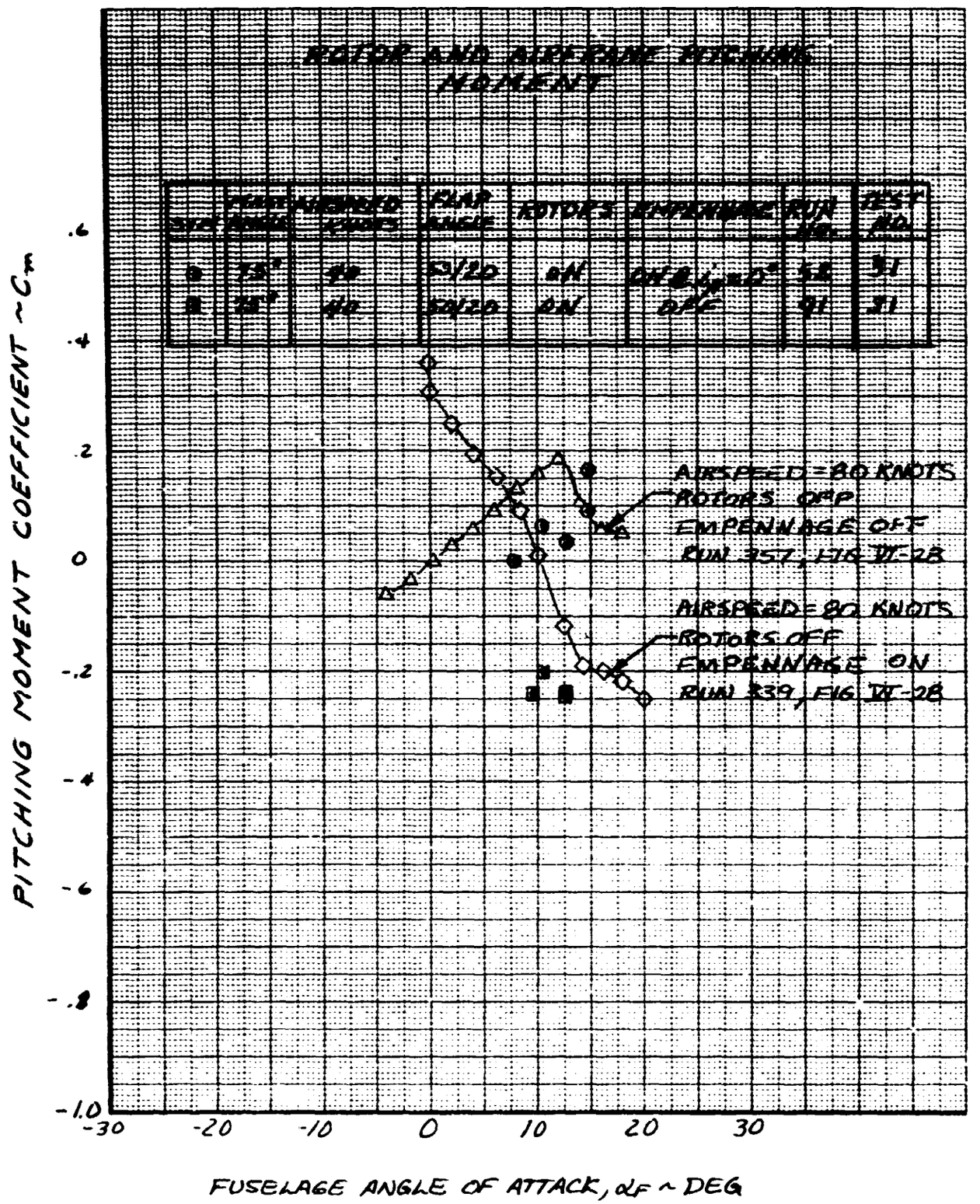

Figure VI-27. Pitching Moment Versus Fuselage Angle of Attack, Nacelle Incidence 75°, Airspeed 40 Knots.

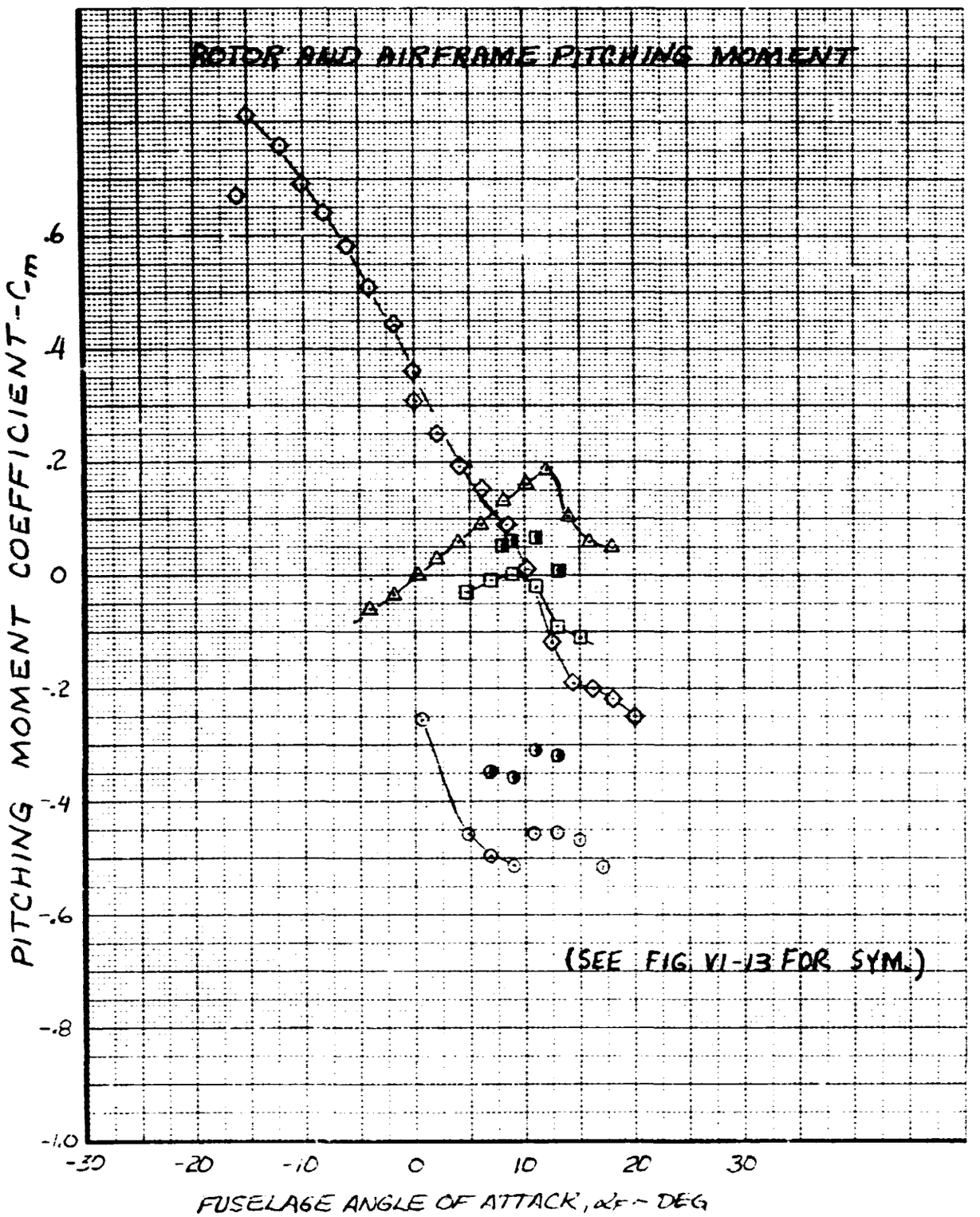

Figure VI-28. Pitching Moment Versus Fuselage Angle of Attack. Nacelle Incidence 75°, Airspeed 80 Knots.

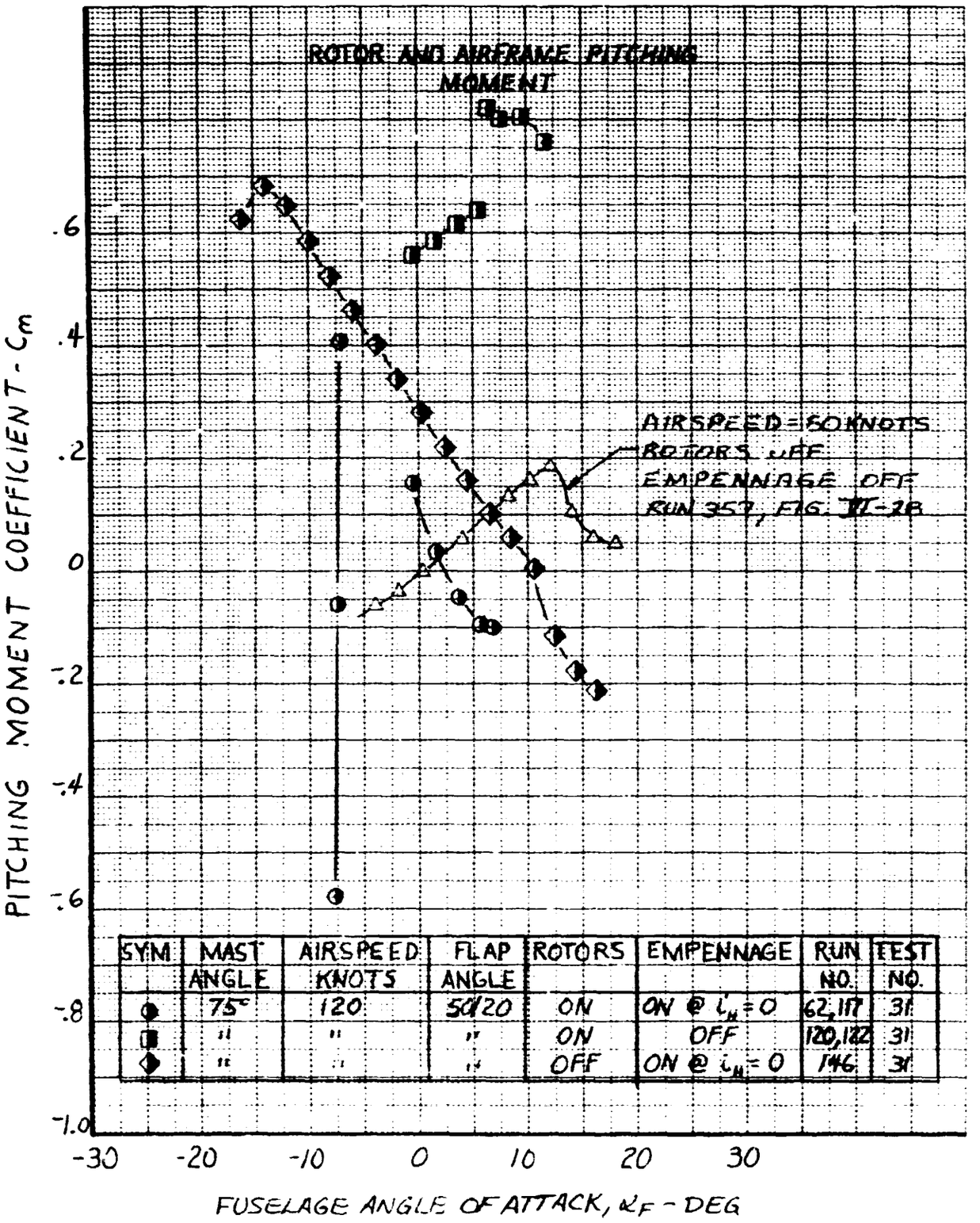

SYM	MAST ANGLE	AIRSPEED KNOTS	FLAP ANGLE	ROTORS	EMPENNAGE	RUN NO.	TEST NO.
●	75°	120	50/20	ON	ON @ $i_H = 0$	62, 117	31
■	"	"	"	ON	OFF	120, 122	31
◆	"	"	"	OFF	ON @ $i_H = 0$	146	31

Figure VI-29. Pitching Moment Versus Fuselage Angle of Attack. Nacelle Incidence 75°. Airspeed 120 Knots.

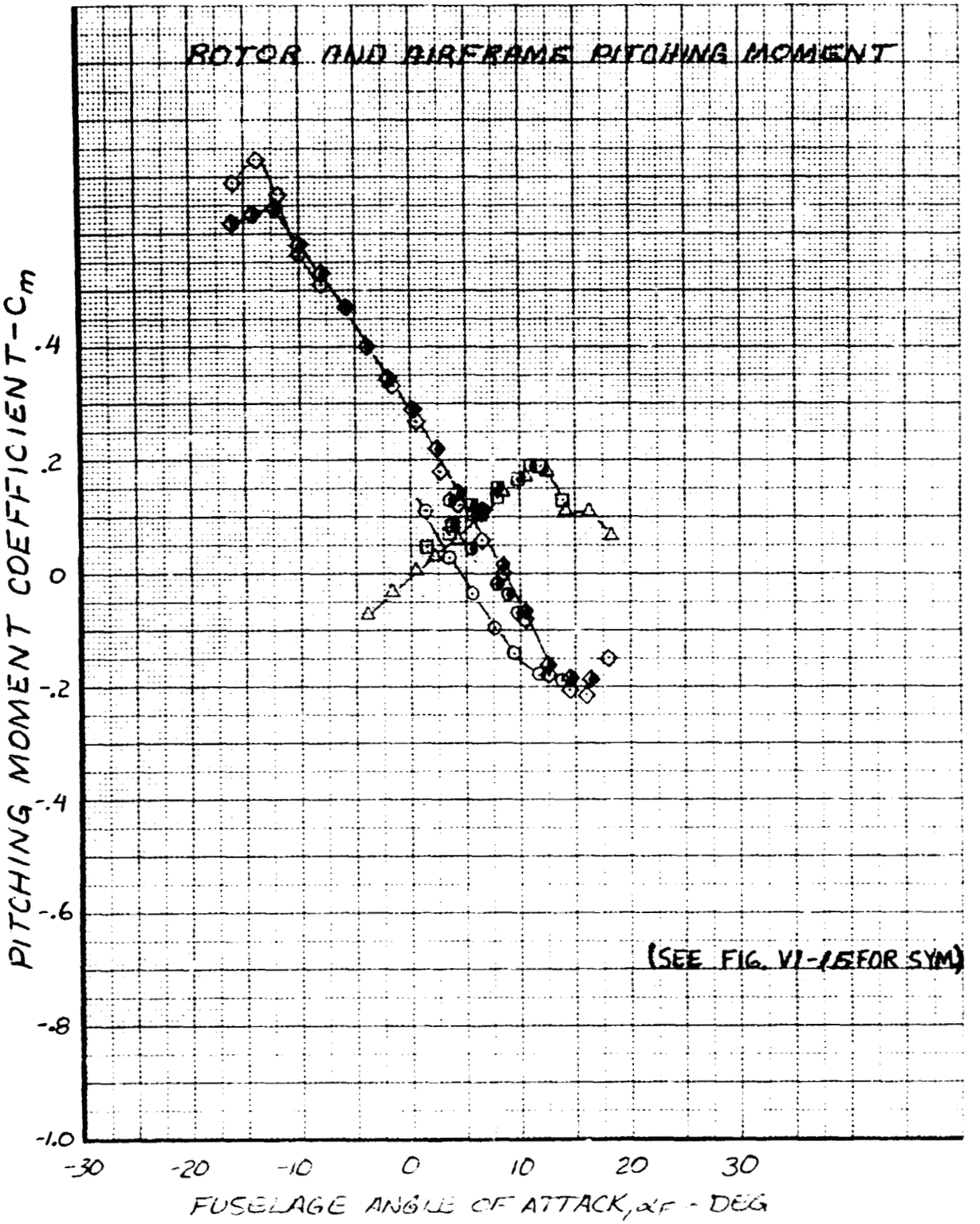

Figure VI-30. Pitching Moment Versus Fuselage Angle of Attack, Nacelle Incidence 60°. Airspeed 120 Knots.

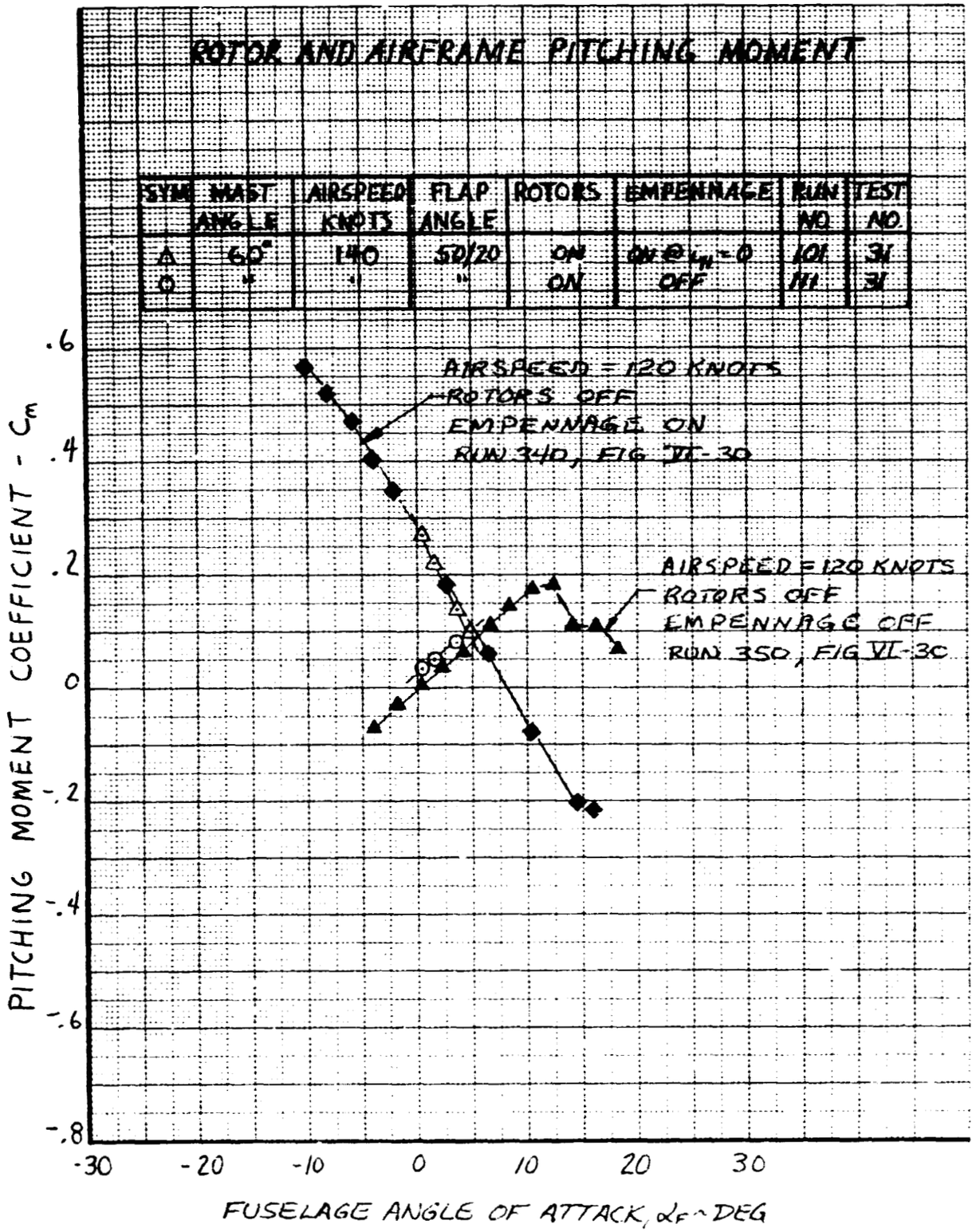

Figure VI-31. Pitching Moment Versus Fuselage Angle of Attack, Nacelle Incidence 60°. Airspeed 140 Knots.

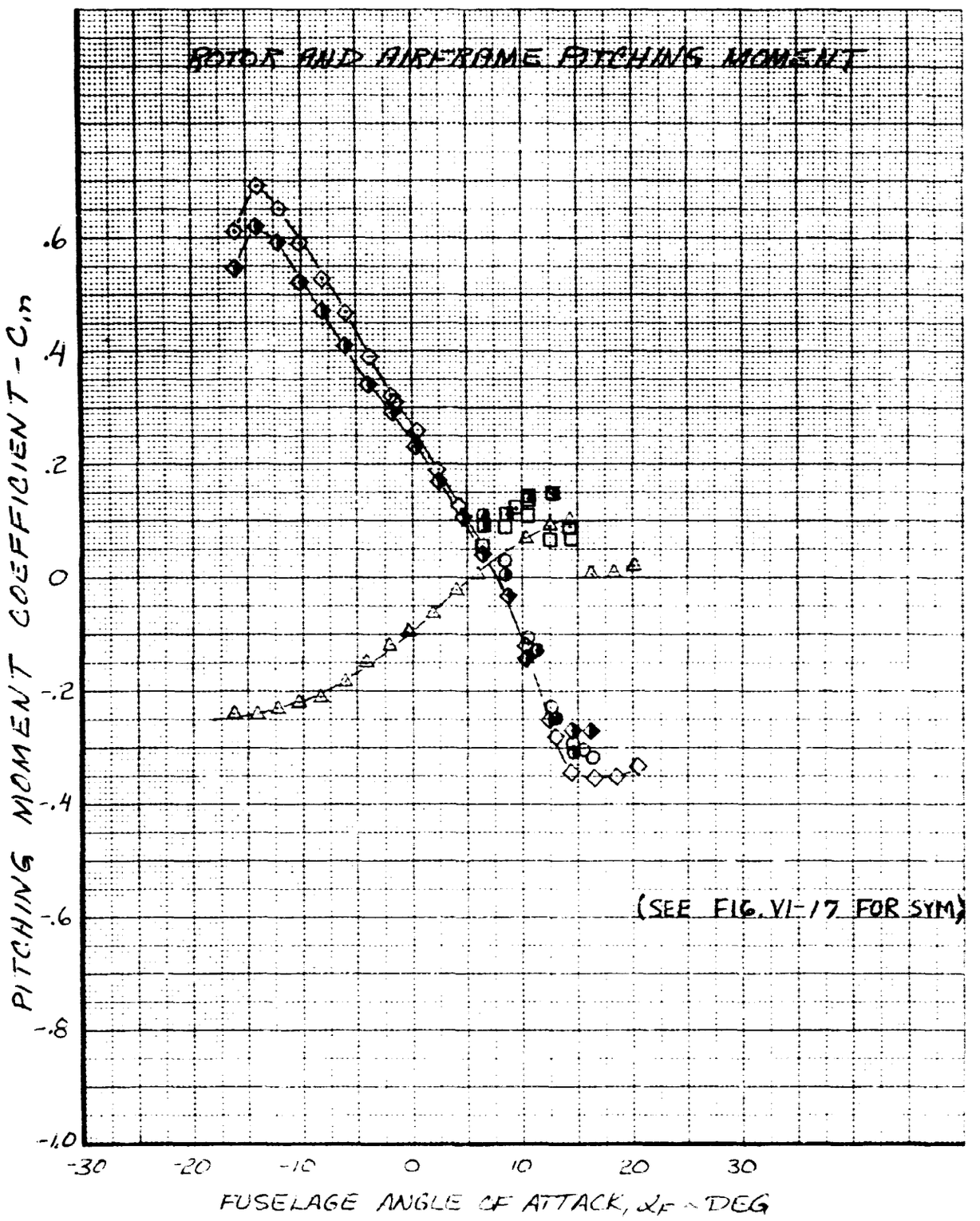

Figure VI-32. Pitching Moment Versus Fuselage Angle of Attack, Nacelle Incidence 30°, Airspeed 120 Knots.

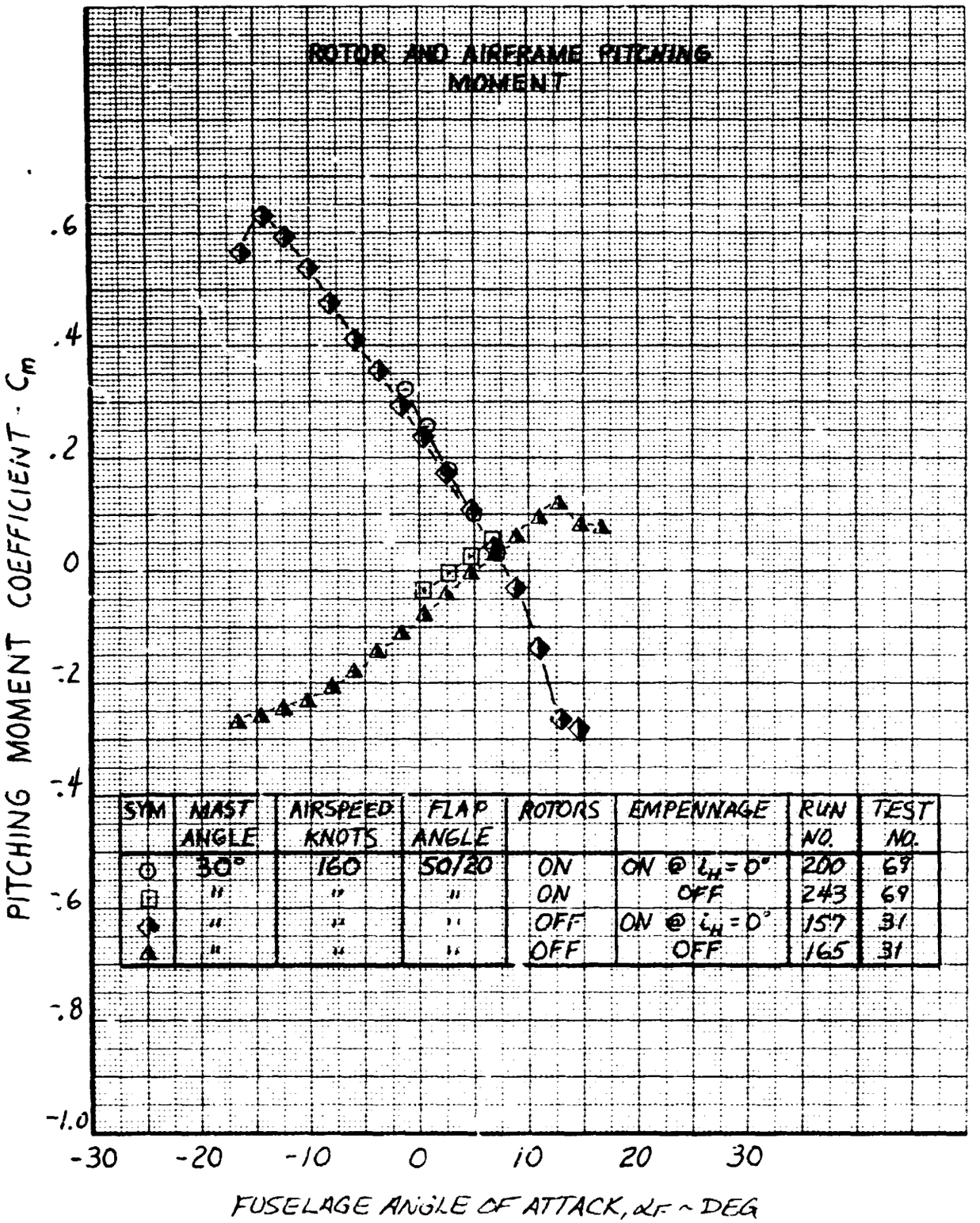

Figure VI-33. Pitching Moment Versus Fuselage Angle of Attack, Nacelle Incidence 30°, Airspeed 160 Knots.

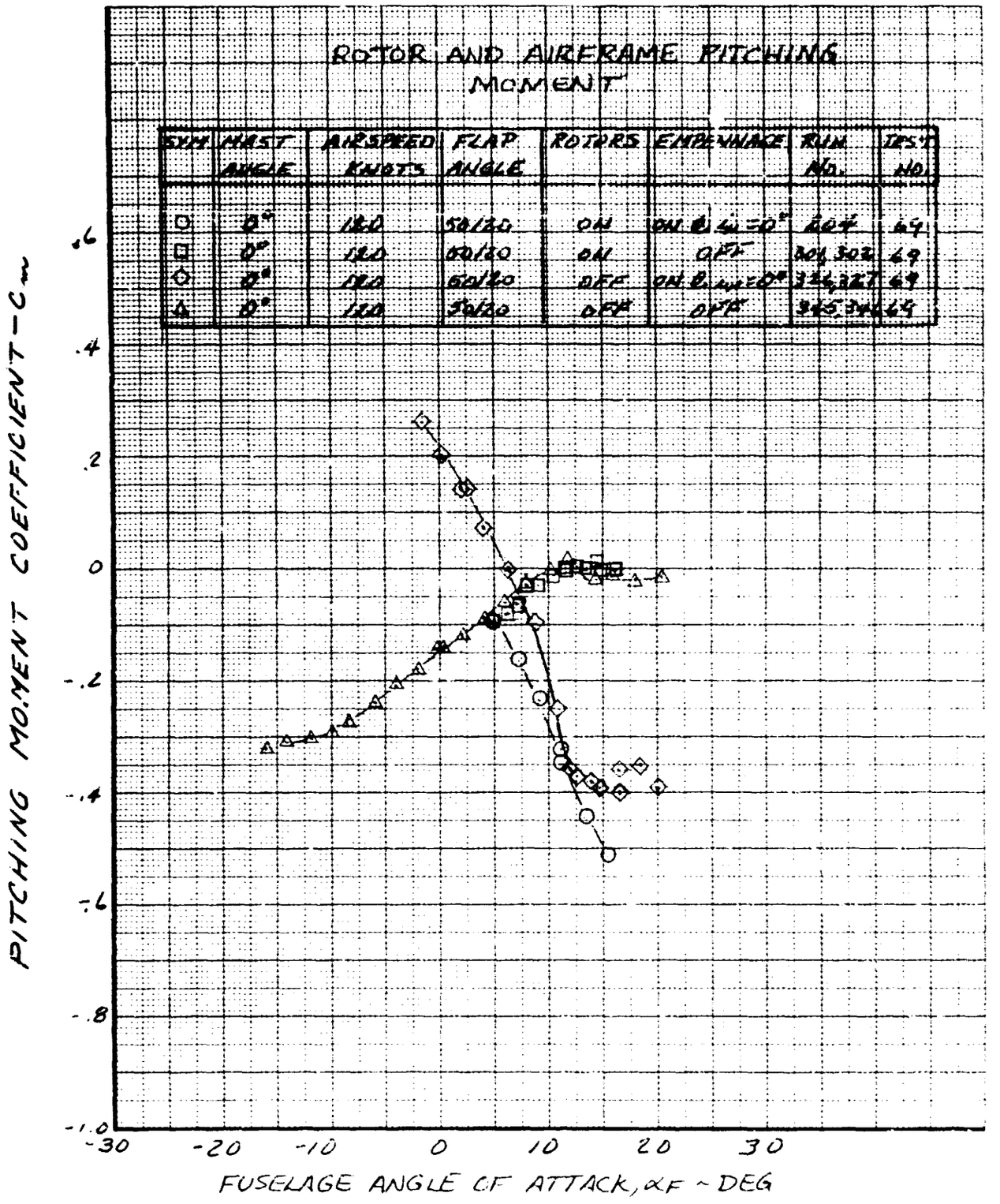

Figure VI-34. Pitching Moment Versus Fuselage Angle of Attack, Nacelle Incidence 0°, Airspeed 120 Knots.

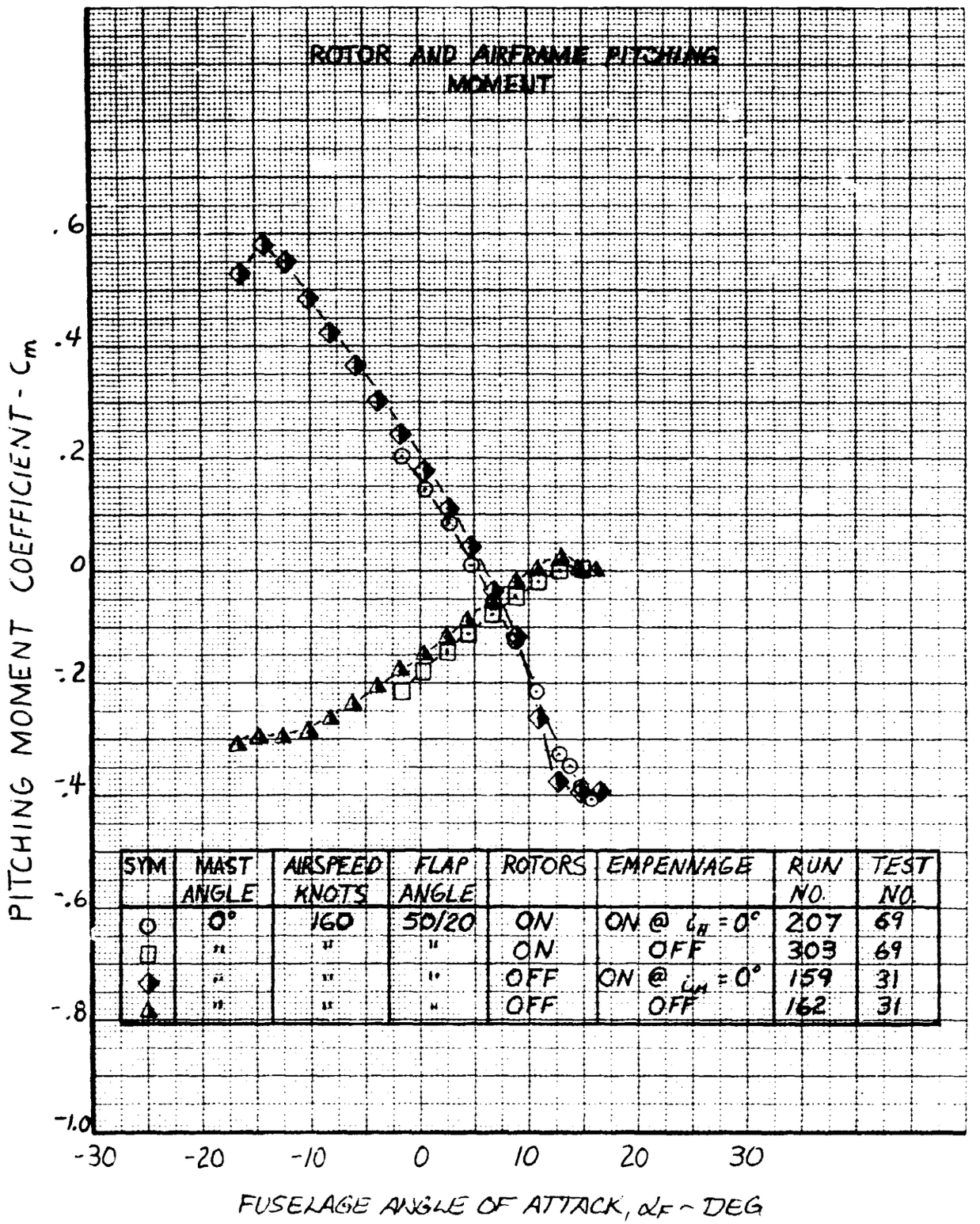

Figure VI-35. Pitching Moment Versus Fuselage Angle of Attack, Nacelle Incidence 0°. Airspeed 160 Knots.

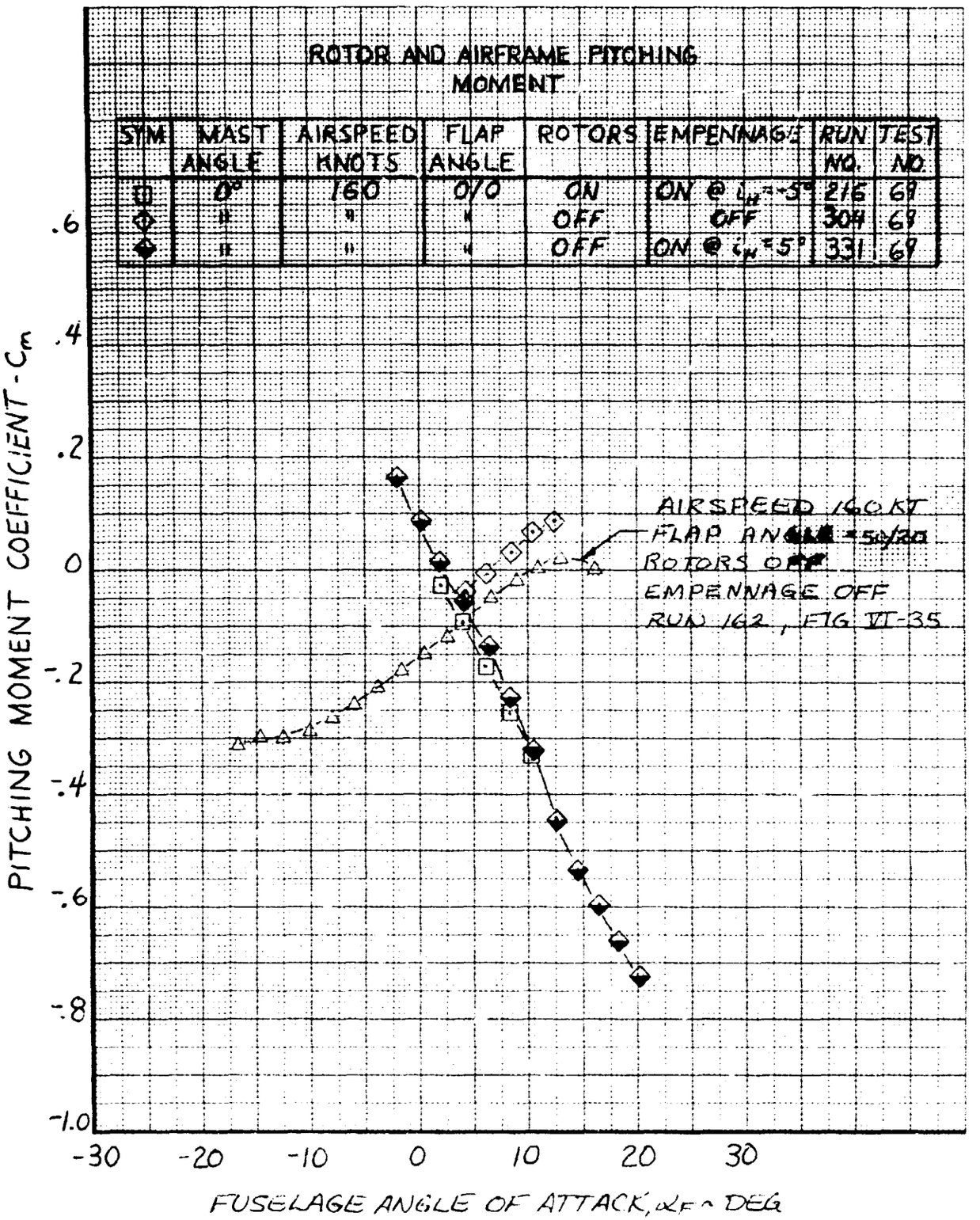

Figure VI-36. Pitching Moment Versus Fuselage Angle of Attack, Nacelle Incidence 0°, Airspeed 160 Knots.

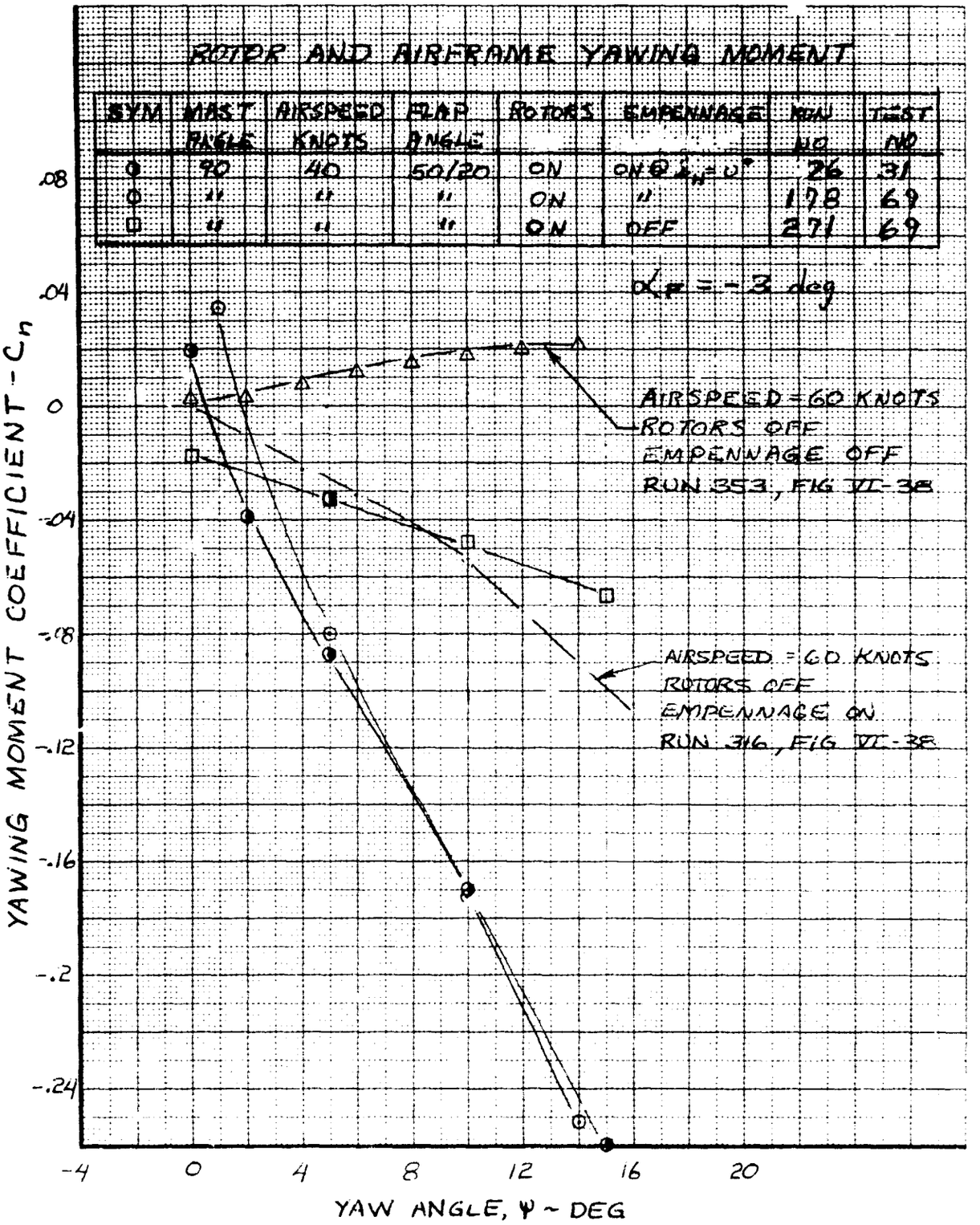

Figure VI-37. Yawing Moment Coefficient Versus Yaw Angle, Nacelle Incidence 90°, Airspeed 40 Knots.

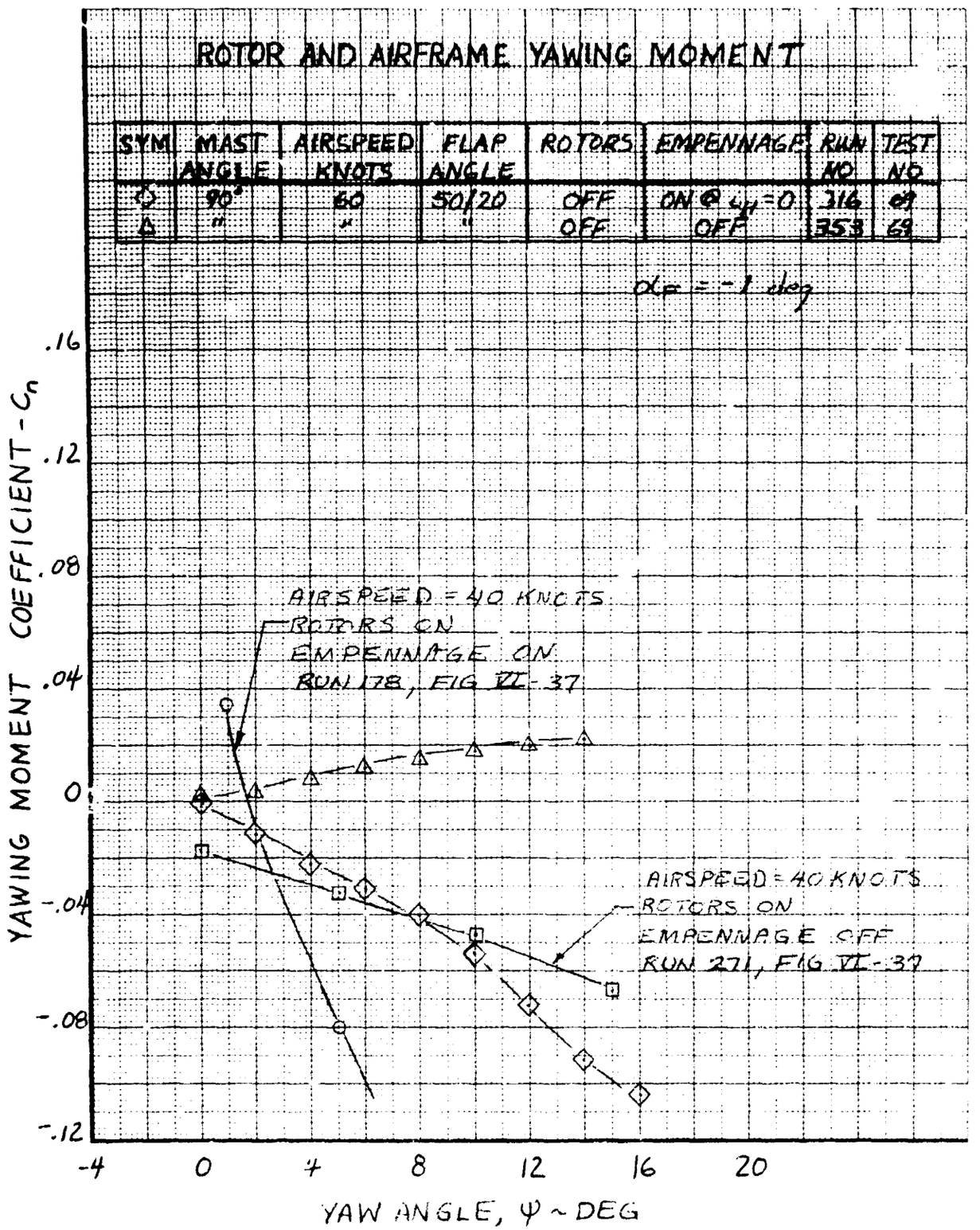

Figure VI-38. Yawing Moment Coefficient Versus Yaw Angle, Nacelle Incidence 90°, Airspeed 60 Knots.

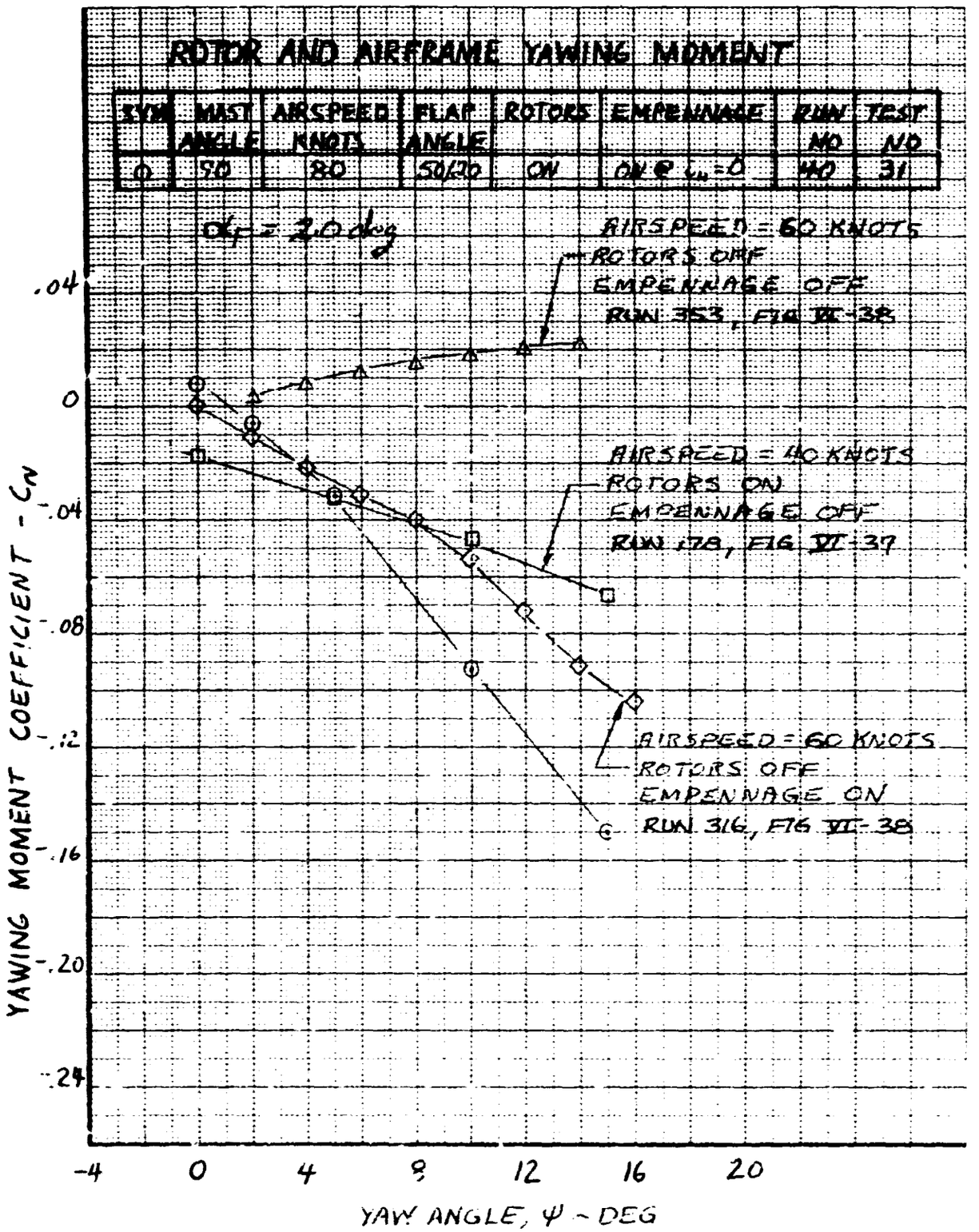

Figure VI-39. Yawing Moment Coefficient Versus Yaw Angle, Nacelle Incidence 90°, Airspeed 80 Knots.

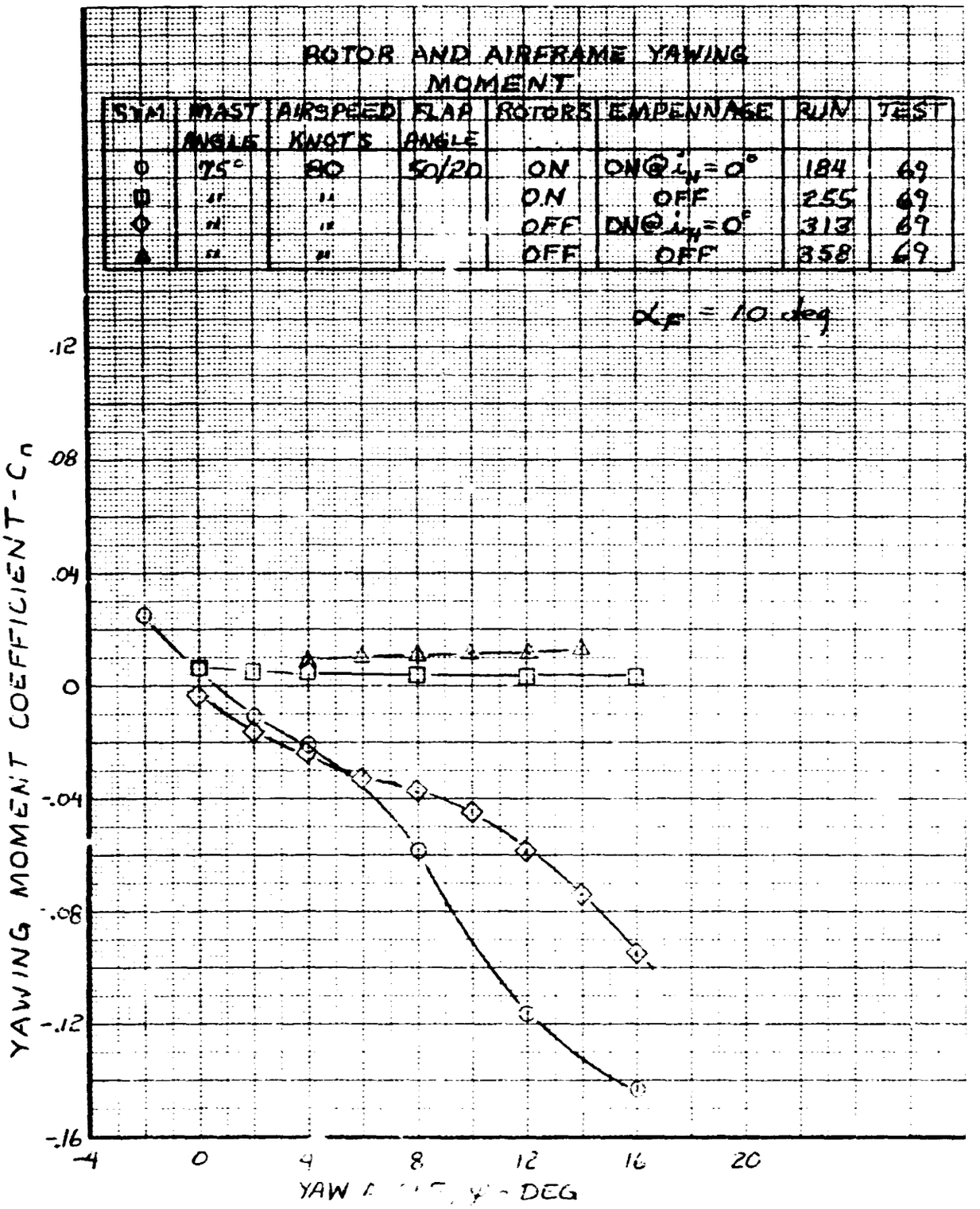

Figure VI-40. Yawing Moment Coefficient Versus Yaw Angle, Nacelle Incidence 75°, Airspeed 80 Knots.

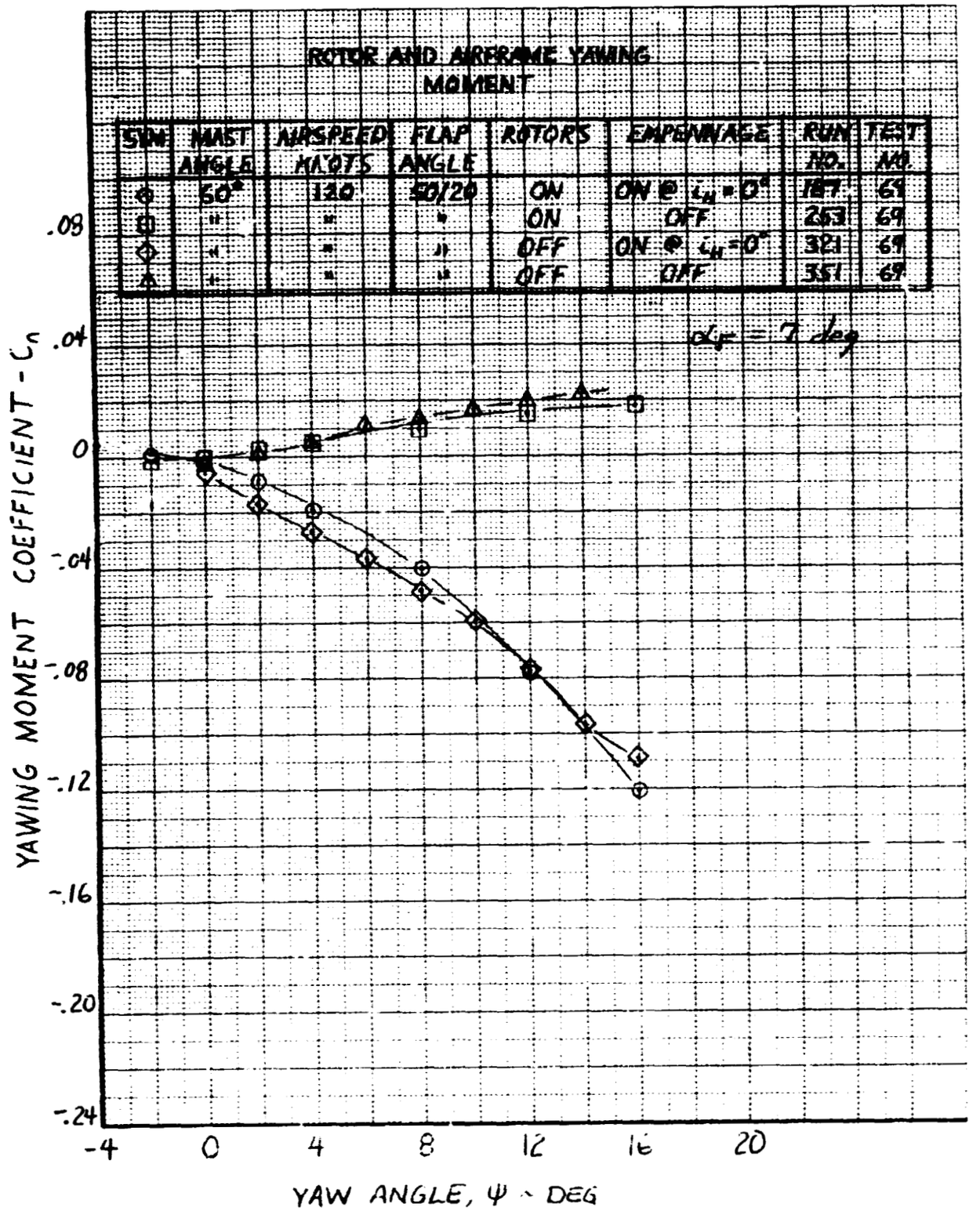

Figure VI-41. Yawing Moment Coefficient Versus Yaw Angle, Nacelle Incidence 60°, Airspeed 120 Knots.

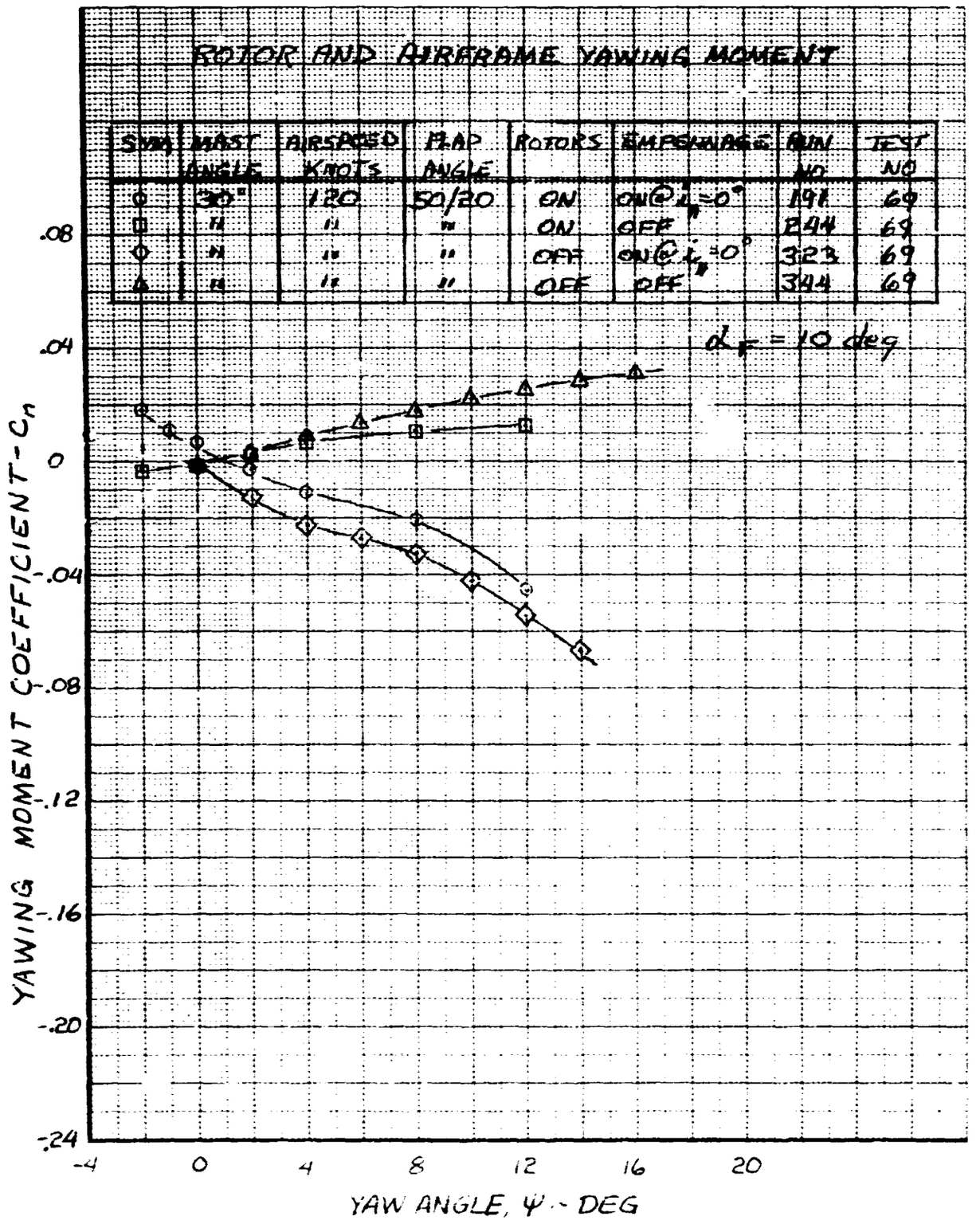

Figure VI-42. Yawing Moment Coefficient Versus Yaw Angle, Nacelle Incidence 30°, Airspeed 120 Knots.

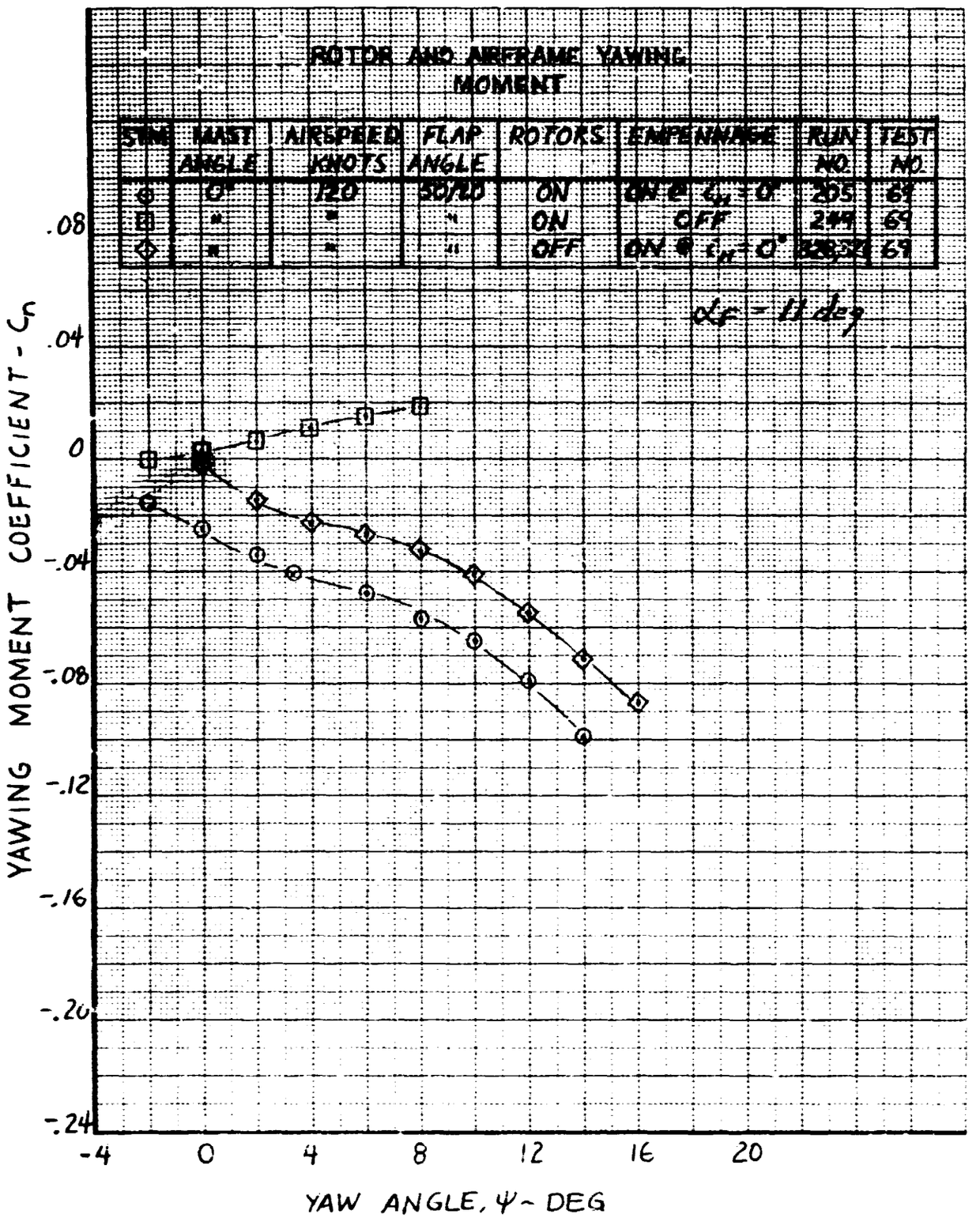

Figure VI-43. Yawing Moment Coefficient Versus Yaw Angle, Nacelle Incidence 0°, Airspeed 120 Knots.

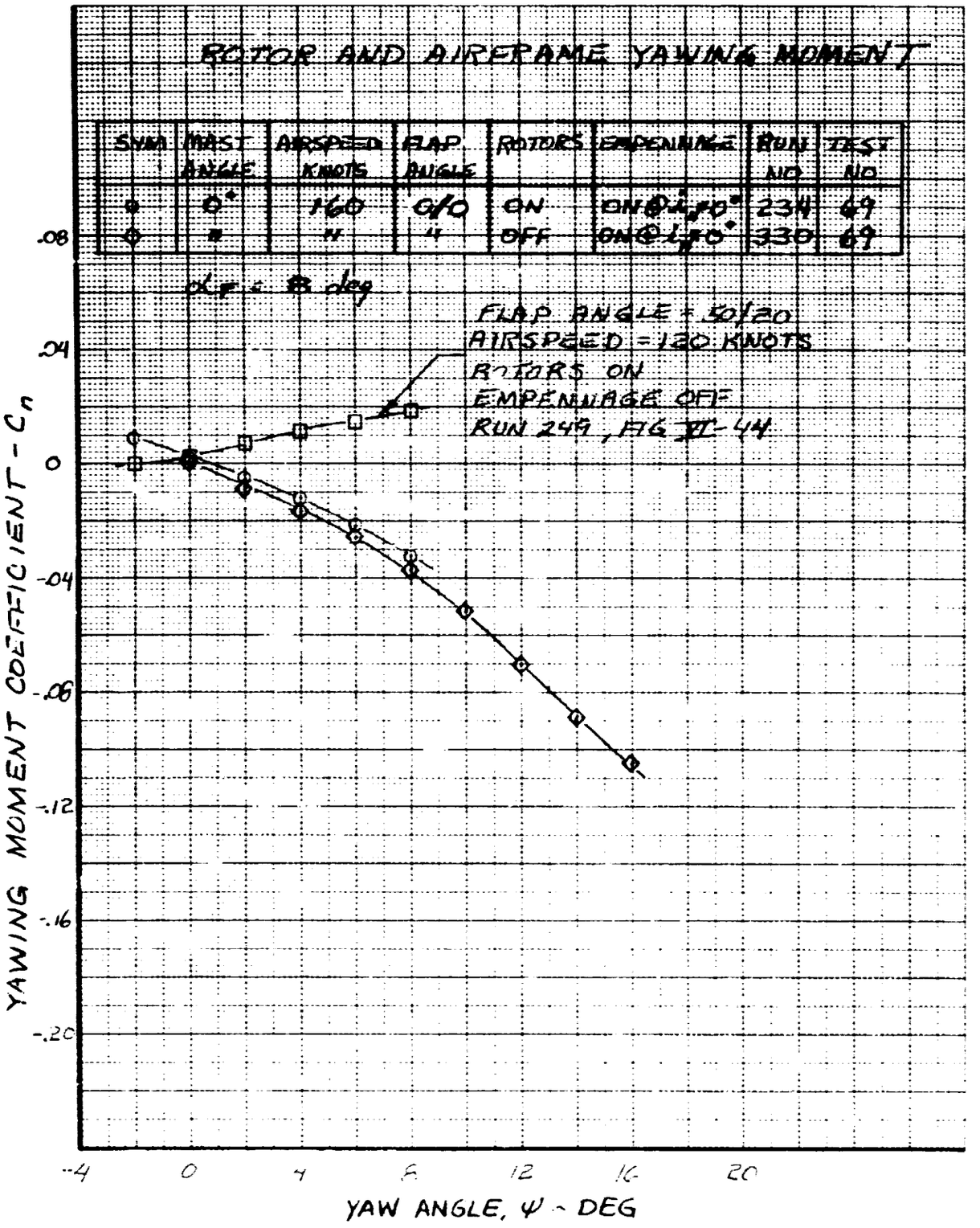

Figure VI-44. Yawing Moment Coefficient Versus Yaw Angle, Nacelle Incidence 0°, Airspeed 160 Knots.

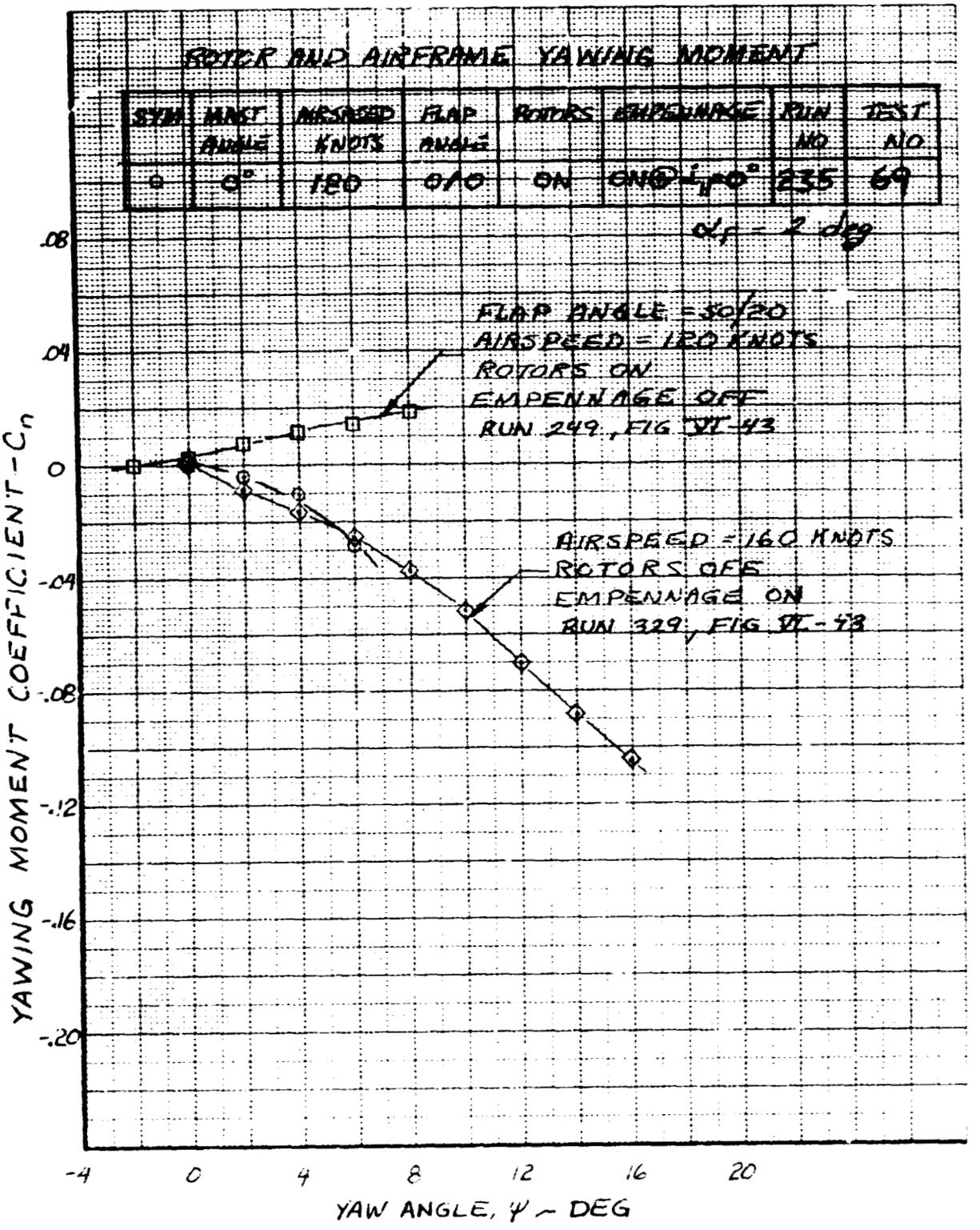

Figure VI-45. Yawing Moment Coefficient Versus Yaw Angle, Nacelle Incidence 0°, Airspeed 180 Knots.

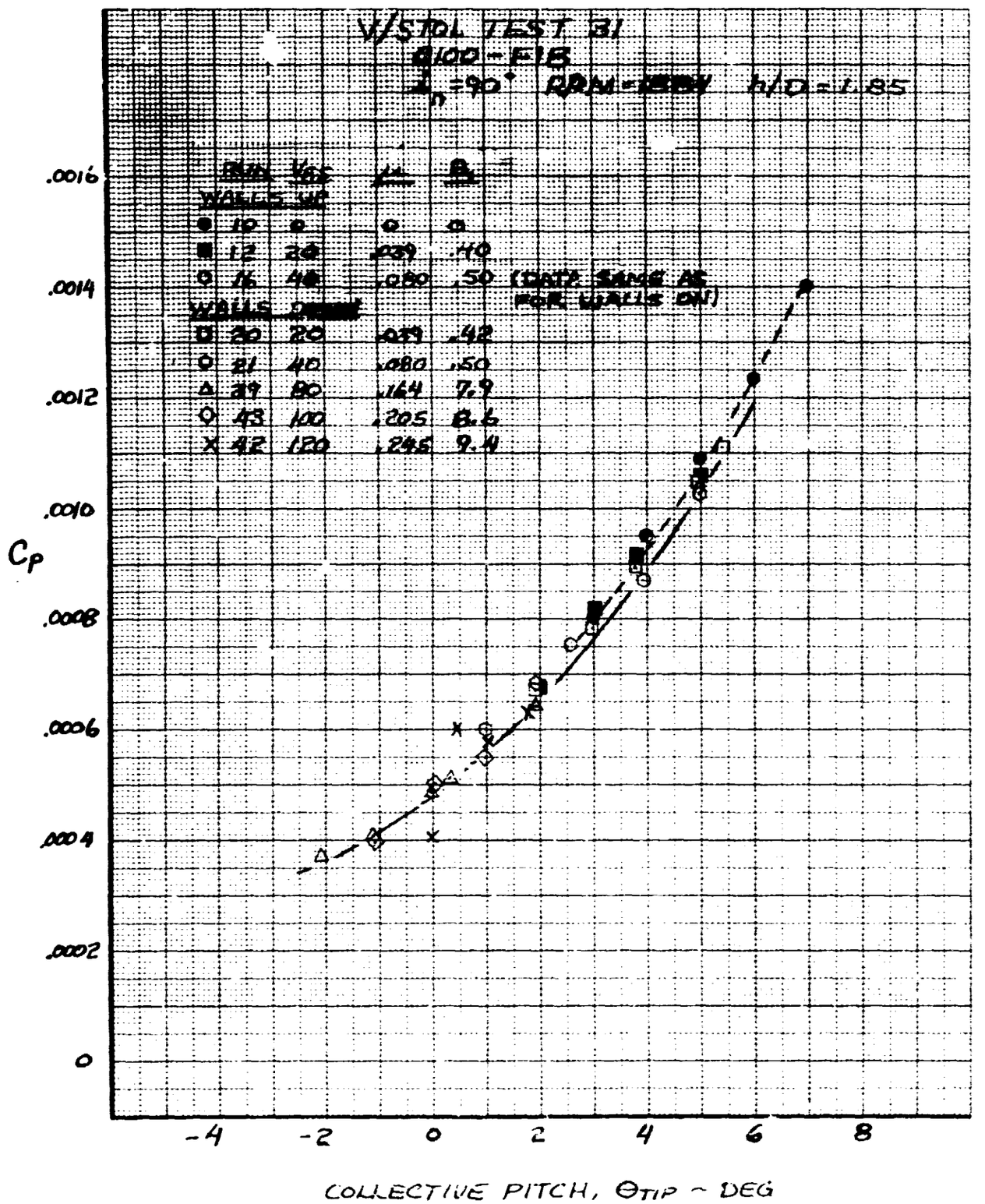

Figure VI-46. Rotor Power/Collective Pitch Variation With Airspeed, Nacelle Incidence 90°, OGE.

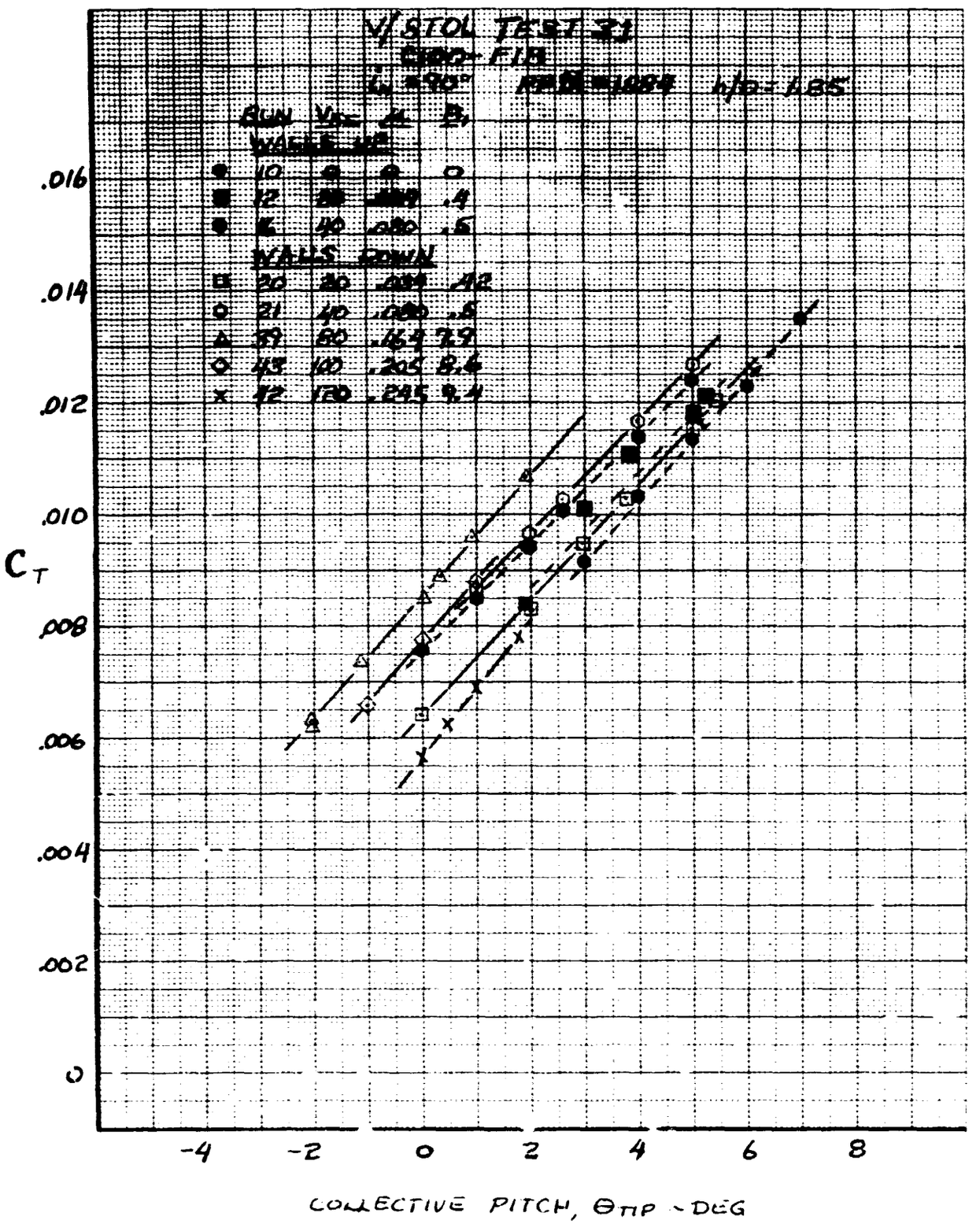

Figure VI-47. Rotor Thrust/Collective Pitch Variation With Airspeed, Nacelle Incidence 90°, OGE.

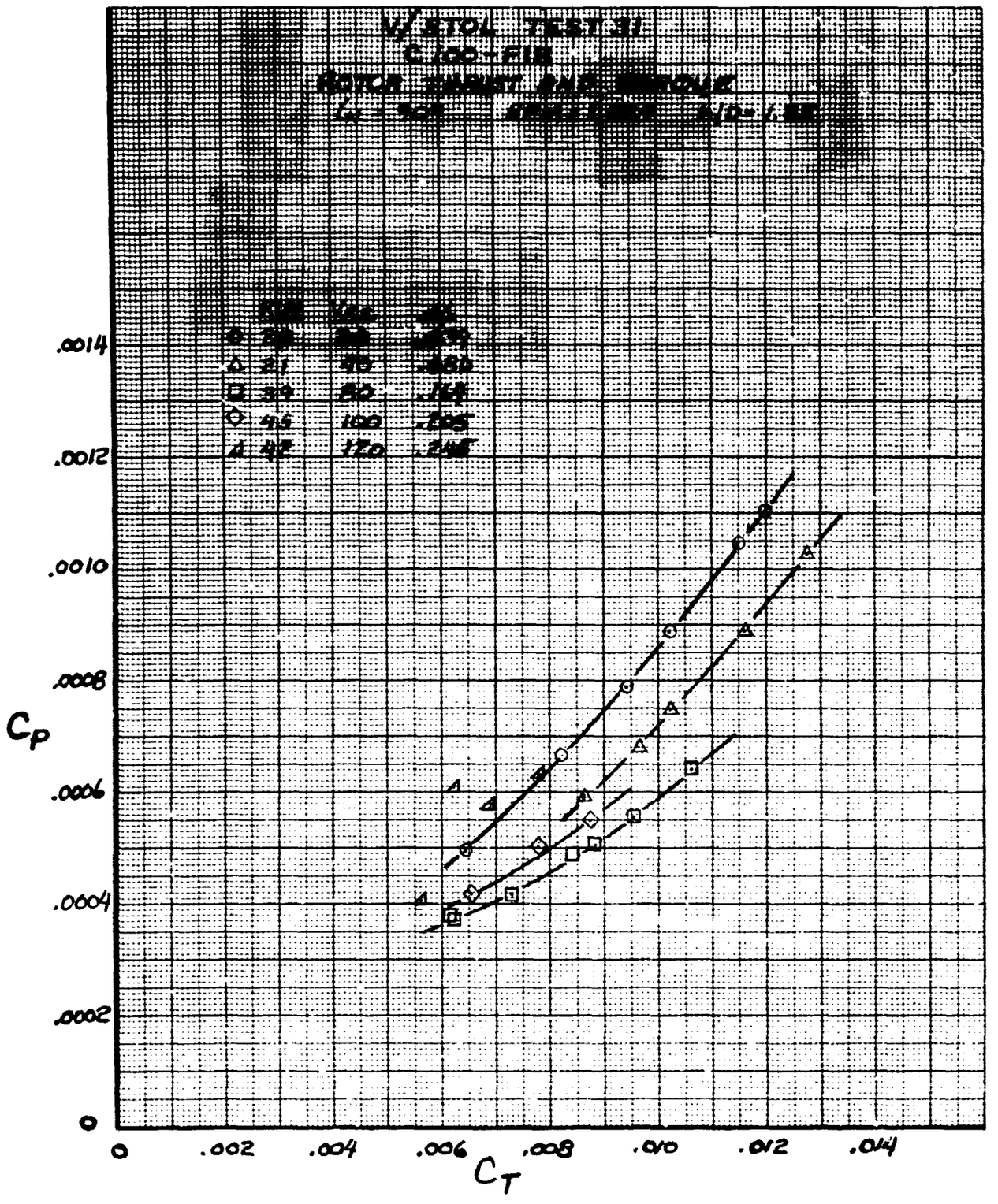

Figure VI-48. Rotor Power/Thrust Variation With Airspeed, Nacelle Incidence 90°, OGE.

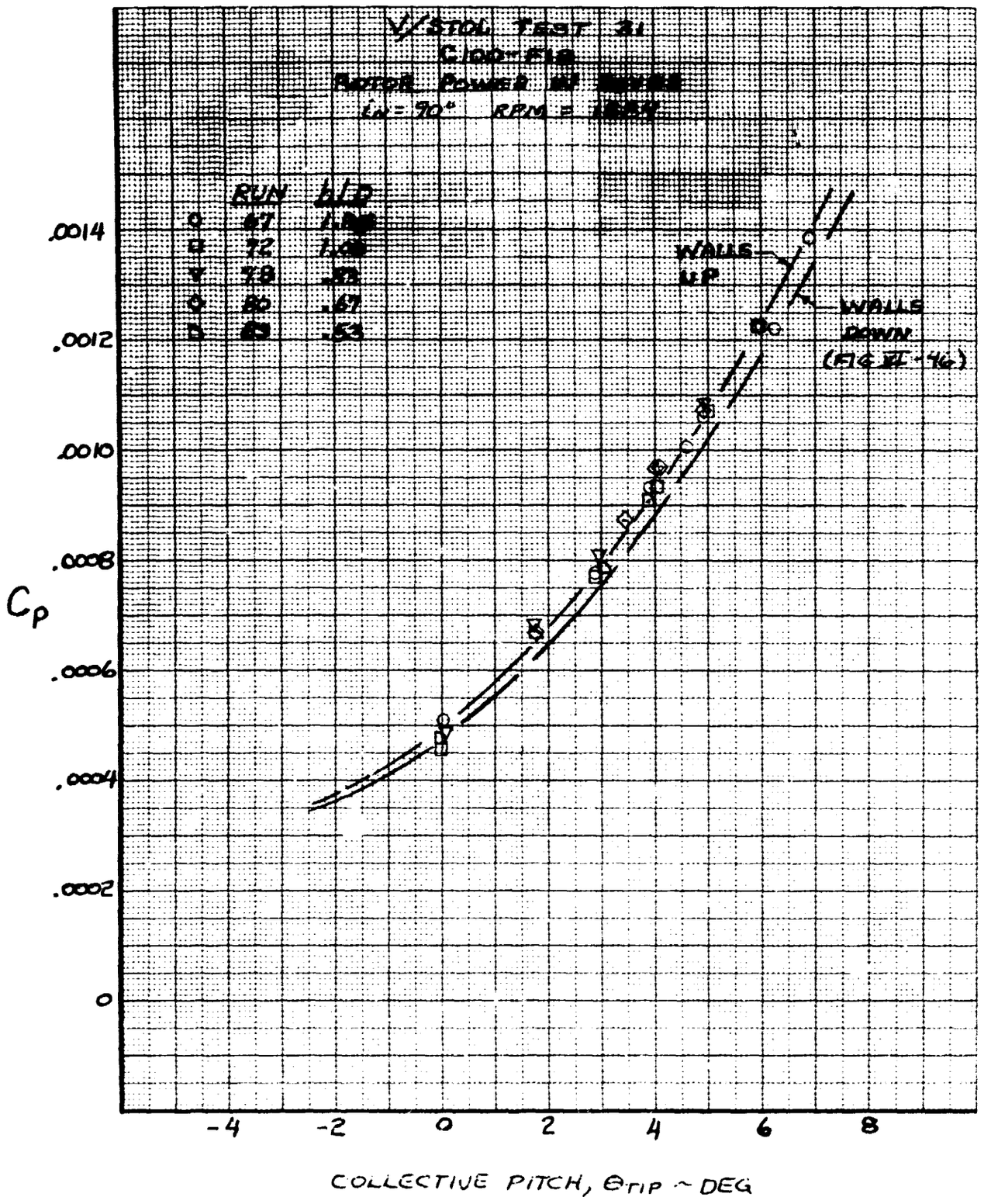

Figure VI-49. Rotor Power/Collective Pitch Variation With Height Above the Ground, Nacelle Incidence 90°.

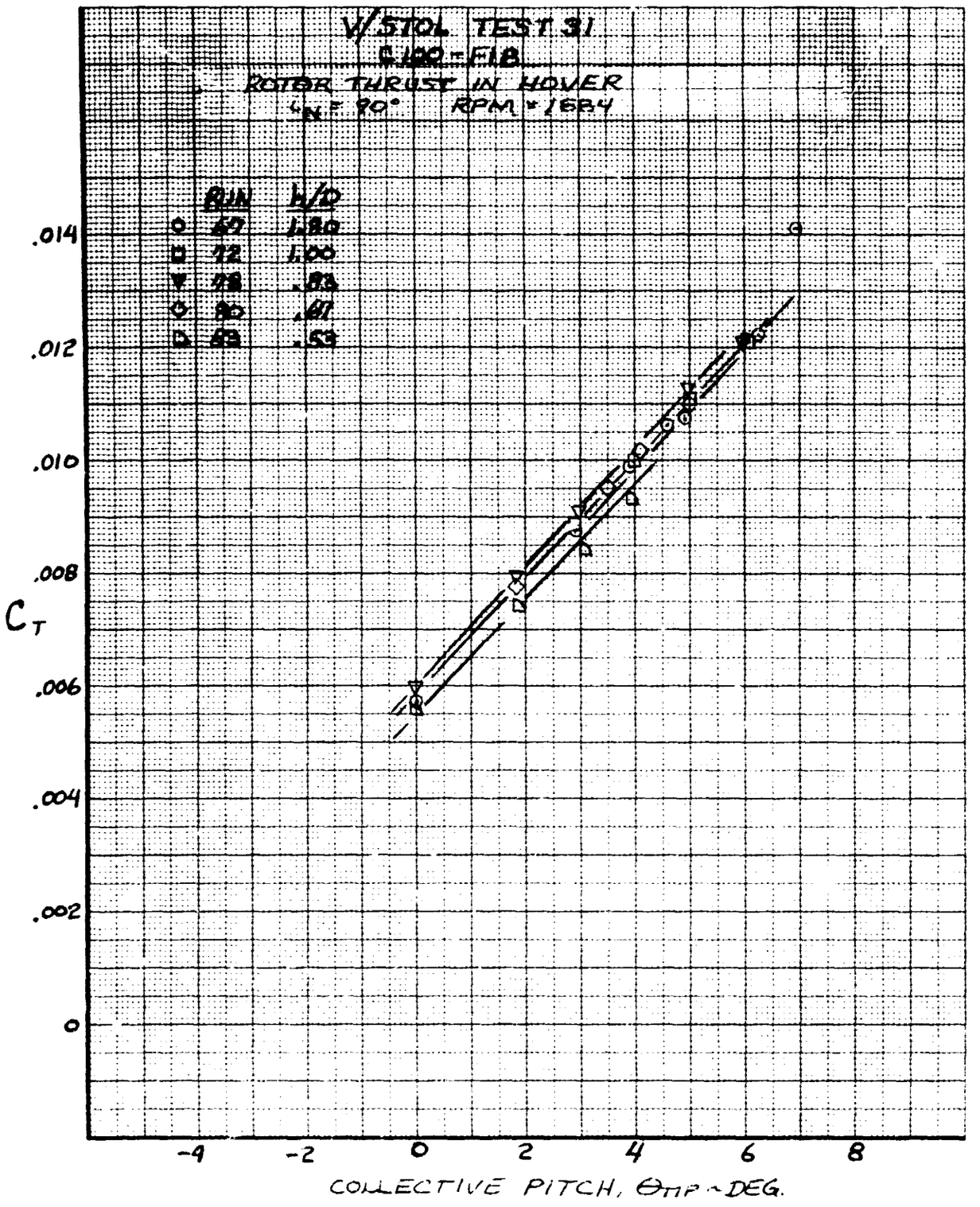

Figure VI-50. Rotor Thrust/Collective Pitch Variation With Height Above the Ground. Nacelle Incidence 90°.

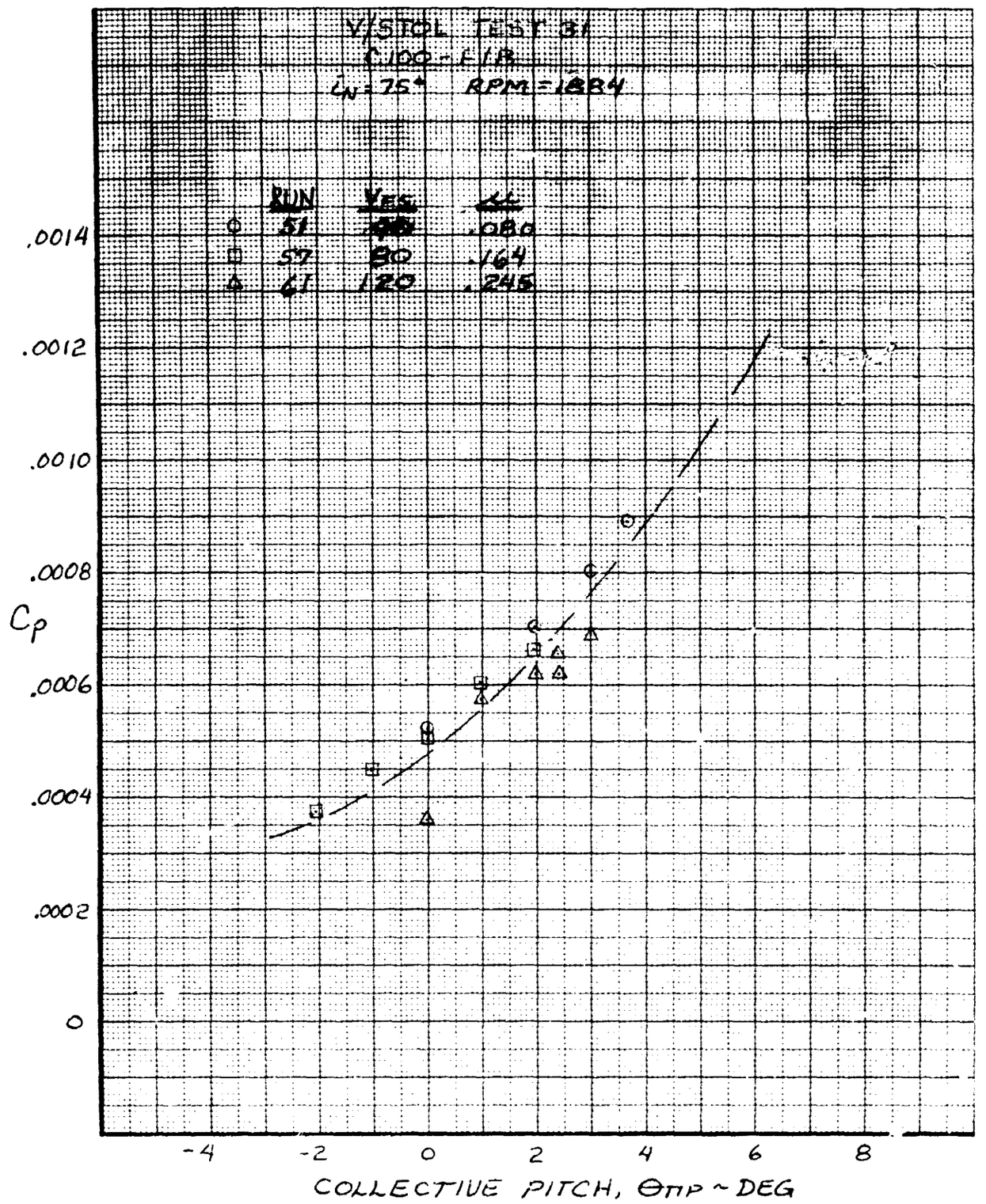

Figure VI-51. Rotor Power/Collective Pitch Variation With Airspeed, Nacelle Incidence 75°, OGE.

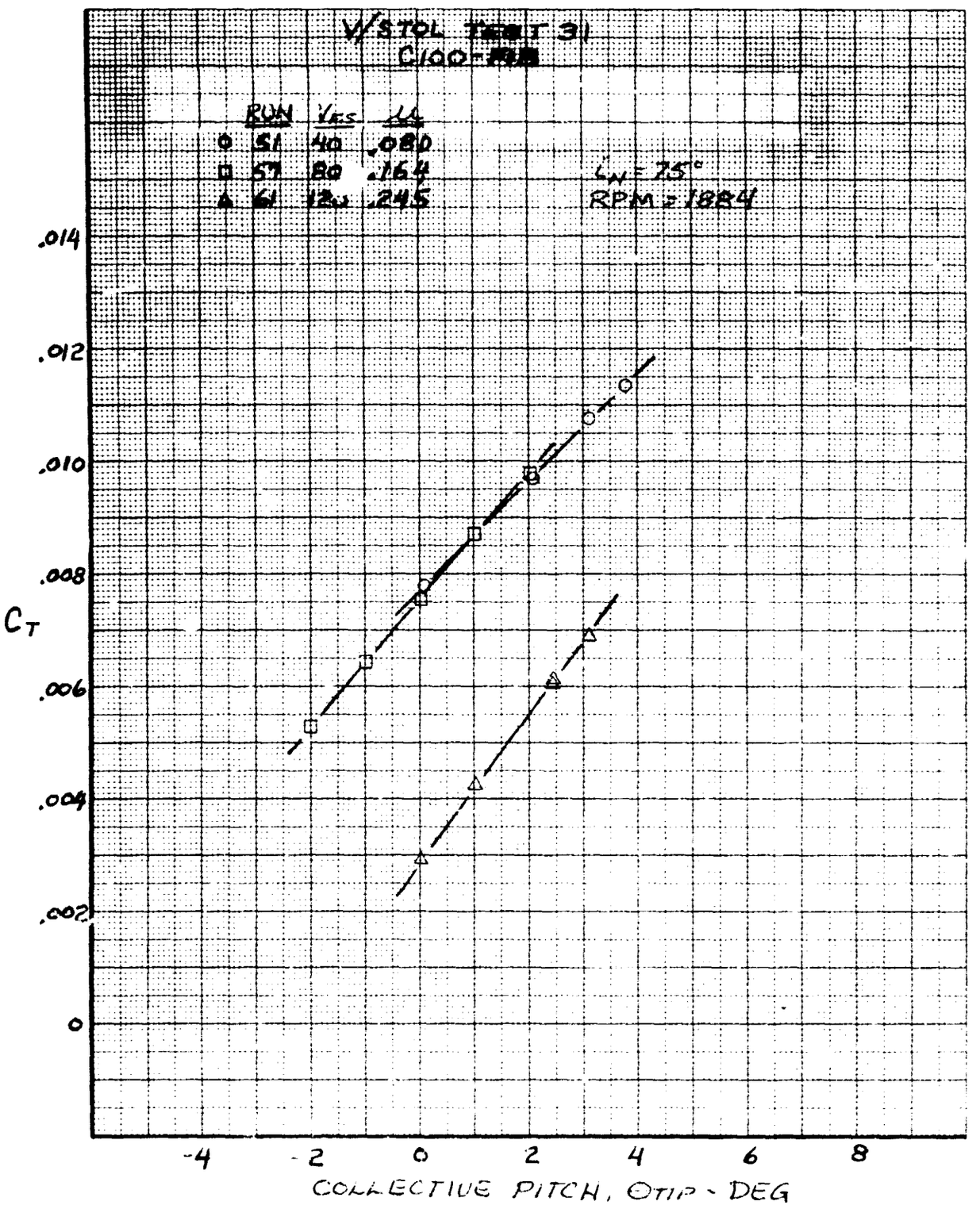

Figure VI-52. Rotor Thrust/Collective Pitch Variation With Airspeed, Nacelle Incidence 75°, OGE.

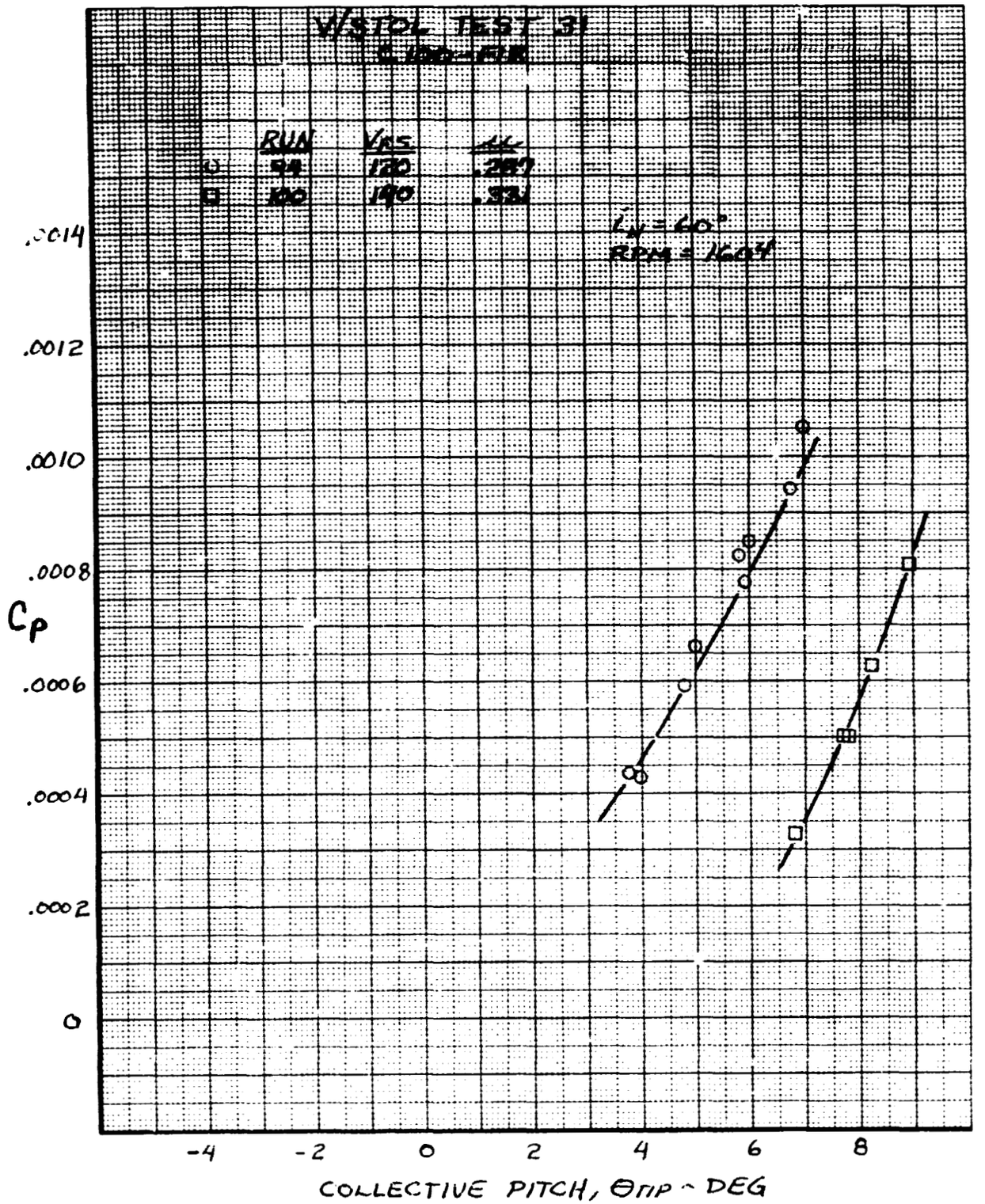

Figure VI-53. Rotor Power/Collective Pitch Variation With Airspeed, Nacelle Incidence 60°, OGE.

C-2

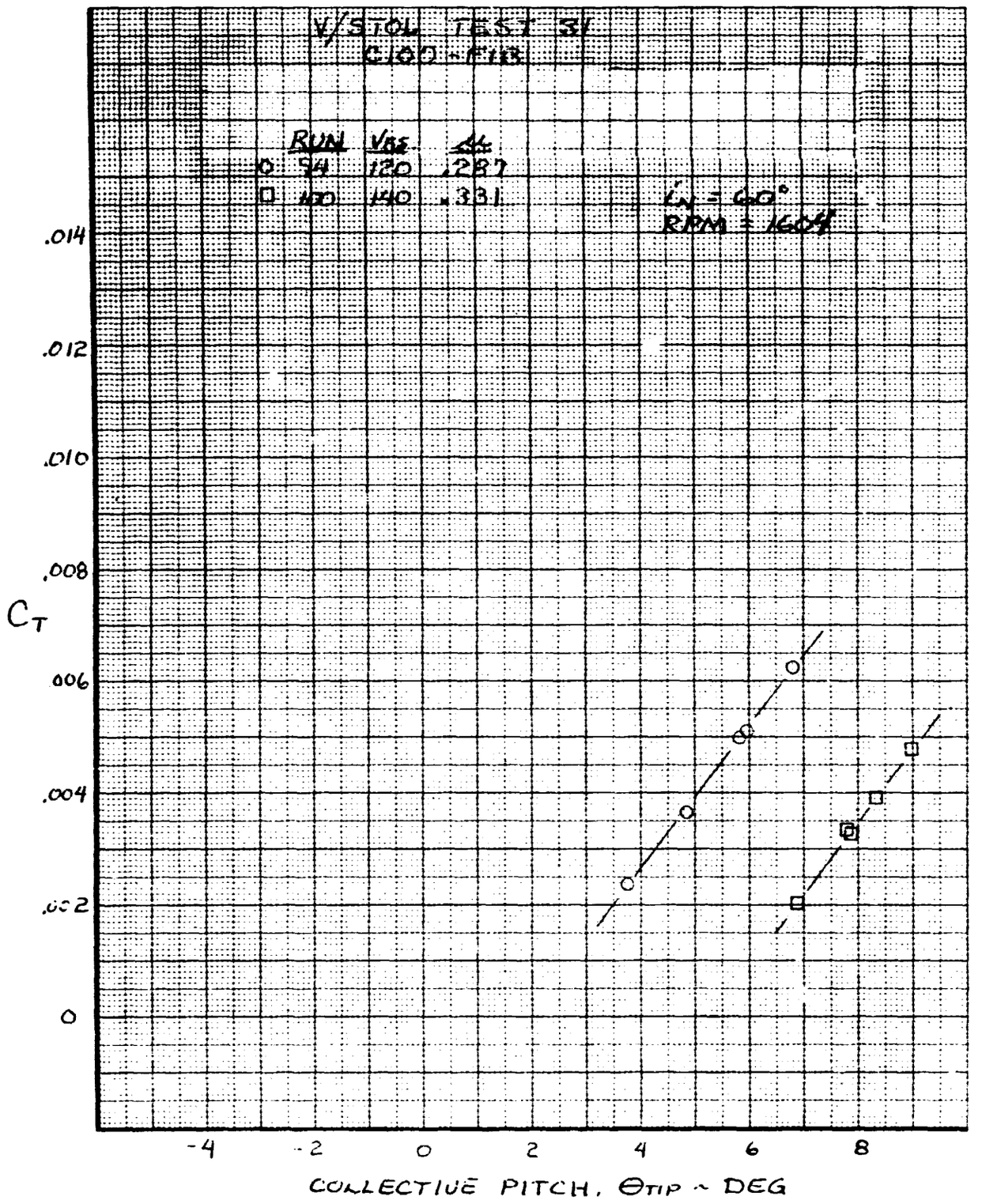

Figure VI-54. Rotor Thrust/Collective Pitch Variation With Airspeed, Nacelle Incidence 60°, OGE.

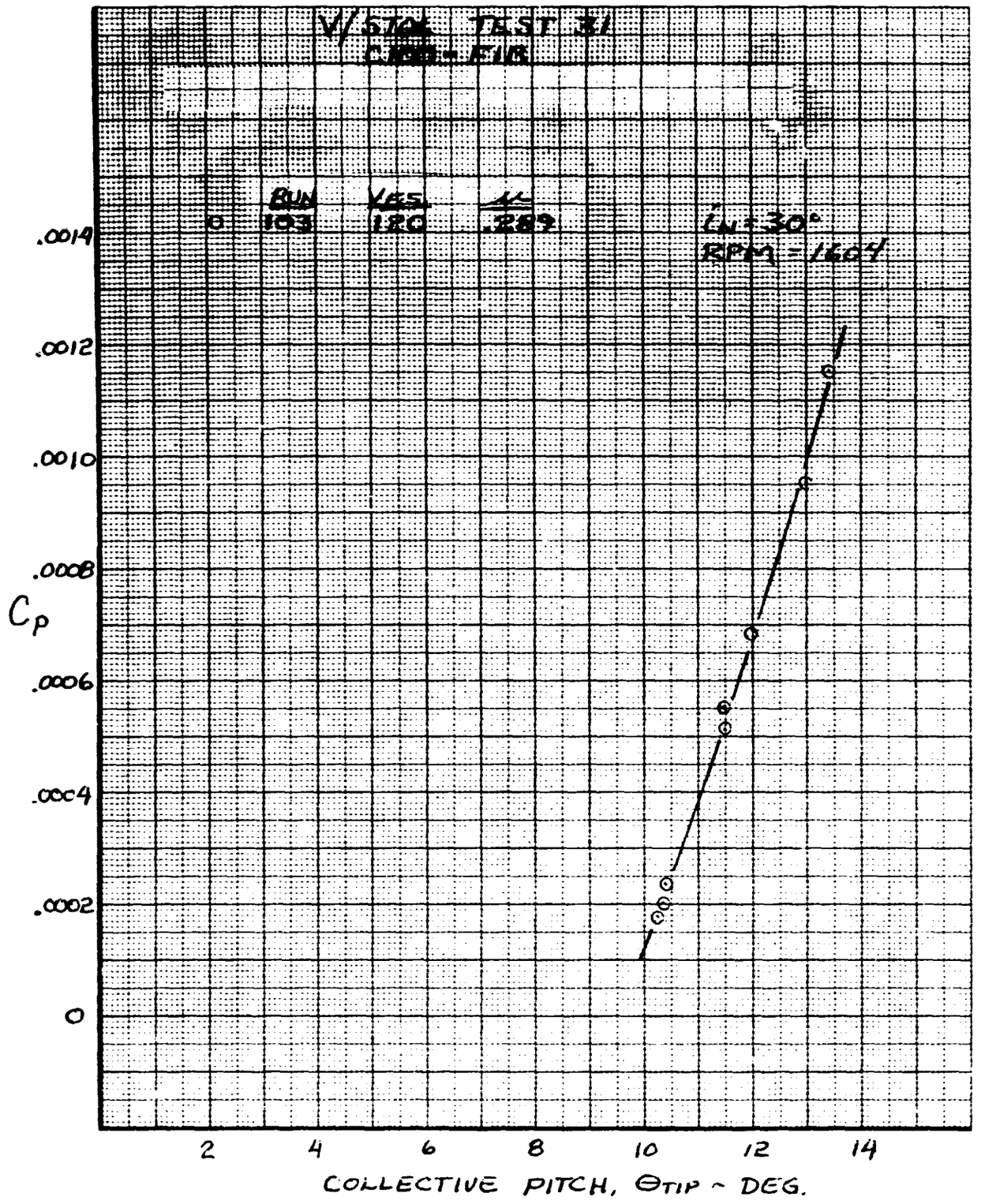

Figure VI-55. Rotor Power/Collective Pitch Variation With Airspeed, Nacelle Incidence 30°, OGE.

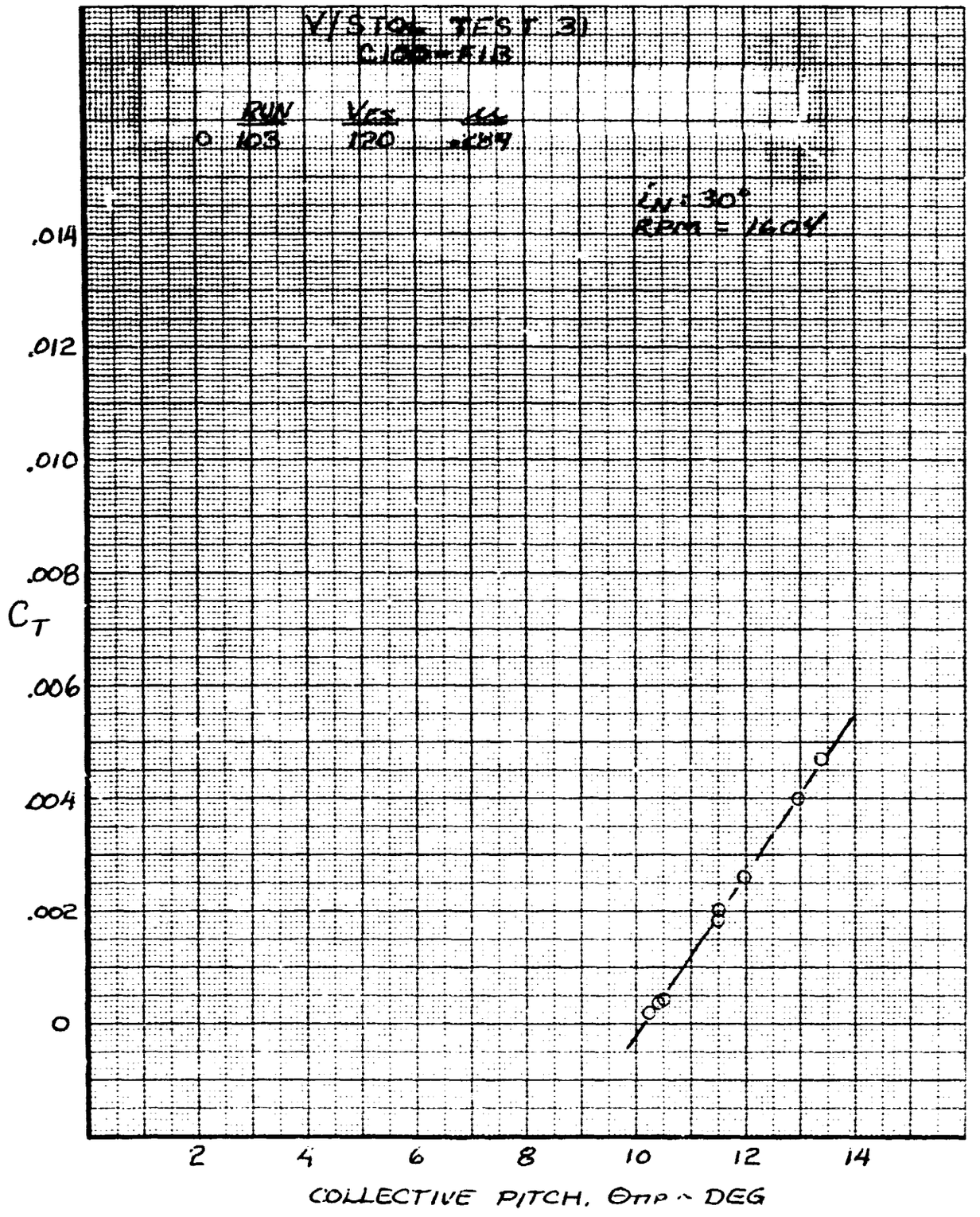

Figure VI-56. Rotor Thrust/Collective Pitch Variation With Airspeed, Nacelle Incidence 30°, OGE.

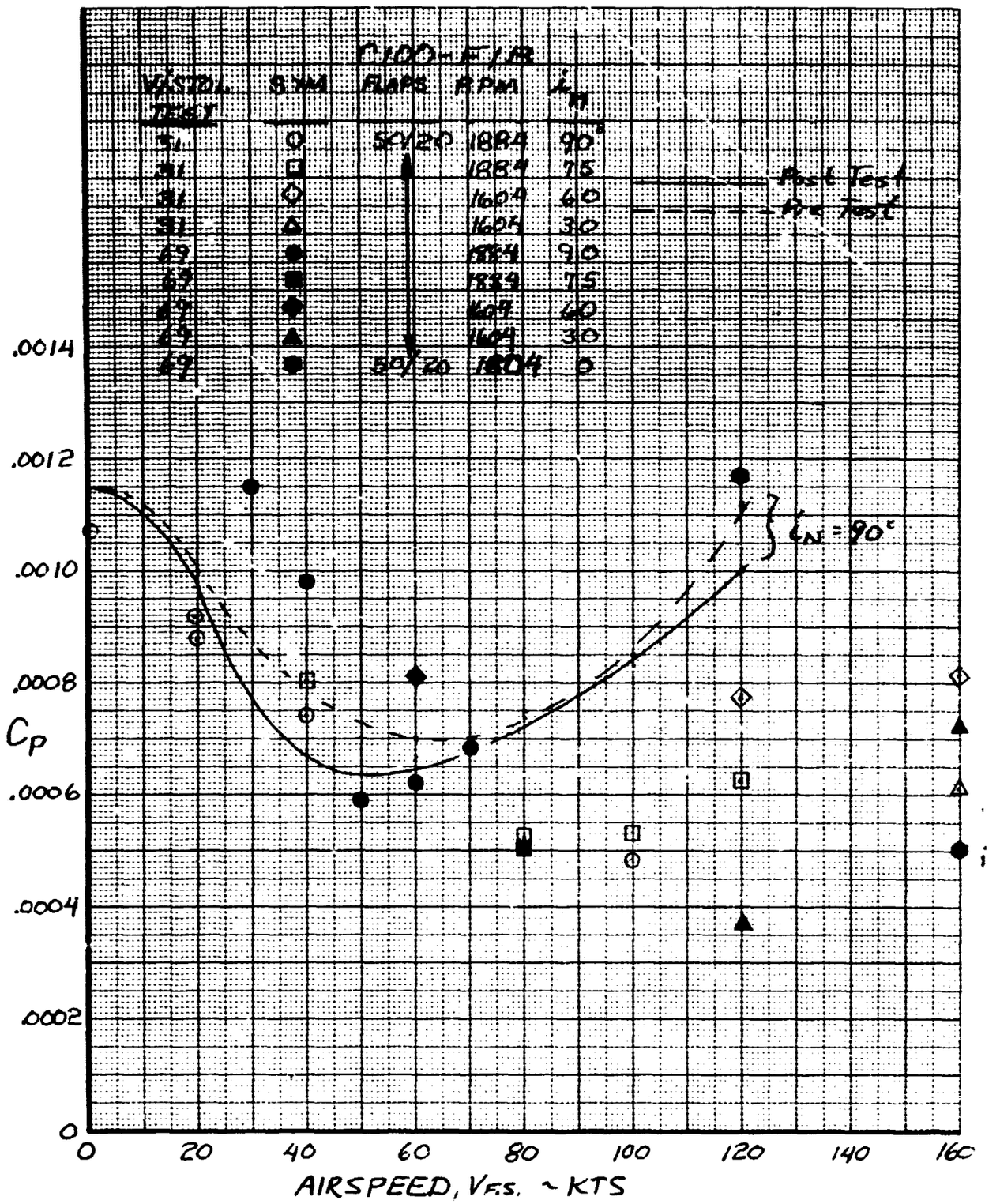

Figure VI-57. Rotor Power Variation With Airspeed and Nacelle Incidence.

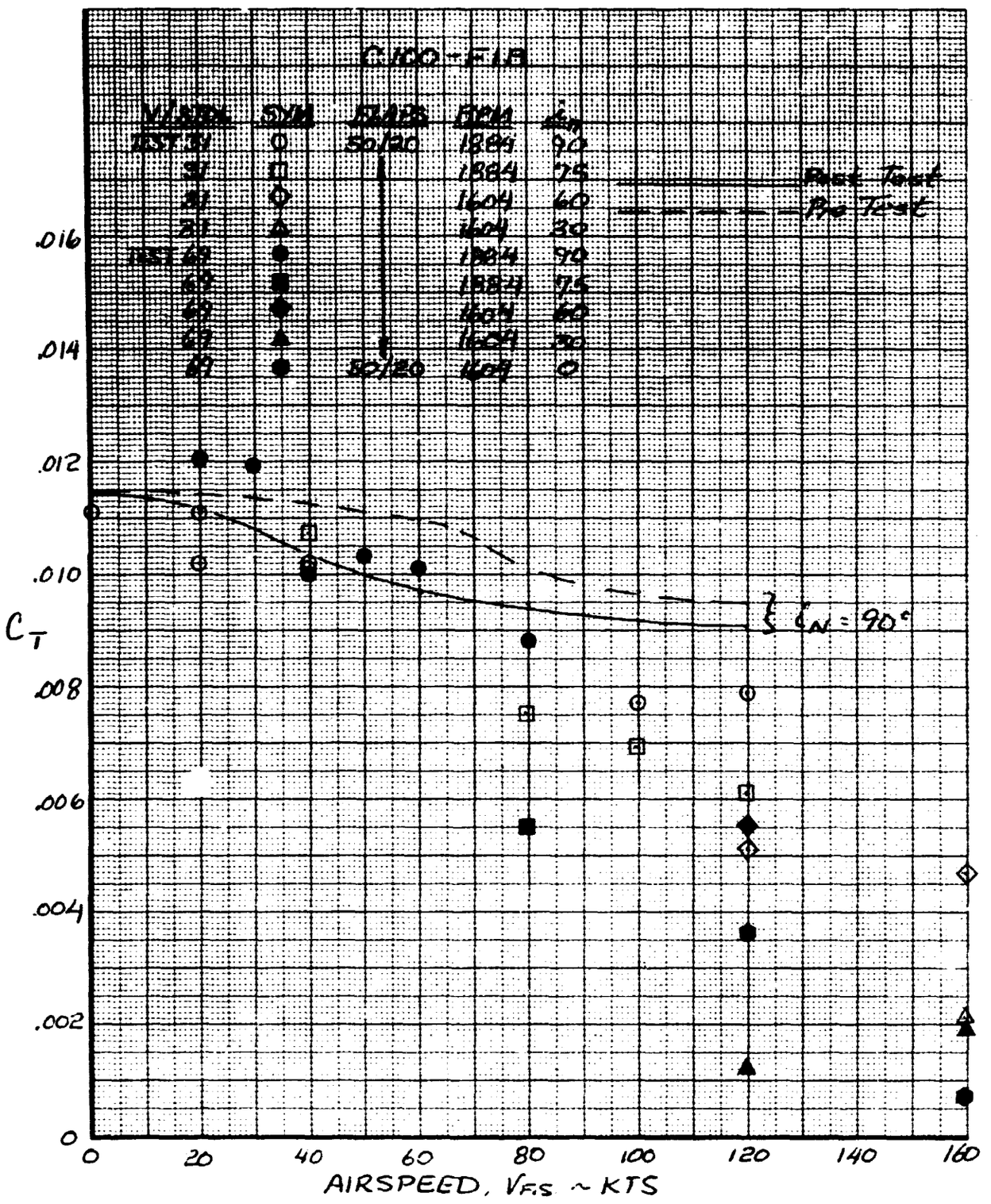

Figure VI-58. Rotor Thrust Variation With Airspeed and Nacelle Incidence.

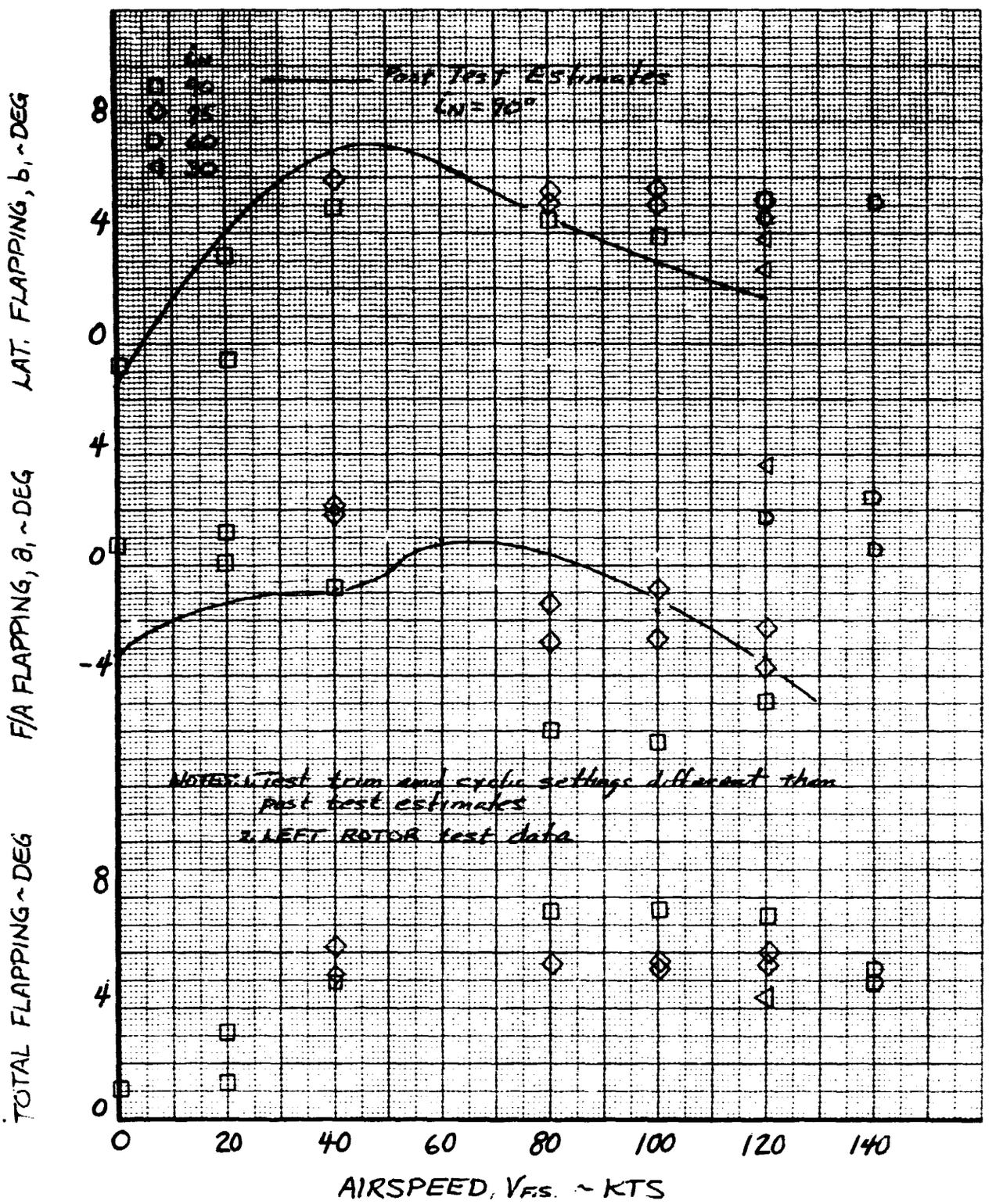

Figure VI-59. Rotor Flapping Variation With Airspeed and Nacelle Incidence.

VII. ANALYSIS OF RESULTS

The information presented in this section includes analysis of test data related to determining the effects of the rotor wake on the airframe applicable to tilt rotor aircraft. The result of this analysis will be used in design of future tilt rotor aircraft and to update the tilt rotor flight simulation mathematical model. Results obtained during this analysis will be used to extend rotor wake effect information obtained during the powered aeroelastic model test.[2]

A. Hover Download

As noted in Section VI.A., the wing download was measured in and out of ground effect and at several flap settings. These test results were compared with other powered tilt rotor model tests[2,6,7] as shown in Figures VII-1 and VII-2. As indicated, this test and Reference 6 are in close agreement while the download for the aeroelastic model[2] is much higher. Also, the other two model tests show the same trend in download variation with flap deflection in that download is not significantly reduced for flap/flaperon deflections greater than 50 degrees.

From these two figures it appears that for a flaperon setting near 50 degrees and OGE, it is possible to have anything from 5.5 percent to 13 percent download. Several parameters were found to be influencing these differences and to have an effect on determining hover wing download. The parameters considered for the various models tested are listed in Table VII-1. Of these, blade twist and percent of wing area under the rotor were found to be the most significant parameter in determining download.

The effect of blade twist is shown in Figure VII-3. A 3.5 percent difference in download was measured between one model with 25 degrees blade twist and another model with 40.9 degrees blade twist. The change in blade twist was also in conjunction with an increase in blocked area under the rotor as shown in Figure VII-4. From the trends shown in these two figures, it is difficult to determine which parameter contributed to the increased download between the two models tested or percentage each contributed. In extrapolating the test results, it appears that the blade twist change may account for about .8 percent and the blockage for 2.2 percent. The remaining 0.5 percent is due to different flap settings. The differences in the models tested make it difficult to establish a generalized design chart, but these figures can be used to give the designer some insight into trends that flaps, blade twist, and blocked area under the rotor have on wing download.

A. (Continued)

The test data would indicate a download on the order of 13 percent for a tilt rotor with 40.9 degrees blade twist, 75 percent blockage, and flap setting of 75/45. This is higher than previously estimated for this configuration. This difference is attributed to a Reynolds number effect. Hoerner[8] shows that the drag of cross-sectional shapes similar to a wing. with flaps deflected, at an angle of attack of -90 degrees is highly dependent on Reynolds number. This effect is shown in Figure VII-5 for the variation of drag coefficient of the cross-section with Reynolds number referenced to wing chord and mean induced velocity from the rotor. Calculation required to correct model scale download to full scale is given in Table VII-2. As noted on Figure VII-5, the drag coefficient was reduced by approximately 50 percent due to Reynolds number changing from model scale to full scale. Therefore, a 13 percent download measured for the model would be approximately 6.5 percent for the full scale aircraft. Other configurations would be similarily reduced.

B. Rotor Wake on Horizontal Stabilizer

The wake characteristics at the horizontal stabilizer were determined using pitching moment data from tail-off, tail-on, and incidence runs. For rotors-off configuration, the wake is the wing downwash angle ($\epsilon_{W/H}$). Rotors on, the wake is the total wake angle (ϵ_T) which includes the wing downwash angle plus the rotor wake ($\epsilon_{R/H}$). As noted earlier, two methods of obtaining the wake effects were used during these tests. During the first tunnel entry, only elevator sweeps were made; whereas, during the second entry, incidence sweeps were used. The following are the equations used to determine the wake for rotors on and off including the equation for elevator and incidence.

Knowing,

$$C_{m_{H_T}} = C_{m_{TAIL\text{-}ON}} - C_{m_{TAIL\text{-}OFF}} \qquad (1)$$

$$= - a_H \eta_{H_T} \bar{V}_H \alpha_H$$

$$C_{m_{i_{H_T}}} = (C_{m\ @\ i_H = -5^o} - C_{m\ @\ i_H = 0})/-5^o \qquad (2)$$

$$= - a_H \eta_{H_T} \bar{V}_H$$

B. (Continued)

$$C_{m_{\delta e_T}} = a_H \eta_{H_T} \bar{V}_H \tau_e \tag{3}$$

then,

$$\alpha_H = C_{m_{H_T}} / C_{m_{i_{H_T}}} = C_{m_{H_T}} / (C_{m_{\delta e_T}} / \tau_e) \tag{4}$$

$$= \alpha_F - \epsilon_T + i_H + \tau_e \delta_e$$

giving,

$$\epsilon_T = \alpha_F - \alpha_H + i_H + \tau_e \delta_e \tag{5}$$

where,

$$\epsilon_T = \epsilon_{W/H} + \epsilon_{R/H} \tag{6}$$

$$\eta_{H_T} = \eta_{H_{WB}} + \eta_{H_R} \tag{7}$$

For rotors-off configurations, the same equations can be used by setting $\epsilon_{R/H}$ and η_{H_R} to zero and replacing ϵ_T and η_{H_T} with $\epsilon_{W/H}$ and $\eta_{H_{WB}}$ respectively.

The horizontal stabilizer lift curve slope was estimated[9] at the test Reynolds number to allow determination of the dynamic pressure ratio (η_{H_T}) at the horizontal stabilizer.

Knowing

$$\bar{V}_H = \frac{S_H \ell_H}{S_W c_W} = 1.31 \tag{8}$$

$$a_H = .054/\text{degree} \tag{9}$$

then,

$$\eta_{H_T} = -C_{m_{i_{H_T}}} / a_H \bar{V}_H \tag{10}$$

B. (Continued)

From the test data, elevator effectiveness (τ_e) was determined from

$$\tau_e = C_{m_{\delta_{e_T}}} / C_{m_{i_{H_T}}} \qquad (11)$$

$$= .54$$

These equations were programmed to accept wind tunnel test pitching moment data. The resulting dynamic pressure ratio and wake angle are shown in Figures VII-6 through VII-11 for both rotor on and rotor off at each nacelle incidence angle tested. These figures show that for nacelle incidence angles of 90 and 75 degrees the rotors produce an upwash and an increase in dynamic pressure. These are similar characteristics as obtained during the aeroelastic model test.[2]

A constant dynamic pressure ratio was used at 60, 80, and 100 knots because only elevator sweeps were made at these speeds. As mentioned above, both incidences and elevator sweeps were shown to be methods of determining wake characteristics on the horizontal stabilizer. As the result of these two tests, the comparison between the two methods is valid only for the angle of attack that the elevator sweep was made or for configurations in which dynamic pressure was not expected to vary much with angle of attack. This was primarily the reason for making incidence sweeps during the second tunnel entry. Although incidence sweeps take longer than elevator sweeps, the test data are much more useful for analysis.

The measured wake angle at nacelle incidence angle of 75 degrees and 120 knots is considered questionable. At this airspeed, the other nacelle incidence angles show closer agreement with rotors-off downwash. No error was found in review of the analysis, but this condition is felt to be inconsistent with trends from this and other model tests.

The upwash from the rotors continually decreases as the nacelles are tilted forward from 60 degrees until the total wake angle is nearly the same as the rotors-off wing downwash value. Some scatter exists in comparing dynamic pressure ratio, but in general becomes that of the rotors-off value also.

As noted earlier, the total wake angle (ϵ_T) at the horizontal stabilizer is made up of the wing downwash ($\epsilon_{W/H}$) and the rotor wake ($\epsilon_{R/H}$). The rotor wake is represented in the tilt

B. (Continued)

rotor simulation math model in terms of the rotor induced velocity. It is computed from the ratio of rotor induced velocity in the plane of the horizontal stabilizer to the rotor induced velocity at the rotor disc ($W_{iR/H}/W_{iR}$) times the mean rotor induced velocity (W_{iR}). These two terms give the velocity of the rotor wake at the horizontal stabilizer (V_{H_R}). In order to obtain these parameters the following equation was used.

$$V_{H_R} = \left(\frac{W_{i_{R/H}}}{W_{i_R}}\right) W_{i_R} = V_{M.S.} \tan \epsilon_{R/H} \tag{12}$$

Therefore,

$$\left(\frac{W_{i_{R/H}}}{W_{i_R}}\right) = V_{M.S.} \tan \epsilon_{R/H} / W_{i_R} \tag{13}$$

Rotor induced velocity (W_{iR}) used was that calculated from the tilt rotor simulation math model corrected to model scale. The induced velocity ratio determined from this test and the aeroelastic model test are summarized in Figure VII-12. Both tests indicate the same trend with airspeed and show that the rotor wake in the plane of the horizontal is effectively eliminated above 120 knots for all nacelle incidence angles. With this type of wake reaction on the horizontal stabilizer, trim aircraft attitude becomes more nose down and longitudinal stick gradients are shallower than originally predicted with linearized rotor wake theory.

It should be noted that the downwash velocity (V_{HR}) is merely a convenient way to represent the rotor wake effects on the horizontal stabilizer and does not represent the actual wake from the rotor. This is illustrated by the fact that the vector sum of the free stream velocity ($V_{M.S.}$) and the downwash velocity (V_{HR}) is not the total velocity indicated by the total dynamic pressure ratio. Furthermore, the variation of downwash velocity with airspeed implies that it increases with airspeed, which is opposite to the momentum theory of rotor induced velocity. With the test data available at this time, it is not possible to separate the effect of the rotor wake on the wing downwash. Wing lift on the inboard section is considerably different with rotors on than with rotors off, and would change the contribution of the wing lift on the wing wake at the empennage. However,

B. (Continued)

combining the dynamic pressure ratio (η_{HT}) and downwash (ϵ_T) does give the correct empennage lift. Additional testing in this area would be required to obtain pressure distribution and local flow velocity data to properly describe these effects. Sideslip was found to reduce the magnitude of the upwash on the horizontal stabilizer as shown in Figure VII-13. The downwash velocity was determined by assuming the total dynamic pressure ratio to be equal to its value at zero sideslip. The reduction in upwash velocity causes a nose-up pitching moment when the aircraft is sideslipped. Comparison is also shown with the aeroelastic model test. Wake effects on the two empennage configurations are nearly the same. Free-flight testing of the aeroelastic model and the rotor simulation tests have shown that only a small amount of longitudinal cyclic stick is required to correct this pitch up and to maintain pitch attitude with yaw.

C. Rotor Wake on Vertical Stabilizer

Rotor wake effects on the vertical stabilizer were partially evaluated in terms of a parameter defined as the rotor sidewash factor (K_β). This is defined as the ratio of the vertical stabilizer yawing moment rotors on to rotors off and indicates the change in dynamic pressure ratio and sidewash due to the rotors. K_β is defined as follows:

$$K_\beta = \frac{\eta_{V_T} (1 - \partial\sigma/\partial\beta) \text{ ON}}{\eta_{V_{WB}} (1 - \partial\sigma/\partial\beta) \text{ OFF}} \qquad (14)$$

Rotor sidewash factor for the conventional vertical fin tested was compared with an H-tail[2] as shown in Figure VII-14. The airspeed shown was the only case in which data were available for both rotors on and rotors off. The conventional fin is shown to have more directional stability during low speed helicopter flight with rotors on than the H-tail configuration. In comparing other configurations tested for the conventional vertical fin with the H-tail, several other items were noted. Rotors off, the directional stability of the conventional fin is reduced for sideslip less than 8 degrees whereas the H-tail has more linear stability characteristics with sideslip. This is generally the case throughout the speed range tested. It would indicate that the effectiveness of the conventional fin is reduced at small sideslip angles due to the wing/fuselage wake. At low sideslip angles, the H-tail is outside this wake. At the higher sideslip angles, the conventional fin passes outside the wake to increase stability. With rotors on, low

C. (Continued)

speed helicopter flight, the rotor wake effect is also different between the two vertical tail configurations. The H-tail fins were shown[2] to be near the center of the vortices of the rotors which reduces directional stability due to reduced dynamic pressure. As the aircraft is sideslipped, the vortex cores shift with respect to the fuselage centerline to increase the effectiveness of the vertical fins. The conventional fin is located outside of these vortices in an area which causes it to have increased stability over that of the H-tail. As airspeed increases and the nacelles are tilted forward, the rotor wake effect decreases and the stability characteristics are similar to that for rotors off.

A comparison of the two fin configurations is shown in Figure VII-15 at zero fuselage angle of attack. At first appearance, both fin configurations show close to the same level of stability. Also shown are the results of additional testing at small angles using the Reference 2 model with a conventional fin. An additional reduction in stability was found for the conventional fin between ±2 degrees. The level of stability provided by this conventional fin configuration was found to be inadequate. Increasing the fin size to give the same level of stability as the H-tail would have required a very large fin. The difference in the two configurations became more apparent at angle of attack when the conventional fin becomes more immersed in the wing/fuselage wake. If low-speed characteristics were the only consideration, the conventional fin would appear to be better, but most of the low speed directional stability is provided by the rotors and SCAS. (Tilt rotor simulation tests, SCAS-off, have shown the handling qualities of the aircraft to be adequate and controllable with the reduced stability of the H-tail during low speed helicopter flight.) In high speed flight, where the fin is more effective and provides the major portion of the directional stability of the aircraft, the H-tail configuration with its linear characteristics were found to be more desirable.

TABLE VII-1. HOVER DOWNLOAD PARAMETERS (FULL SCALE)

Test	V/STOL 31/39	301-099-002[2]	TR-71-62[6]	200-094-270[7]
Wing Area(1), $m^2(ft^2)$	65.59 (706)	15.61 (168)	54.07 (582)	10.78 (116)
Wing Chord, m(ft)	3.38 (11.1)	1.59 (5.22)	2.62 (8.6)	1.14 (3.75)
Disc Area, $m^2(ft^2)$	182.46 (1964)	45.61 (491)	220.7 (2376)	38.55 (415)
Blade Twist, deg	25	40.9	37.0	10/20
Rotor Diam, m(ft)	15.24 (50)	7.62 (25)	16.76 (55)	7.62 (25)
S_W'/S_W(2)	.62	.75	.705	.65
c_f/c_w	.275	.25	.24	.22/.44
ℓ_m/D	.204	.187	.125	.161

(1) Measured between centerline of rotors, S_W

(2) Wing area under rotor disc, S_W'

TABLE VII-2. HOVER DOWNLOAD

Test	V/STOL 31/69	301-099-002[2]	TR-71-62[6]	200-094-270[7]
Model Scale	1/10	1/5	1/10	1/4
C_T	.1147	.111	.0085	.0042
V_T, m/sec (fps)				
Model Scale	150.26 (493)	100.58 (330)	228.6 (750)	169.77 (557)
Full Scale	250.55 (822)	225.55 (740)	228.6 (750)	212.14 (696)
W_{iR}(1), m/sec (fps)				
Model Scale	12.98 (42.6)	8.59 (28.2)		
Full Scale	21.64 (71.0)	19.23 (63.1)		
R_N(2)				
Model Scale	4.8×10^5	3.04×10^5		
Full Scale	8.0×10^6	3.36×10^6		

(1) Rotor induced velocity computed using the digital tilt rotor simulation program

(2) $R_N = \frac{1.5 * W_{iR} * C_W}{\nu}$

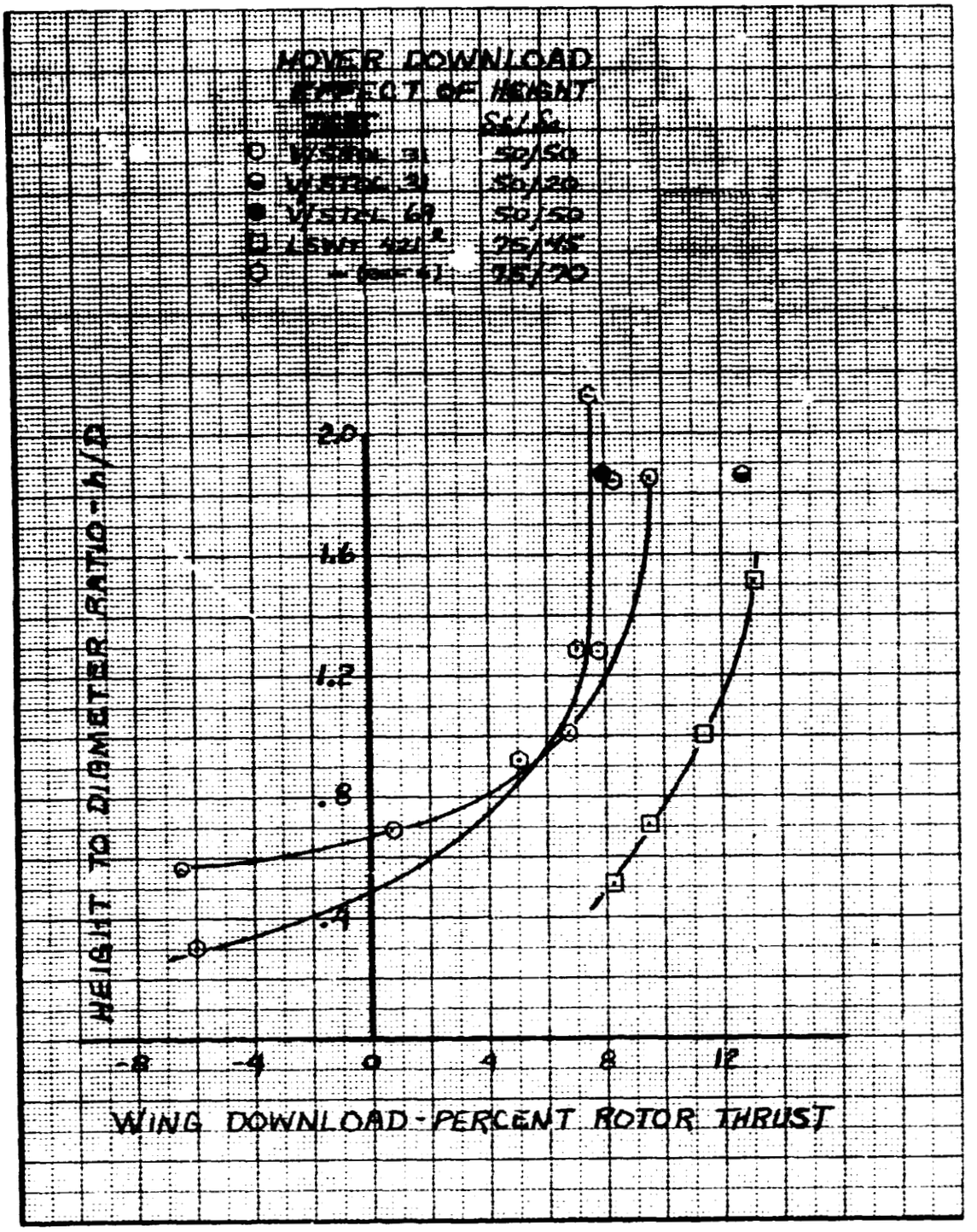

Figure VII-1. Wing Download Comparison in Hover.

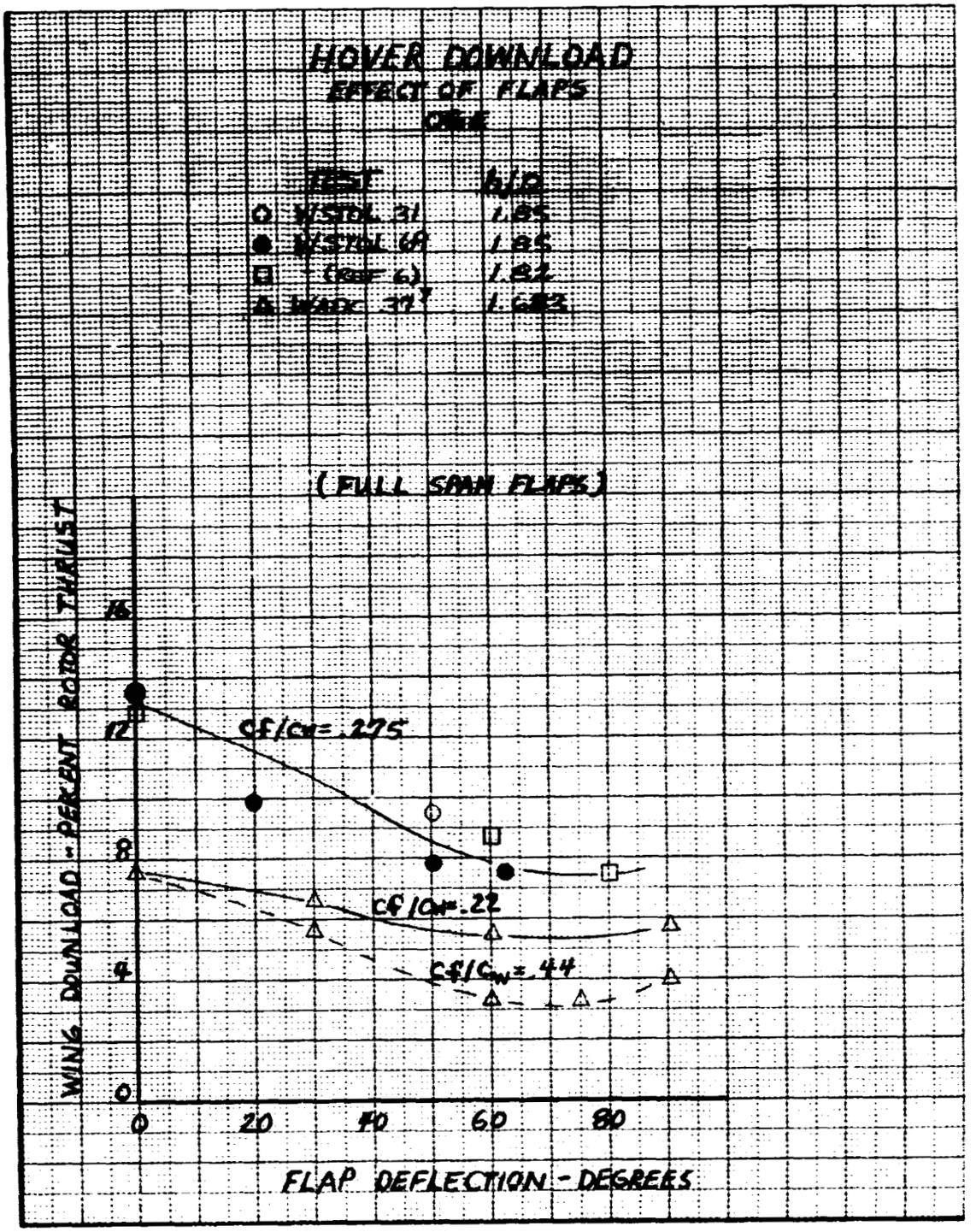

Figure VII-2. Wing Download Comparison in Hover for Flap Deflection, OGE.

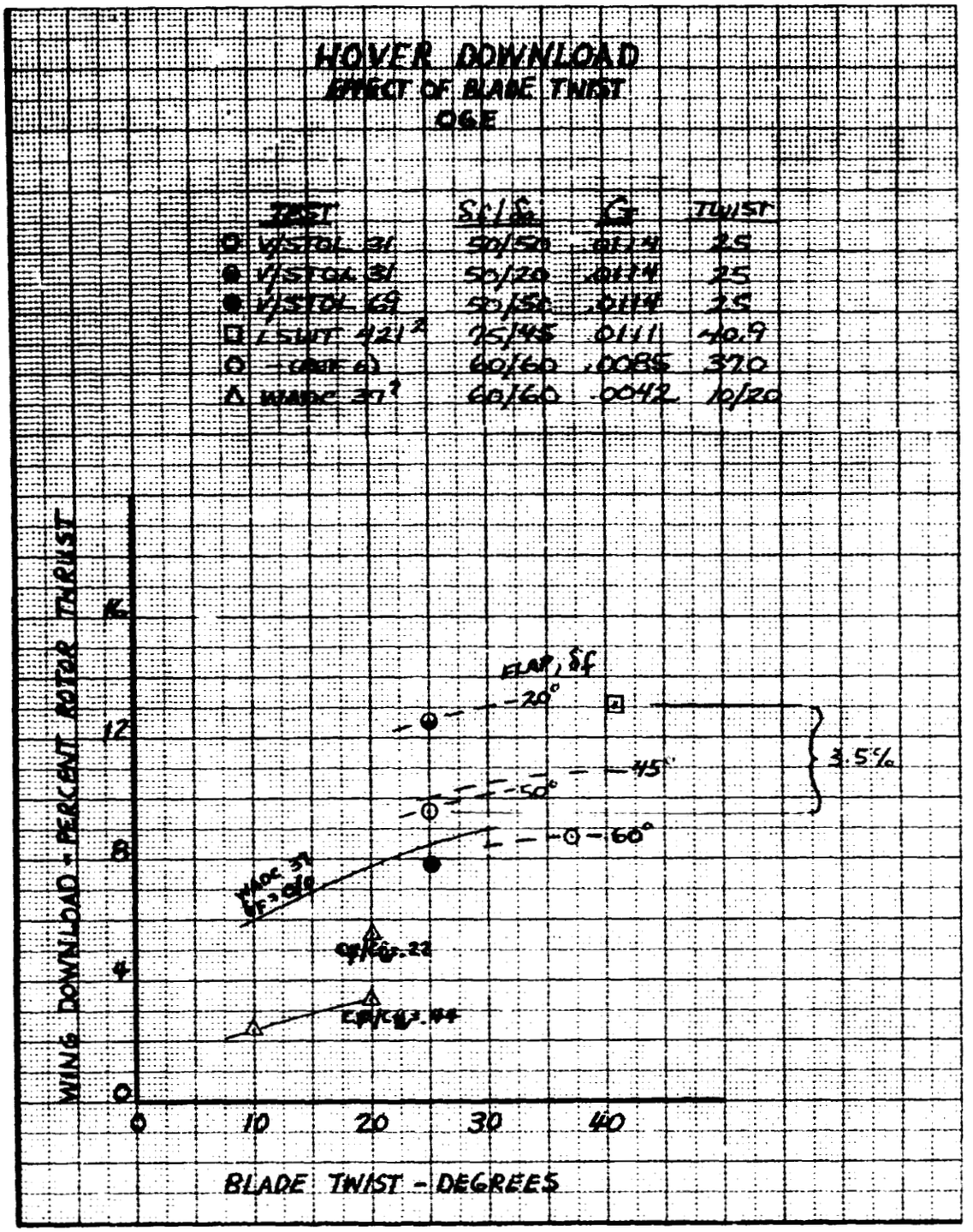

Figure VII-3. Wing Download Comparison in Hover for Blade Twist, OGE.

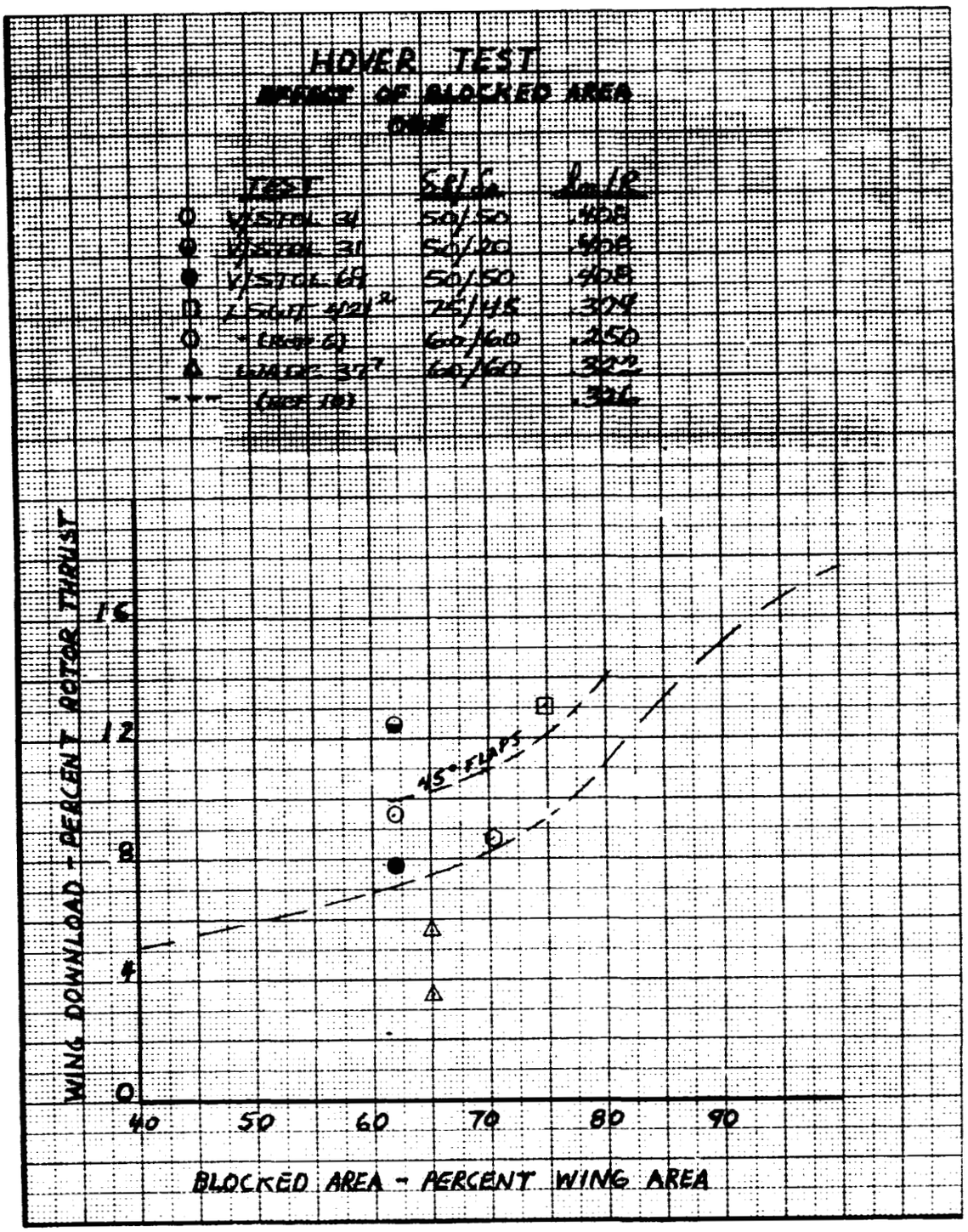

Figure VII-4. Wing Download Comparison in Hover for Blocked Area, OGE.

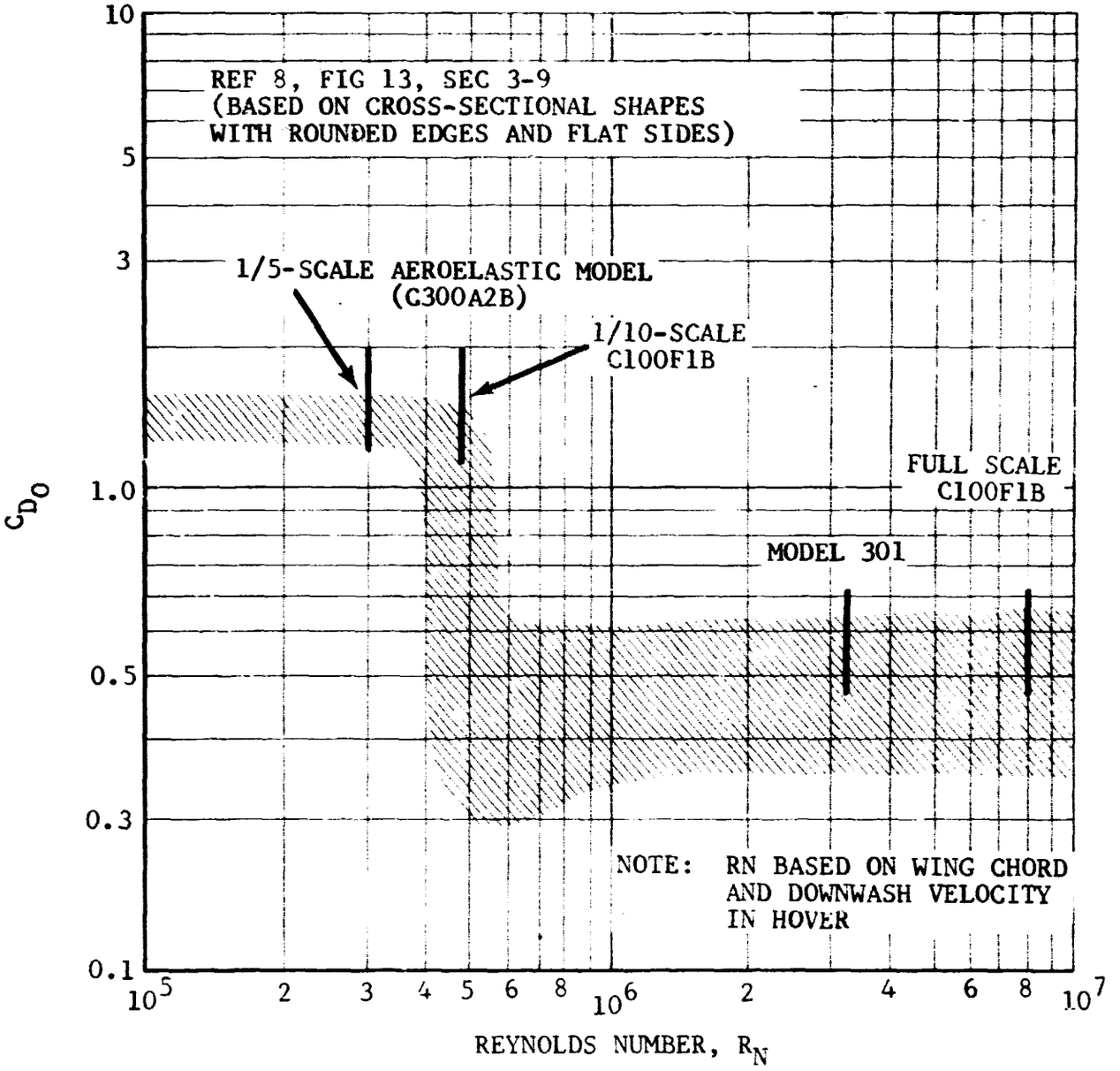

Figure VII-5. Variation of Wing Drag Coefficient at $\alpha_w = -90°$ with Reynolds Number.

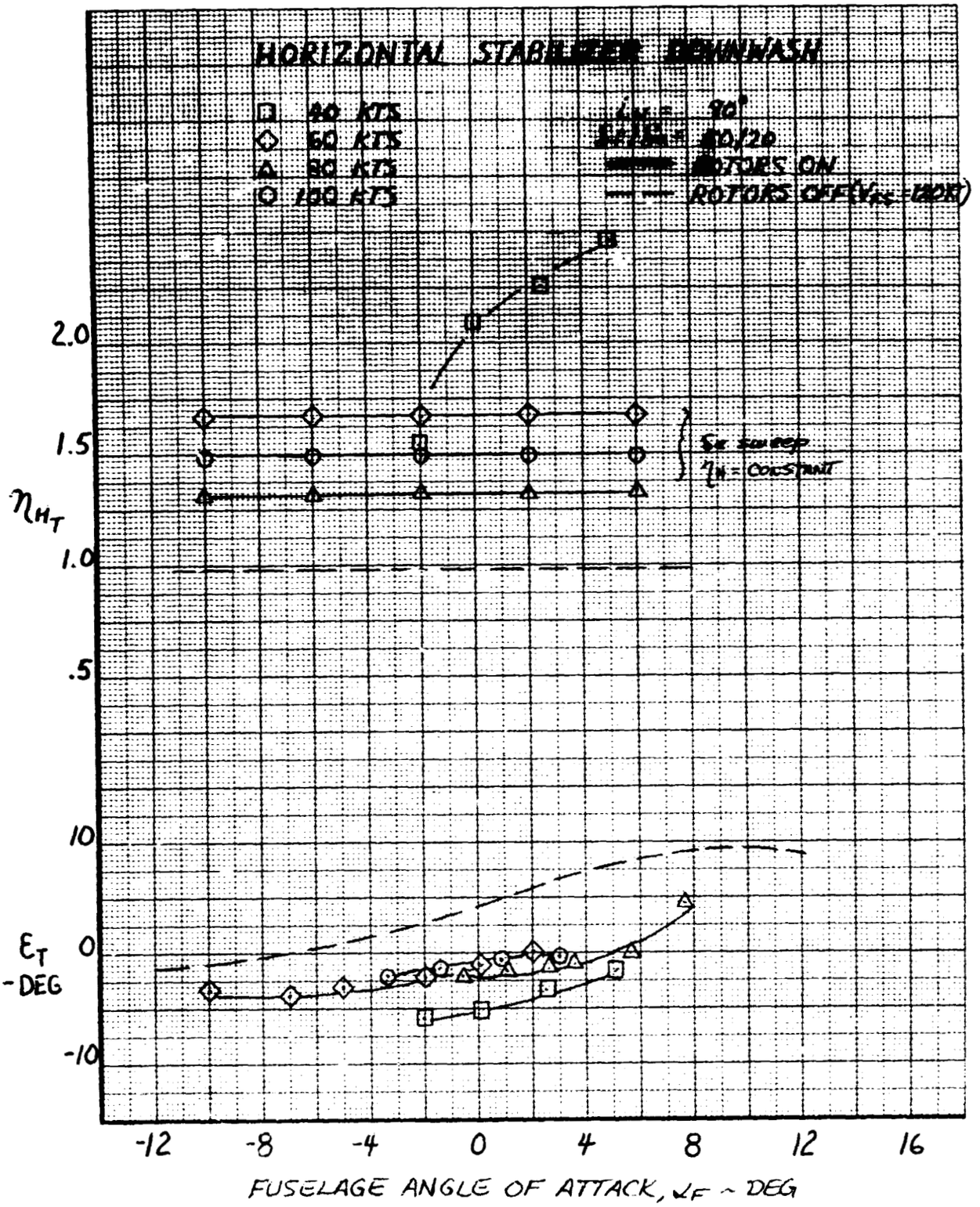

Figure VII-6. Horizontal Stabilizer Aerodynamic Characteristics, Nacelle Incidence 90°.

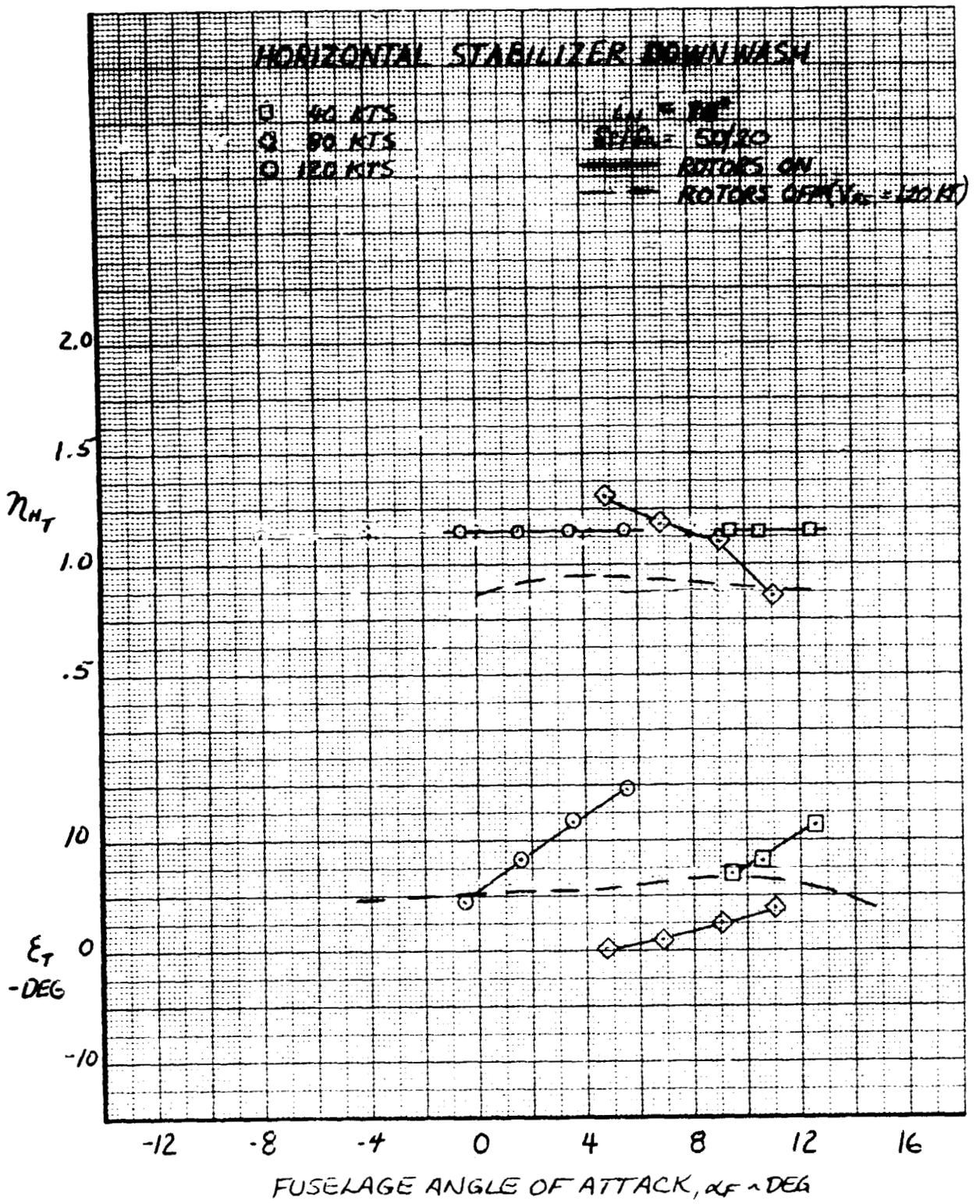

Figure VII-7. Horizontal Stabilizer Aerodynamic Characteristics, Nacelle Incidence 75°.

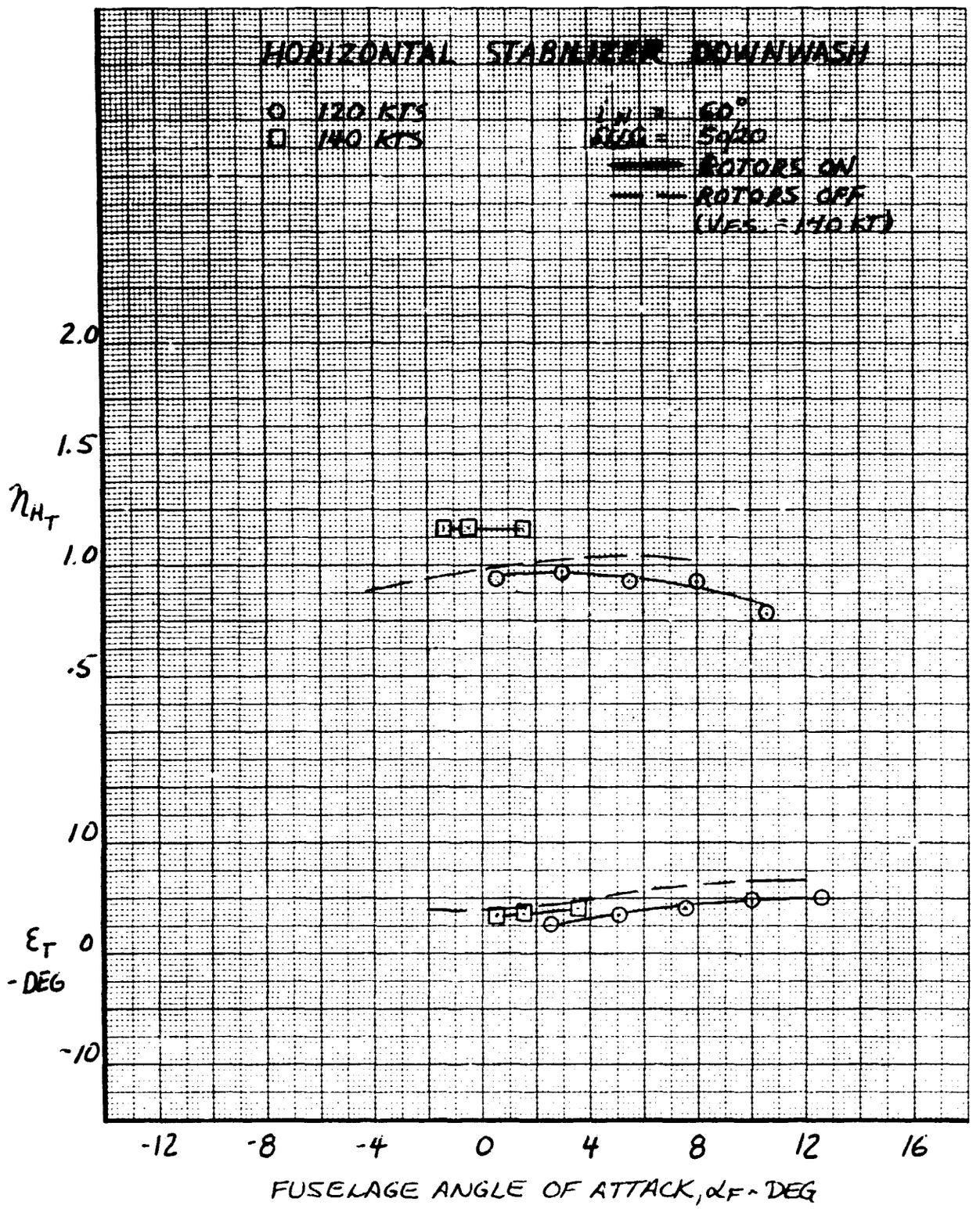

Figure VII-8. Horizontal Stabilizer Aerodynamic Characteristics, Nacelle Incidence 60°.

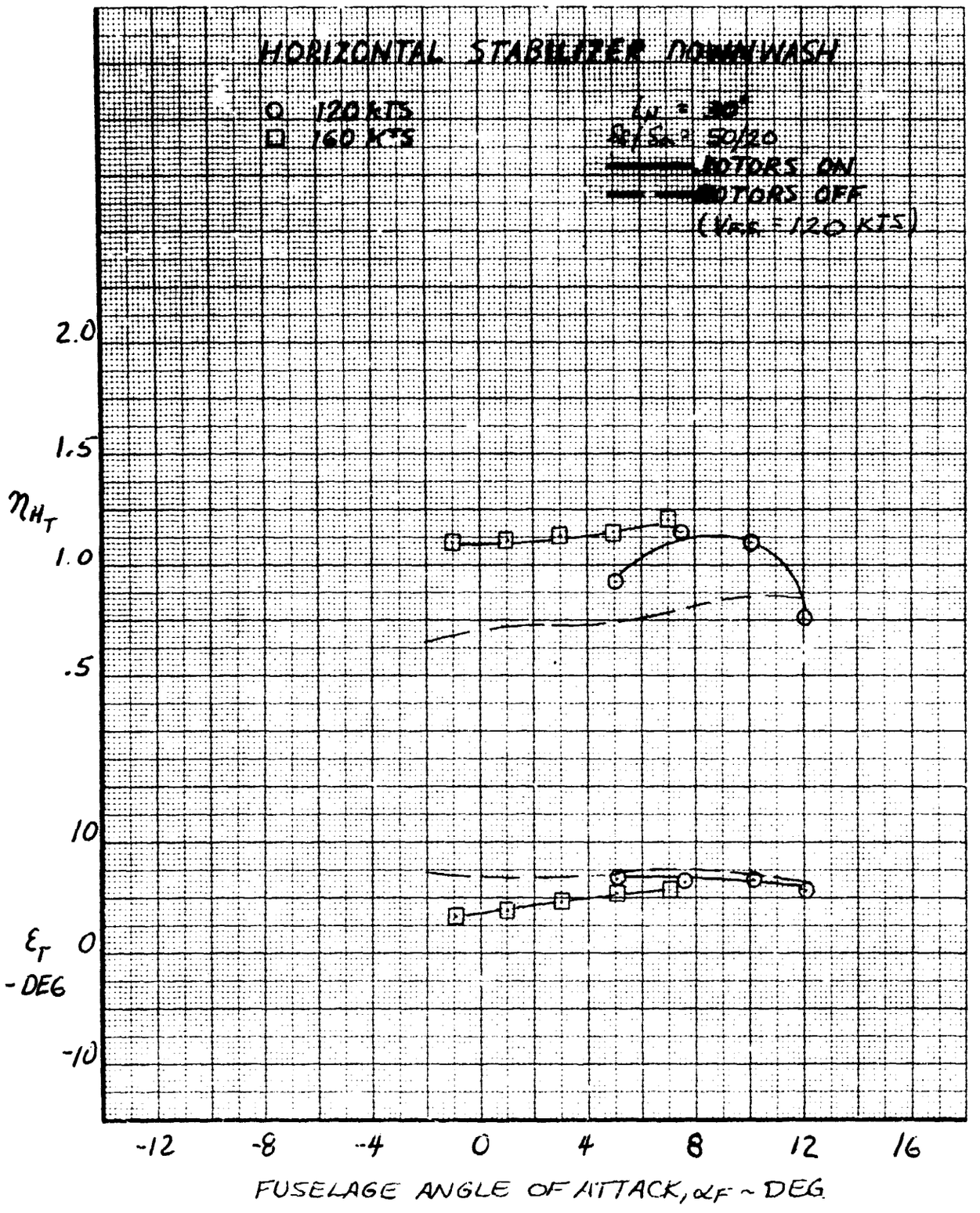

Figure VII-9. Horizontal Stabilizer Aerodynamic Characteristics, Nacelle Incidence 30°.

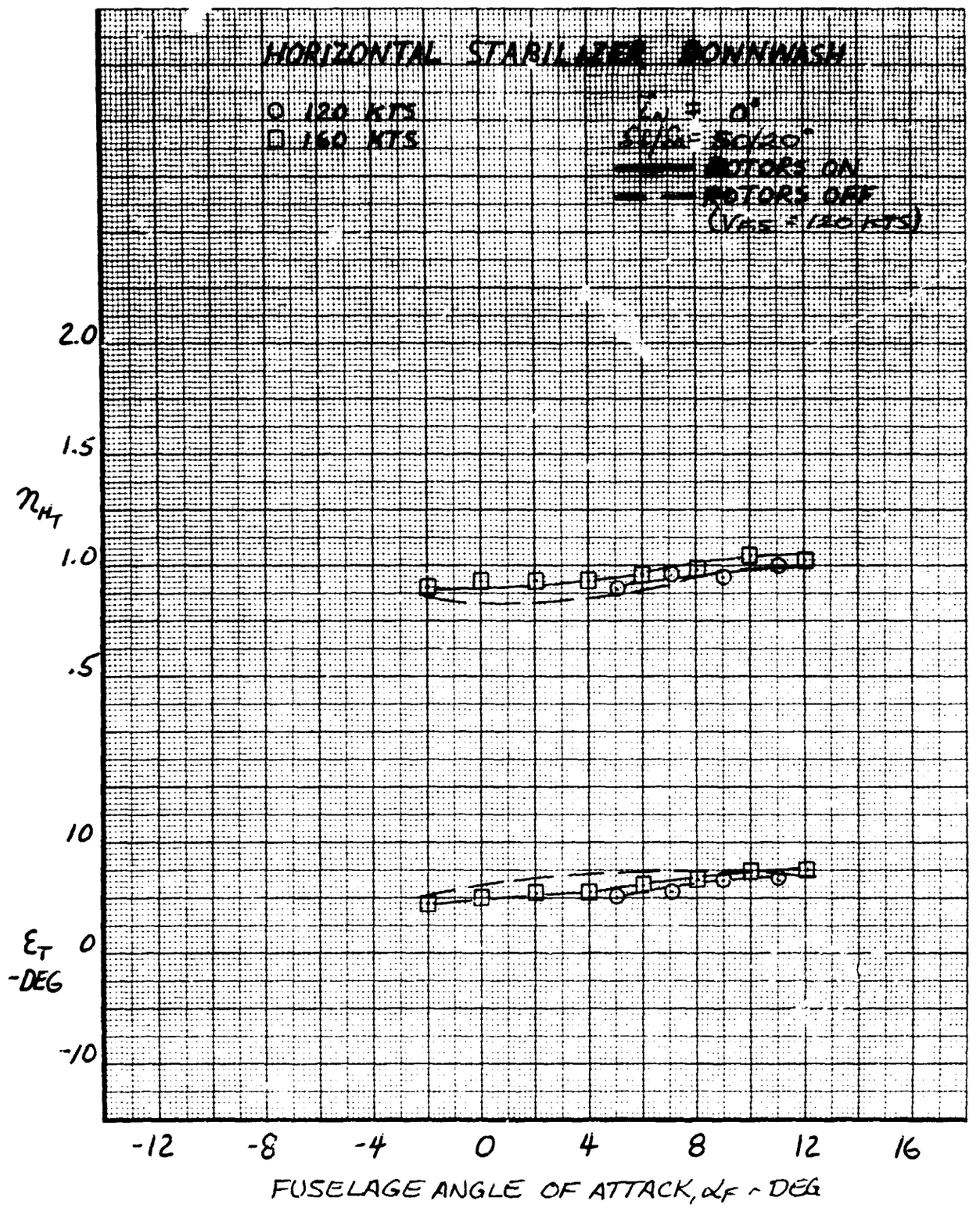

Figure VII-10 Horizontal Stabilizer Aerodynamic Characteristics, Nacelle Incidence 0°.

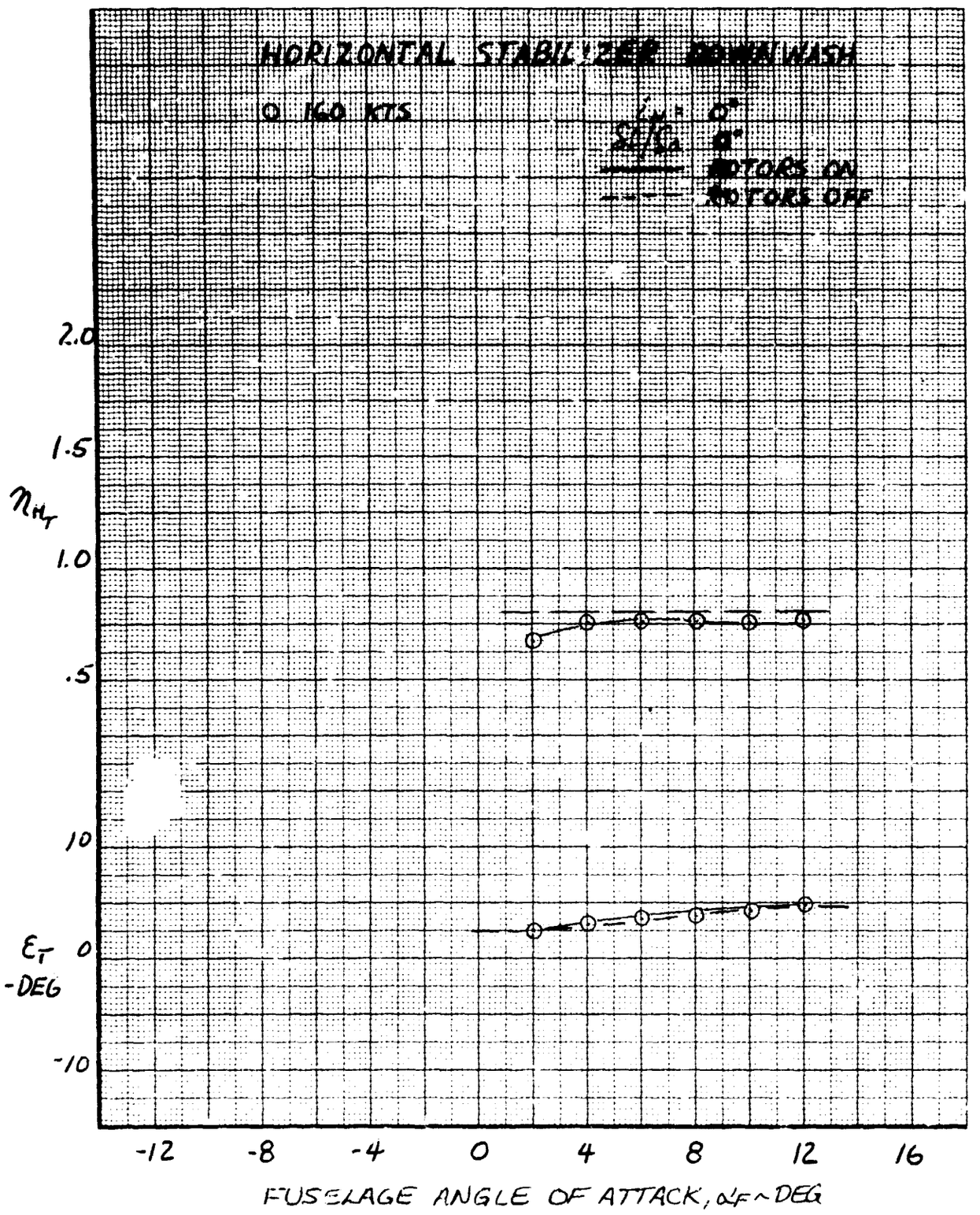

Figure VII-11. Horizontal Stabilizer Aerodynamic Characteristics, Nacelle Incidence 0°, Flaps Up.

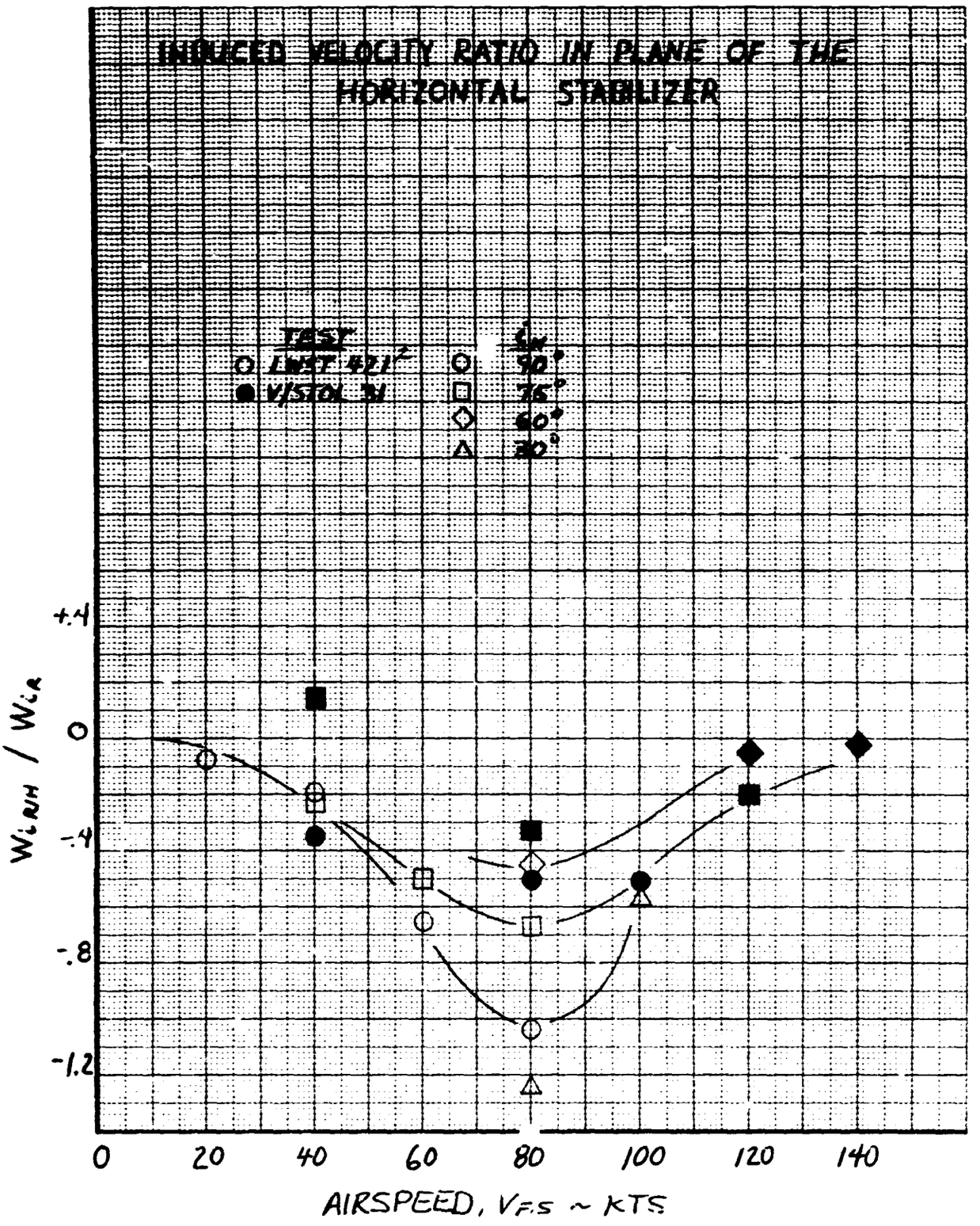

Figure VII-12. Induced Velocity Ratio in Plane of the Horizontal Stabilizer.

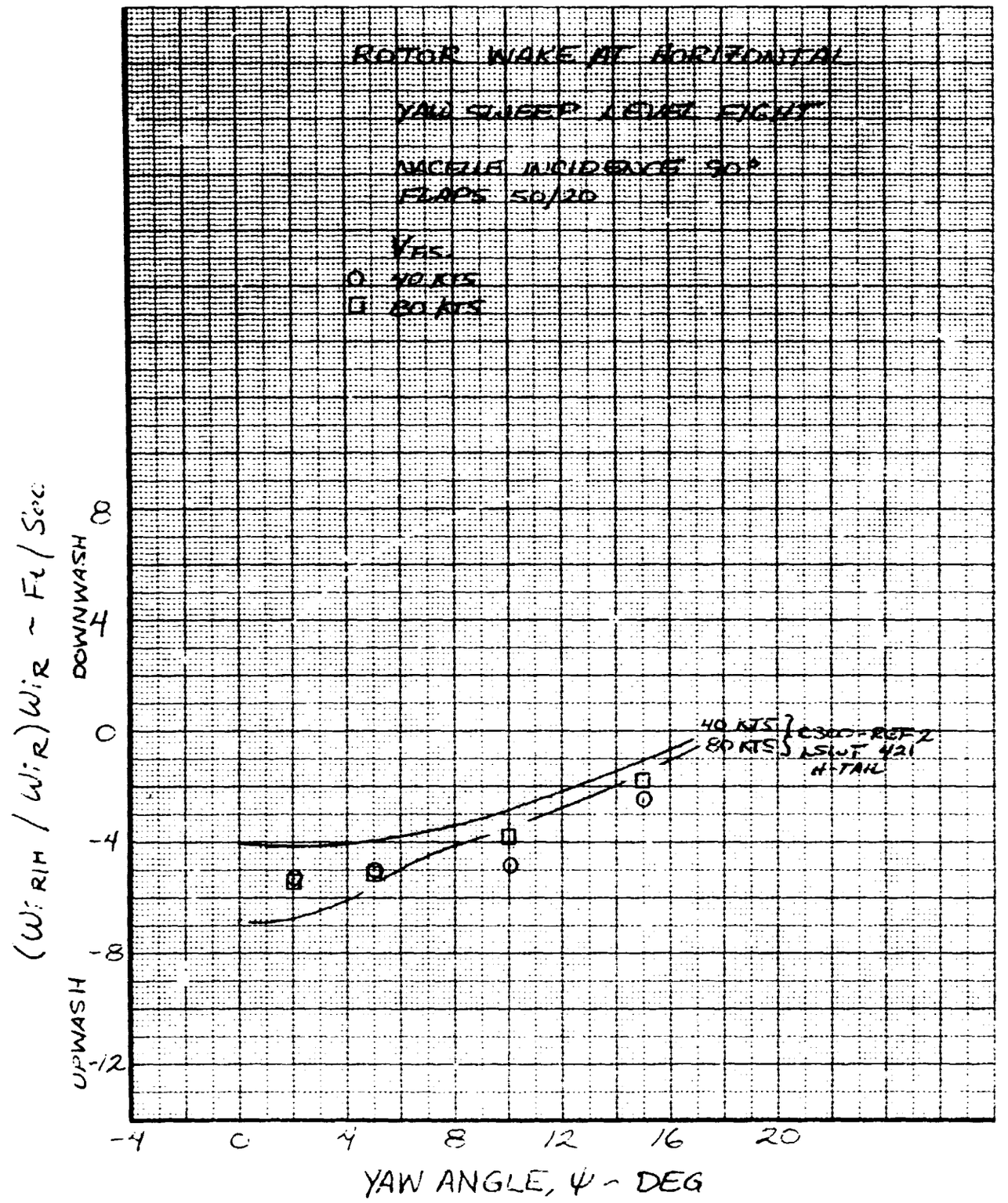

Figure VII-13. Effect of Yaw Angle on Rotor Wake Upwash at Horizontal Stabilizer, Nacelle Incidence 90°.

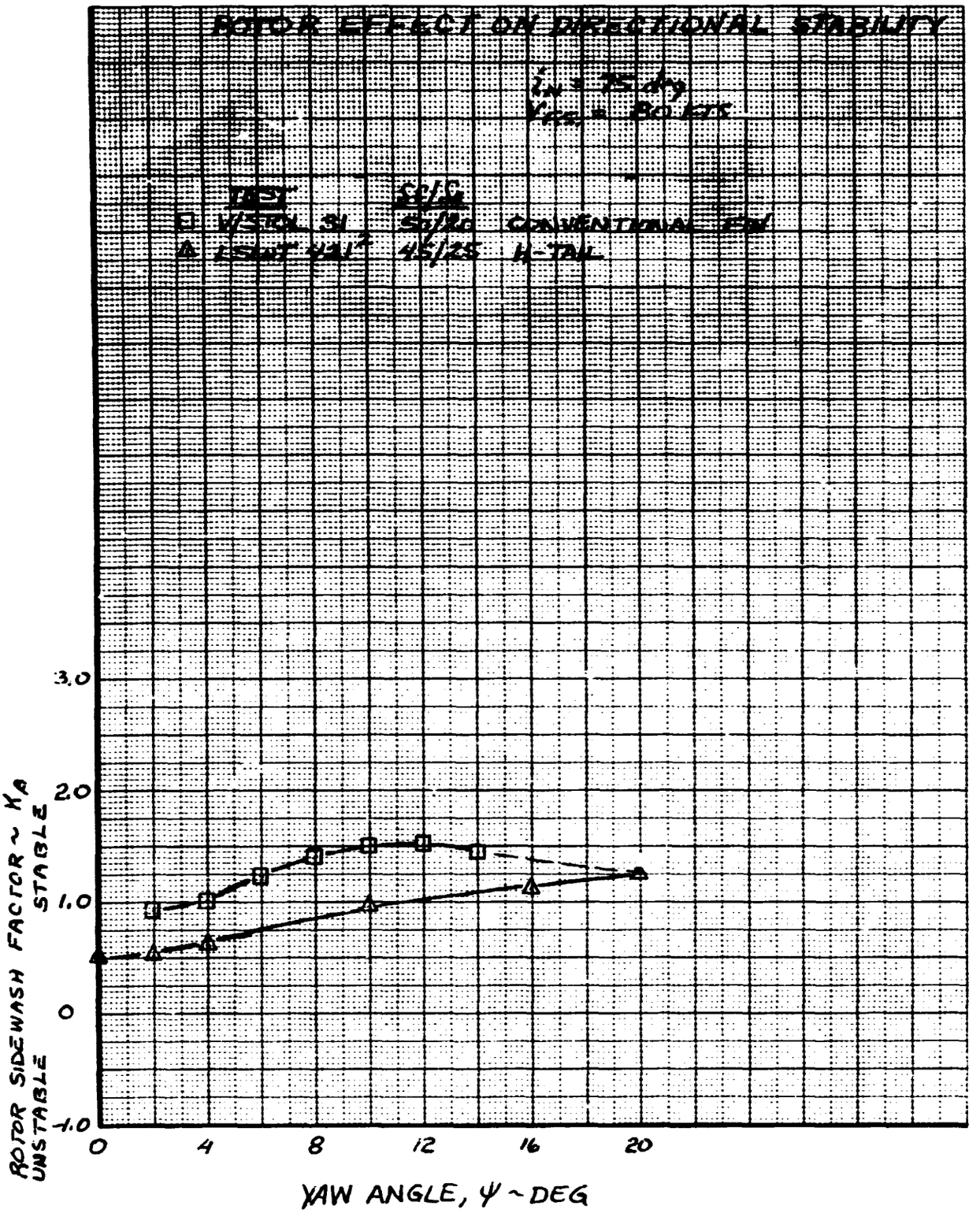

Figure VII-14. Effect of Rotor Wake on Directional Stability, Nacelle Incidence 75°.

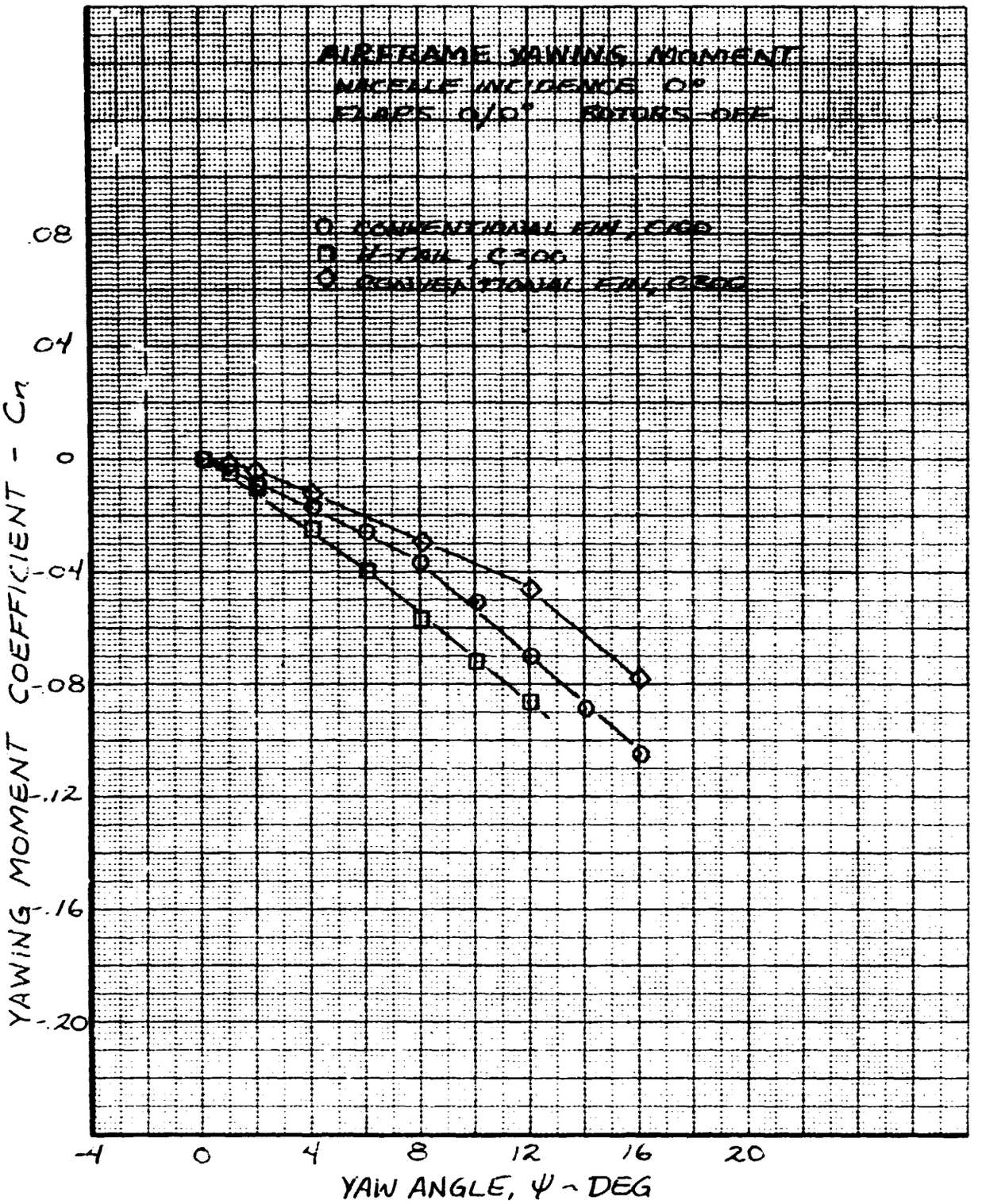

Figure VII-15. Effect of Fin Configuration on Yawing Moment Coefficient.

VIII. CONCLUSIONS

The following conclusions are made from analysis of the test data:

A. Roll Stability - IGE

Static roll stability characteristics obtained during hover tests in ground effect were in agreement at small roll angles with that determined during other model tests. A roll instability is obtained as the aircraft approaches touchdown between h/D = 1.67 and .60 with the maximum instability occurring at h/D = .85. This instability does not appear to present a significant problem for current generation tilt rotor aircraft with the improved control power available and addition of SCAS.

B. Wing Download

Characteristics of wing download were determined during hover in and out of ground effect, with flap deflection, and in forward flight. Hover download in addition to being a function of h/D and flap deflection was found to be influenced by blade twist, percent blockage area of the wing under the rotor, and Reynolds number.

Very little improvement in relieving wing download during hover was obtained for flap deflections above 50 degrees. Results indicate that most of the reduction in download is due to flaperon deflection rather than flap deflection. Download was also found to increase with increasing blade twist and the blocked area under the rotor. Hover download measured during model tests are subject to Reynolds number effect. For the configurations tested, the download for the full-scale aircraft would be approximately 50 percent lower than the model scale value. The full-scale aircraft is estimated to have a 6.5 percent download OGE.

Rotor/wing lift sharing during forward flight was determined. Results indicated that the wing lift is not influenced by the rotor wake above 40 knots and that the wing begins to contribute lift at an airspeed of 35 knots. Above 120 knots and nacelle incidence angle of less than 60 degrees, the rotor wake was found to not contribute much to wing lift.

C. Rotor Wake on the Empennage

During low speed helicopter and conversion flight the interaction between the rotor wake and the horizontal stabilizer

C. (Continued)

is such to produce a nose down pitching moment. This results from a net upwash effect and increased dynamic pressure on the horizontal stabilizer from the rotors. Rotor wake effects are essentially eliminated at airspeeds above 120 knots.

Rotor wake effects on the vertical fin during low speed helicopter were found to be less apparent on the conventional vertical fin than for the H-tail. This is not compatible with the low directional stability characteristics observed for the XV-3 which also had a conventional vertical fin. Additional empennage testing using the same model would be desirable to describe the rotor wake effect for different empennage configurations. Directional stability of the H-tail during high speed flight is more linear with yaw angle than the conventional fin.

As the result of these tests and analyses, the following items have been incorporated in the tilt rotor simulation math model:

1. Improved the wing download variation with flaps, ground effect, and airspeed;

2. Modified the induced velocity variation at the empennage; and

3. Modified the roll stability in-ground-effect.

IX. LIST OF REFERENCES

1. Wilson, J.: "NASA-Langley Research Center V/STOL Wind Tunnel Test Results of Powered Force Tilt Rotor Aircraft," NASA-Langley TM, to be published.

2. BHC Report 301-099-002, "V/STOL Tilt Rotor Study - Volume VI, Hover, Low Speed and Conversion Tests of a Tilt Rotor Aeroelastic Model," NASA CR 114615, May 15, 1973.

3. BHC Report 299-199-084, "Proposal for Wind Tunnel Tests of a Powered Tilt Rotor Force Model," March 1972.

4. BHC Report 301-099-001, "V/STOL Tilt Rotor Study - Volume V, A Mathematical Model for Real Time Flight Simulation of the Bell Model 301 Tilt Rotor Research Aircraft," NASA CR 114614, April 13, 1973.

5. Marr, R.: "Handling Qualities Evaluation of the XV-15 Tilt Rotor Aircraft," American Helicopter Society Preprint No. 840, May 1974.

6. Anon: "Volume V, Wind Tunnel Test of a Powered Tilt Rotor Performance Model," AFFDL-TR-71-62, October 1971.

7. BHC Report 200-094-270, "Results of the Wind Tunnel Tests of the Quarter-Scale Semi-Span Model of the Bell XV-3 Tilting-Rotor Convertiplane," September 18, 1958.

8. Hoerner, S. F.: Fluid-Dynamic Drag, 1965.

9. Anon: USAF Stability and Control Datcom, Air Force Flight Dynamics Laboratory, Wright-Patterson Air Force Base, October 1960 (Rev. February 1972).

10. McKee, J. W.: "Experimental Investigation of the Drag of Flat Plates and Cylinders in the Slip Stream of a Hovering Rotor," NACA TN 4239, April 1958.

APPENDIX A

Run Schedule Summary

(A description of the configuration code is given in Table V-2, page V-5.)

RUN SCHEDULE SUMMARY
MODEL C100-F1B LANGLEY V/STOL TEST 31

RUN NO.		$V_{F.S.}$ (KTS)	iN (DEG)	CONFIG. NO.	RPM	h/D
10	Walls Up - Coll. Sweep	0	90	1-2-6	1884	
11	- Cyclic	0				
12	- Coll.	20				
13	- α	20				
14	- ψ	20				
15	Void					
16	- Coll.	40				
17	- α					
18	Void					
19	Walls Up - ψ	40				
20	Walls Dn - Coll.	20				
21	- Coll.	40				
22	- α					
23	- Cyclic					
24	- $\Delta\theta_1$					
25	- ΔB_1					
26	- ψ					
27	- δ_e					
28				1-2-6		
29	- α			2-0-6		
30	- ψ					
31	- Coll.	40				
32	- Coll.	80				
33	Void					
34	- ψ					
35	Void		90			
36	- α		0	2-0-6		
37				1-2-6		
38						
39						
40	- ψ	80				
41	- Coll.	120				
42	- Coll.	120				
43	- Coll.	100				
44	- δ_e					
45	- Cyclic					
46	- $\Delta\theta$					
47	- α	100				
48	- Cyclic	80	0	1-2-6	1884	
49	- V	40,80,100,120	15	1-2-5	1604	
50	- V	40,80,100,120			1884	
51	- Coll.	40				
52	- α					
53	- δ_e					
54	- Cyclic					
55	- $\Delta\theta$					
56	Walls Dn - ΔB_1 Sweep	40	15	1-2-5	1884	

RUN SCHEDULE SUMMARY
MODEL C100-F1B LANGLEY V/STOL TEST 31
(Continued)

RUN NO.		$V_{F.S.}$ (KTS)	i_N (DEG)	CONFIG. NO.	RPM	h/D
57	Walls Dn - Coll. Sweep	80	15	1-2-5	1884	
58	- α	↓	↓	↓	↓	
59	- δ_e	↓	↓	↓	↓	
60	- Cyclic	80	↓	↓	↓	
61	- Coll.	120	↓	↓	↓	
62	- α	↓	↓	↓	↓	
63	- δ_e	↓	↓	↓	↓	
64	- Cyclic	↓	↓	↓	↓	
65	- $\Delta\theta$	↓	↓	↓	↓	
66	Walls Dn - ΔB_1	120	15	1-2-5	↓	
67	Walls Up - Coll.	0	0	1-2-6	↓	1.84
68	- Cyclic	↓	↓	↓	↓	
69	- ΔB_1	↓	↓	↓	↓	
70	- ϕ	↓	↓	↓	↓	
71	- $\Delta\theta$	↓	↓	↓	↓	1.84
72	- Coll.	↓	↓	↓	↓	1.00
73	- α	↓	↓	↓	↓	
74	- Cyclic	↓	↓	↓	↓	
75	- ϕ	↓	↓	↓	↓	
76	- δ_e	↓	↓	↓	↓	
77	- $\Delta\theta$	↓	↓	↓	↓	1.00
78	- Coll.	↓	↓	↓	↓	.83
79	- ϕ	↓	↓	↓	↓	.83
80	- Coll.	↓	↓	↓	↓	.67
81	Void	↓	↓	↓	↓	.67
82	- ϕ	↓	↓	↓	↓	.67
83	- Coll.	↓	↓	↓	↓	.53
84	- Cyclic	↓	↓	↓	↓	.53
85	- Cyclic	↓	↓	↓	↓	.53
86	- ϕ	↓	↓	↓	↓	.53
87	Walls Up - δ_e	0	↓	1-2-6	↓	
88	Walls Dn - Coll.	100	↓	2-0-6	↓	
89	- α	100	0	2-0-6	↓	
90	- Coll.	40	15	2-0-5	↓	
91	- α	40	15	2-0-5	↓	
92	- Coll.	80	15	2-0-5	↓	
93	- α	80	15	2-0-5	1884	
94	- Coll.	120	30	1-2-4	1604	
95	- α	↓	↓	↓	↓	
96	- δ_e	↓	↓	↓	↓	
97	- Cyclic	↓	↓	↓	↓	
98	- $\Delta\theta$	↓	↓	↓	↓	
99	Walls Dn - ΔB_1 Sweep	120	30	1-2-4	1604	

RUN SCHEDULE SUMMARY
MODEL C100-F1B LANGLEY V/STOL TEST 31
(Continued)

RUN NO.		$V_{F.S.}$ (KTS)	iN (DEG)	CONFIG NO.	RPM	h/D
100	Walls Dn - Coll. Sweep	140	30	1-2-4	1604	
101	- α	140	30	1-2-4		
102	- δ_e	140	30	1-2-4		
103	- Coll.	120	60	1-2-2		
104	- α					
105	- δ_e					
106	- Cyclic					
107	- ΔB_1		60	1-2-2		
108	- Coll.		30	2-0-4		
109	- α	120	30	2-0-4		
110	- Coll.	140	30	2-0-4		
111	- α	140	30	2-0-4		
112	- Coll.	120	60	2-0-2		
113	- Coll.	120	60	2-0-2		
114	- Coll.	120	60	2-0-2		
115	- α	120	60	2-0-2	1604	
116	- Coll.	80	15	1-2-5	1884	
117	- α	80		1-2-5		
118	- δ_e	80		1-2-5		
119	- Coll.	120		2-0-5		
120	- α	120		2-0-5		
121	- Coll.	80		2-0-6		
122	- α	80	15			
123	- Coll.	20	0			
124	- α	20				
125	- Coll.	40				
126	- α	40				
127	- ψ	20				
128	Walls Dn - ψ Sweep	40		2-0-6	1884	
	End of Powered Test					
129	Walls Up - ϕ Sweep	0		1-2-6	0	
	Rotors Off Test					
130	Walls Dn - α	80		3-2-6		
131	- α	120				
132	- α	160				
133	- ψ	160				
134	- ψ Sweep	120				
135	- ψ (α = 5°)	160				
136	- ψ (α = 10°)					
137	- ψ (α = -10°)					
138	- δ_e Sweep					
139	- δ_e					
140	Walls Dn - α Sweep	160	0	3-2-6	0	

RUN SCHEDULE SUMMARY
MODEL C100-F1B LANGLEY V/STOL TEST 31
(Continued)

RUN NO.		$V_{F.S.}$ (KTS)	i_N (DEG)	CONFIG. NO.	RPM	h/D
141	Walls Dn - ψ Sweep	160	0	3-2-6	0	
142	- ψ (α = -5°)	160	↓	3-2-6	↓	
143	- δ_e Sweep	120		3-2-6		
144	- δ_e ↓	160	↓	3-3-6		
145	- α	160	0	3-3-6		
146	- α	120	15	3-2-5		
147	- ψ	160	15	3-2-5		
148	- ψ Sweep	160	15	3-2-5		
149	- ψ (α = -10°)	160	15	3-2-5		
150	- α Sweep	120	30	3-2-4		
151	- α	160	30	3-2-4		
152	- ψ	160	30	3-2-4		
153	- α	120	45	3-2-3		
154	- α	160	45	3-2-3		
155	- ψ	160	45	3-2-3		
156	- α	120	60	3-2-2		
157	- α	160	60	3-2-2		
158	- ψ	↓	60	3-2-2		
159	- α		90	3-2-0		
160	- δ_e		↓	3-2-0		
161	- ψ			3-2-0		
162	- α			4-0-0		
163	- ψ		90	4-0-0		
164	- α		60	4-0-2		
165	- ψ		60	4-0-2		
166	- α		30	4-0-4		
167	- ψ		30	4-0-4		
168	- α Sweep		0	4-0-6		
169	- ψ (α = 0°)		0	4-0-6		
170	- ψ (α = 10°)	↓	0	4-0-6	↓	
171	Walls Dn - ψ (α = -10°)	160	0	4-0-6	0	

RUN SCHEDULE SUMMARY
MODEL C100-F1B LANGLEY V/STOL TEST 69

RUN NO.		$V_{F.S.}$ (KTS)	i_N (DEG)	CONFIG. NO.	RPM	h/D
176	Walls Dn - Coll. Sweep	40	90	1-2-6	1884	
177	- α	40	90	1-2-6		
178	- ψ	40	90	1-2-6		
179	- α	40	90	1-1-6		
180	- α	80	75	1-1-5		
181	- α			1-1-5		
182	- α			1-2-5		
183	- Coll.			1-2-5		
184	- ψ	80	75	1-2-5	1884	
185	- Coll.	120	60	1-2-4	1604	
186	- α			1-2-4		
187	- ψ			1-2-4		
188	- α		60	1-1-4		
189	- α	120	30	1-1-2		
190	- α	160		1-1-2		
191	- ψ	120		1-2-2		
192	- Coll.	120				
193	- α	120				
194	- Coll.	160				
195	- Cyclic					
196	- δ_e Sweep					
197	- Roll Tare					
198	- ψ Sweep					
199	- Roll Tare					
200	- α Sweep	160	30	1-2-2		
201	- Roll Tare		0			
202	- Thrust Checks					
203	- Coll. Sweep	120		1-2-0		
204	- α	120				
205	- ψ	120				
206	- Coll.	160				
207	- α	160				
208	- ψ Sweep	160		1-2-0		
209	- Thrust Checks					
210	- Thrust Checks					
211	- α Sweep	120		1-1-0		
212	- δ_e	120				
213	- α	160				
214	- δ_e				1604	
215	- Coll.			5-2-0	1372	
216	- α					
217	- δ_e	160				
218	- Coll	180				
219	- α	180				
220	Walls Dn - δ_e Sweep	180	0	5-2-0	1372	

RUN SCHEDULE SUMMARY
MODEL C100-F1B LANGLEY V/STOL TEST 69
(Continued)

RUN NO.		$V_{F.S.}$ (KTS)	i_N (DEG)	CONFIG. NO.	RPM	h/D
221	Walls Dn - Coll. Sweep	120	0	1-2-0	1372	
222	- α	120				
223	- δ_e	120				
224	- ψ	120				
225	- Coll.	180				
226	- α	180				
227	- ψ	180			1372	
228	- δ_e	160			1604	
229	- δ_e	120		1-2-0	1604	
230	- α	120		1-1-0	1372	
231	- α	180		1-1-0		
232	- α	160		5-1-0		
233	- α	180		5-1-0		
234	- ψ	160		5-2-0		
235	- ψ	180				
236	- α	160				
237	- α	160				
238	- α	180		5-2-0		
239	- ψ	120		9-2-0		
240	- α	120	0	9-2-0	1372	
241	- α	120	30	2-0-2	1604	
242	- α	120		2-0-2		
243	- α	160		2-0-2		
244	- ψ	120		2-4-2		
245	- α	120		2-4-2		
246	- α	160		2-4-2		
247	- ψ	160	30	2-4-2		
248	- α	120	0	2-4-0		
249	- ψ	120	0	2-4-0		
250	- α	160	0	2-4-0		
251	- ψ	160	0	2-4-0		
252	- α	120	60	2-4-4		
253	- ψ	120	60	2-4-4		
254	- α	120	60	2-4-4		
255	Walls Dn - ψ	120	60	2-4-4	1604	
256	Walls Up - Coll.	0	90	1-2-6	1884	
257	- α	20				
258	- α	30				
259	- α	40				
260	- α	50				
261	- α	60		1-2-6		
262	- α	20		1-1-6		
263	- α	30				
264	- α	40				
265	- α	50				
266	Walls Up - ψ Sweep	40	90	1-1-6	1884	

RUN SCHEDULE SUMMARY
MODEL C100-F1B LANGLEY V/STOL TEST 69
(Continued)

RUN NO.			$V_{F.S.}$ (KTS)	i_N (DEG)	CONFIG. NO.	RPM	h/D
267	Walls Up - α	Sweep	20	90	2-4-6	1884	
268	- α		30				
269	- α		40				
270	- α		50				
271	Walls Up - ψ	Sweep	40		2-4-6		
272	Walls Dn - α	Sweep, Slots Open	20		1-2-6		
273	- α		30				
274	- α		40				
275	- α		50				
276	- α	Sweep, Slots Open	60				
277	- α		20				
278	- α		30				
279	- α		40				
280	- α		50				
281			80				
282			80				
283	- α		40		1-2-6		
284	- Coll.		0		5-2-6		1.83
285	- Coll.				5-2-6		
286	- Coll.				5-2-6		
287	- Coll.				5-2-6		
288	- Roll				1-2-6		1.83
289	- Roll						1.0
290	- Roll						.83
291	- Roll						.67
292	- Roll	Sweep	0				.53
293	- α	Sweep	60				
294	- α		50	90	1-2-6	1884	
295	- α		120	60	1-2-4	1604	
296	- ψ		120	60	1-2-4		
297	- α		120	30	1-2-2		
298	- ψ		120	30	1-2-2		
299	- α		160	30	1-2-2		
300	- ψ		160	30	1-2-2	1604	
301	- α		120	0	2-0-0	1372	
302	- α		120	0	2-0-0	1604	
303	- α		160	0	2-0-0	1604	
304	- α		160	0	6-0-0	1372	
305	Rotors Off						
306	- α		60	90	3-2-6	--	
307	- α		120	90	3-2-6		
308	- α		80	90	3-1-6		
309	- α		160	90	3-1-6		
310	- α		80	75	3-1-5		
311	Walls Dn - α	Sweep	80	75	3-1-5	--	

RUN SCHEDULE SUMMARY
MODEL C100-F1B LANGLEY V/STOL TEST 69
(Continued)

RUN NO.			$V_{F.S.}$ (KTS)	i_N (DEG)	CONFIG. NO.	RPM	h/D
312	Walls Dn - α	Sweep	80	75	3-2-5	--	
313	- ψ		80	75	3-2-5		
314	- α		60	90	3-2-6		
315	- α		120	90	3-2-6		
316	- ψ		60	90	3-2-6		
317	- ψ		120	90	3-2-6		
318	- α		80	90	3-1-6		
319	- α		120	60	3-1-4		
320	- α			60	3-2-4		
321	- ψ			60	3-2-4		
322	- α			30	3-2-2		
323	- ψ			30	3-2-2		
324	- α			30	3-1-2		
325	- α			0	3-1-0		
326	- α				3-2-0		
327	- α				3-2-0		
328	- ψ				3-2-0		
329	- ψ		120		3-2-0		
330	- ψ		160		6-2-0		
331	- α						
332	- δ_e						
333	- δ_e	Sweep					
334	- α	Sweep, Upside Dn	160				
335	- α	Sweep, Upside Dn	60		6-2-0		
336	- ψ	Sweep, Rt Aileron Dn	160		9-2-0		
337	- ψ	Sweep, Lt Aileron Dn	160	0	9-2-0		
338							
339	- α	Sweep	80	75	3-2-5		
340	- α		120	60	3-2-4		
341	- α			30	3-2-2		
342	- α			30	4-4-2		
343	- α			30	4-4-2		
344	- ψ			30	4-4-2		
345	- α			0	4-4-0		
346	- α				4-4-0		
347	- ψ				4-4-0		
348	- ψ				6-4-0		
349	- α			0	6-4-0		
350	- α			60	4-4-4		
351	- ψ		120	60	4-4-4		
352	- α		60	90	4-4-6		
353	- ψ		60	90	4-4-6		
354	- ψ		120	90	4-4-6		
355	- α		120	90	4-4-6		
356	- α		60	75	4-4-5		
357	- α		80	75	4-4-5		
358	- ψ		80	75	4-4-5		
359	Walls Dn - α	Sweep	160	75	4-4-5	--	